SSEC No.87.08.H1.

Rainfall over the Tropical Oceans During Special Observing Periods Of the Global Weather Experiment

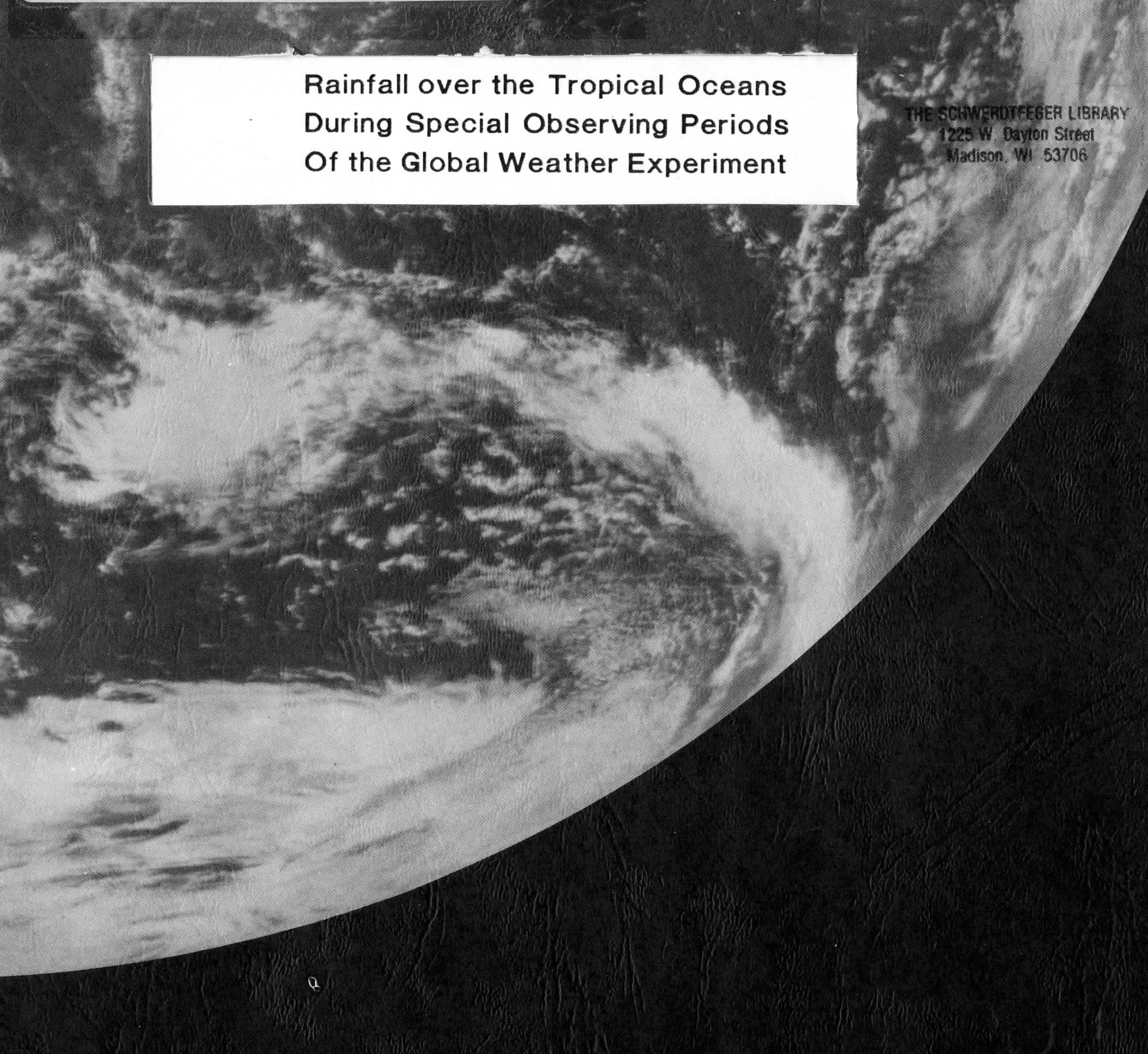

A REPORT

from the space science and engineering center
the university of wisconsin-madison
madison, wisconsin

Rainfall over the Tropical Oceans During Special Observing Periods Of the Global Weather Experiment

Final Report to

The National Oceanic and Atmospheric Administration

for

Rainfall over the Tropical Oceans During the Special Observing Periods Of the Global Weather Experiment

Grant No. NA85AA-D-CA061

University of Wisconsin Account 144-W442

for the period of

15 March 1985 to 28 February 1987

submitted by

Barry B. Hinton

Space Science and Engineering Center
University of Wisconsin-Madison
1225 West Dayton Street
Madison, WI 53706
(608) 262-0544

August 1987

SUMMARY

This report presents work on rain rate estimation over the tropics for the Special Observing Periods of The Global Weather Experiment. Emphasis is first placed on a discussion of calibration and attendant difficulties. After this machine readable products, available to other investigators, are described. The products are also summarized as contour plots for each day processed.

CONTENTS

ACKNOWLEDGEMENTS

We are grateful to NOAA for the financial support necessary to carry out this research. The investigators acknowledge and appreciate the direct contributions of the following SSEC staff: Gail Dengle, David Santek, Bob Gifford, Dana Davis, Roseann Johnson, Ann LaForce, Brian Auvine, Janeane Stuessy, and David Martin. We are especially grateful, also, to Phil Arkin, of NOAA's Climatic Analysis Center.

Rainfall over the Tropical Oceans During the Special Observing Periods of the Global Weather Experiment

1. INTRODUCTION

The subject of this report is research carried out by the University of Wisconsin-Madison Space Science and Engineering Center under Grant No. NA85AA-D-CA061, administered by NOAA.

1.1 Purposes of this Report

This report summarizes work carried out over the life of this grant, 15 March 1985-28 February 1987, thereby satisfying the final technical reporting requirements. Below we briefly review the context of the study, and its the two general accomplishments:

> *Development and calibration of a practical rain estimation technique for the tropical oceans.*
>
> *Production of a set of rain estimates for the Intensive Observation Periods of the Global Weather Experiment which is readily exportable to other investigators.*

1.2 Scope of this Report

Certain scientific conclusions drawn from, but beyond the results presented here, are to be published in the scientific literature. The volume of information produced, is great and it is not practical to reduce it all to printed form here. Consequently, this report is summarizing, rather than a comprehensive documentation of the work performed.

2. BACKGROUND

2.1 Need for this Study

Long range weather prediction and climate simulation require representation of atmospheric thermal energy sources and sinks. Two kinds of processes account for most of the energy cycle. These are: [1] conversions, within the atmosphere, between mechanical and thermal energy on the one hand and [2] the input and loss of thermal and mechanical energy from the atmosphere. However, these processes are correlated, which results in the organization seen in atmospheric processes.

In numerical models the actual mechanisms responsible for these correlations are represented in simplified "parameterized" form. It is then crucial to know whether, or not, these parameterizations have captured the essential nature of the process. Thus, it is reasonable to investigate whether the precipitation --a major conversion and heating process-- is correctly described.

Rain gauge data are dense enough to provide most (but by no means all) the required information over continental areas for the applications intended here. For other purposes, such as crop forecasting or hydrological application over small domains, the existing gauge networks are inadequate in many regions--even over inhabited land areas. However, there is a notable lack of data over the oceans, especially the southern oceans, for any application. Consequently, we have produced a data set suitable for verifying global scale tropical precipitation for the intensive observation periods (IOPs) of the 1979 Global Weather Experiment.

Further, similar techniques are now being developed for continuing use by geostationary weather satellite operating agencies around the globe. Our research contributes to the understanding and interpretation of the resulting "precipitation indices", which will have several applications extending outside of meteorology. For example Cooper [1986], discussing the work of Levitus [1986], has shown that there are regions in the tropical oceans where the component of the current in the upper few hundred meters that is driven by the horizontal density gradient, is determined as much by salinity variations as by sea surface temperature variations. Therefore, it is ultimately desirable to advance remote sensing techniques for ocean rainfall as a means of monitoring salinity changes. The data set we have produced is too short to be directly useful in this context, but our work verifies the feasibility of integrating data from several satellites.

2.2 Tools and Data for Rain Estimation

Recently one of our investigators, Martin, reviewed 19 remote sensing (and remote sensing combined with *in situ* data) methods which have been used.[1] Many of these methods are too complex, or require too much expensive, labor-intensive "human analysis" for routine use on a nearly global scale. Similarly, some other methods presuppose auxiliary information not available on a global scale, or or not available frequently enough (except possibly from the model itself, which compromises the desired independence of the precipitation field)[2].

What remains is a group of methods whose essential feature is an association of rain with cloud height. A measure of this height is the remotely sensed cloud top temperature or "OLR" (outgoing longwave radiation). These methods can be very simple. For example, one of the more

---

[1] 1. Report of the Workshop on Global Large-Scale Precipitation Data Sets for the World Climate Research Programme at Camp Springs Maryland, USA, 24-26 July 1985 (WCRP Report 1182).

[2] 2. Further information of several of these techniques can be found in Barrett and Martin's book [1981].

widely applied ones, the GOES Precipitation Index or GPI, [Arkin, 1979, 1983] assigns a fixed rain rate (3 $mm\ h^{-1}$) to any cloud colder than 235°K. Yet, the performance of these methods often compares favorably with more complex methods [see *e. g.* Wylie and Laitsch, 1983].

Because of the limited life and variability of raining systems in the tropics, including a substantial diurnal modulation, a sampling frequency of several observations per day is required to observe daily rain in a 2.5° latitude by 2.5° longitude grid cell [Richards and Arkin, 1981; Wylie and Laitsch, 1983]. For the Global Weather Experiment 11μ data from geostationary spacecraft are available over the entire tropical belt much of the time[1] These images are available at half hour intervals, or in some cases even more frequently. Moreover, the sensors all have a spatial resolution the order of 8 km at the subsatellite point or 14 km where the satellite is seen at a zenith angle of 55° from the earth. This provides at least 300 samples in each grid cell for each time interval.

---

[1] Unfortunately, there are interruptions in the data. The IR sensor of Goes IO (on station over the Indian Ocean) failed. Goes E (viewing the central Atlantic Ocean to mid USA) did not always scan the Southern Hemisphere due to a problem with the scan drive.

3. ACCOMPLISHMENTS

3.1 Calibration

In view of the foregoing, we decided to adopt a simple IR method on the 2.5° lat-lon grid. However, we were not satisfied with the step-function nature of The GPI at a specific threshold temperature as described above and as shown in (1).

$$\mathrm{GPI} = \begin{cases} 0 \ mm/d & \text{if } T_{ir} > 235^{\circ}K \\ 72 \ mm/d & \text{if } T_{ir} < 235^{\circ}K \end{cases} \qquad (1)$$

Earlier investigations over both land and ocean had suggested that there is useful quantitative information on rain rate in the cloud top temperature [*e.g.* Wylie and Laitsch, 1983; Hinton and Martin, 1986; Robertson, 1985; Richards and Arkin, 1981]. Therefore, we determined to heed the results of these previous works, and to establish a "calibration curve". A brief description of the procedure follows.

SUMMARY OF PROCEDURE FOR GENERATING CALIBRATION DATA SET

1. Microwave radiometer data, from the SMMR on Nimbus-7, were used to select areas where rain was indicated within the over-water coverage sectors of the NOAA weather radars along the Gulf of Mexico coast plus the Atlantic sector of the Daytona Beach radar as shown in Fig. 1.

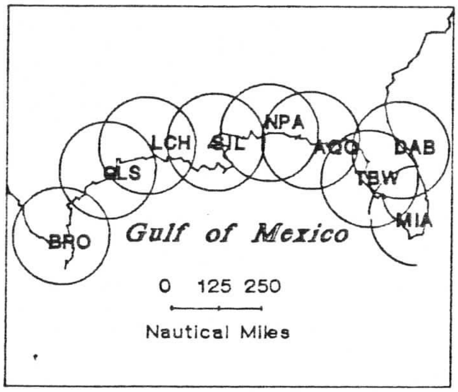

Fig. 1 Radar locations.

2. Microfilm records were obtained for as many of the cases as possible. These were reviewed for quality, and for data in the appropriate time window. Some of the films had to be discarded because of poor quality of exposure or processing. In some cases the lack of image sharpness did not permit reliable reading of time, range indicators, or elevation indicators.

3. The surviving images, listed in Table 1, were digitized on a scanning photometer with a 0.02 *mm* spot size, resulting in radar images with about 500 picture elements in both the vertical and horizontal dimensions. This resolution was adequate to preserve the spatial resolution of the original images. Using data on the radar's location, the images were "navigated" to establish the correspondence between the image elements and geographical coordinates.

Table 1. Radar data used. YYDDD represents year and day, HHMM are hours and minutes of the data (UT). SMMR time, in HHMM form, indicates Nimbus-7 overpass.

	Radar			GOES			SMMR
File	ID	/ Location	:	YYDDD	HHMM --	HHMM :	Time
1	SIL	30°16'N	89°46'W	79054	1730	1800	1743
6	LCH	30°07'N	93°13'W	79054	1730	1800	1743
2	NPA	20°21'N	87°19'W	79242	1700	1730	1711
27	SIL	30°16'N	89°46'W	79242	1700	1730	
3	NPA	20°21'N	87°19'W	79236	1700	1730	1703
11	AQQ	29°43'N	85°02'W	79236	1700	1730	
13	TBW	27°42'N	82°24'W	79236	1700	1730	
4	NPA	20°21'N	87°19'W	79052	1700	1730	1706
12	AQQ	29°43'N	85°02'W	79052	1700	1730	
5	LCH	30°07'N	93°13'W	79200	1730	1800	1752
7	DAB	29°11'N	81°03'W	79214	0500	0530	0529
8	GLS	29°18'N	94°48'W	79244	1730	1800	1750
10	BRO	25°54'N	97°26'W	79244	0600	0630	0617
9	GLS	29°18'N	94°48'W	79036	1700	1730	1729
14	MIA	24°43'N	80°17'W	79028	0500	0530	0516
15	AQQ	29°43'N	85°02'W	79012	1700	1730	0540
25	TBW	27°42'N	82°24'W	79012	0530	0600	
16	NPA	20°21'N	87°19'W	79182	0530	0600	0552
17	NPA	20°21'N	87°19'W	79030	0530	0600	1724
19	SIL	30°16'N	89°46'W	79030	1700	1730	
18	LCH	30°07'N	93°13'W	79304	0600	0630	0607
22	SIL	30°16'N	89°46'W	79304	0600	0630	
20	DAB	29°11'N	81°03'W	79274	0500	0530	0519
24	MIA	24°43'N	80°17'W	79274	0500	0530	
21	NPA	20°21'N	87°19'W	79198	0530	0600	0540
23	AQQ	29°43'N	85°02'W	79198	0530	0600	
26	TBW	27°42'N	82°24'W	79126	1700	1730	1713

4. GOES infrared window channel images were obtained for times close to the times of the radar images (usually within 3 minutes). These were transformed or "remapped" to the same image projection as the radar and displayed, in register, on a McIDAS video terminal. This allowed us to verify that the remapping had been done correctly, that the correct images had been paired and the like. Sample images are shown in Fig. 2.

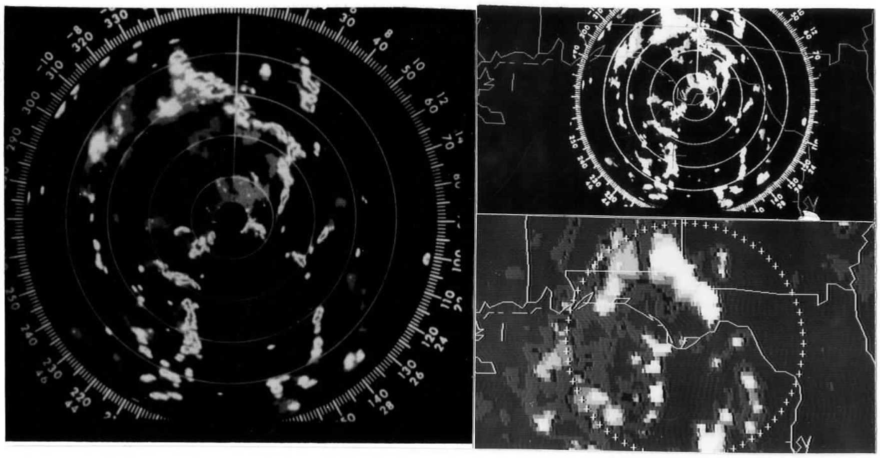

Fig. 2 Radar and satellite data illustrating calibration. The left panel is a reprint of the radar microfilm for station AQQ on day 236 of 1979 at about 17:03 GMT. The upper right panel is a hardcopy rendition of the video display of the digitized version of the radar data. The lower right panel is the corresponding infrared image display from GOES-E. The GOES display has been enhanced to emphasize cold clouds.

5. An analyst selected appropriate data points. Unfortunately, the exposure and processing variations, mentioned above, resulted in the "digitized" radar video processor levels having a band of digital count levels in our re-digitization process. Further, artifacts on the radar images, such as permanent clutter and range markers could not be distinguished from true echoes on the basis of digital value alone. In addition, all reflectivity levels are represented photographically in only three shades of gray. That is, the video processor output, when judged by digital value alone, is ambiguous. One has to consider the surrounding context. Thus, fully automatic processing of the images to form a data set was not practical. Therefore an analyst was used to avoid the artifacts and interpret the gray levels (to remove the ambiguities). All the factors mentioned are readily seen in the radar image shown above in Fig. 2.

In the discussion which follows we may think of the calibration data as a set 221 records, where each record consists of one radar observation of reflectivity, re-expressed as a rain rate, and one value of a corresponding infrared cloud top temperature observed by GOES-E. Before discussing three ways of treating this data set, we will look at a few general characteristics.

Fig. 3 illustrates the spread in T_{ir}, cloud top infrared temperature (actually inferred from radiance, assuming all radiation is emitted by the cloud as a black body), and the nominal spread in rain rate for the video processor levels, (z) present in the data set. The values z=0,1,2,3 nominally correspond to rain rates R of 0, 4, 17, and 44 $mm \cdot h^{-1}$. The spread in R is taken to be $0.4 \cdot R$ for $R>2$, but 2 for $R<2$. The mean and spread values of T_{ir} illustrated in Fig. 3 are deduced from observations when they are sorted according to z.

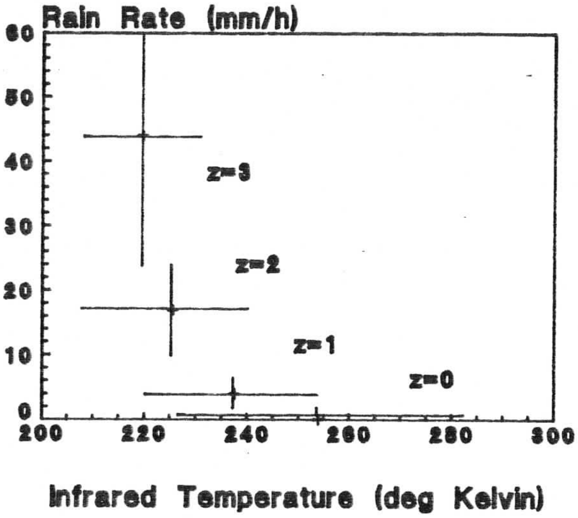

Fig. 3 Means and variances of cloud top infrared temperatures for radar reflectivity factors zero through three.

Table 2 shows the distribution of calibration points in 10°K T_{ir} bins, while Table 3 shows it by z-value. It is important to note that these distributions do **not** necessarily reflect the population characteristics of the tropical oceans. A least squares fit to the *observed* tropical T_{ir} distribution for 5 January 1979 is shown in Fig. 3 along with the distribution for the calibration data. The parabolic curve (restricted to T_{ir}<271°K) is an excellent fit to the observed tropical data, explaining 98.6 % of the total variation.

Table 2. Distribution of T_{ir} values in calibration data.

T_{ir}	n	Mean	Mode	Std. Dev.	Skewness	Kurtosis
<200	1	0	0	0	0	0
200-210	11	27.2	42	14.7	-0.06	-1.86
210-220	51	17.4	17	16.7	0.52	-1.27
220-230	37	9.5	4	14.1	1.68	1.48
230-240	20	8.2	0	12.9	2.02	3.38
240-250	27	7.4	0	11.8	2.08	4.41
250-260	21	2.1	0	15.2	2.97	10.78
260-270	18	3.4	0	5.3	2.06	3.73
270-280	9	0	0	0	0	0
280-290	10	0.8	0	1.7	1.78	1.41
290-300	16	0	0	0	0	0

Table 3. Distributions of T_{ir} for fixed values of Z.

Z-Value:	0	1	2	3
Sample size	103	53	37	28
Mean	253.8	239.1	225.4	219.5
Mode	291	225	215	216
Std. dev.	27.3	18.7	16.8	10.5
Skewness	-0.01	0.34	1.14	1.25
Kurtosis	-1.29	-0.67	0.47	1.94

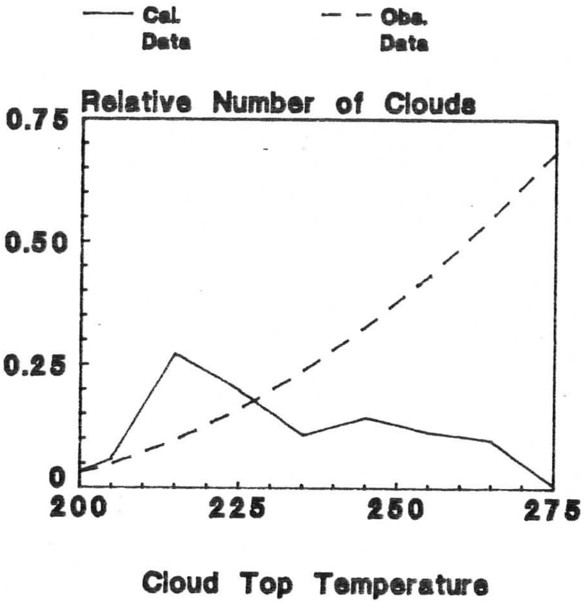

Fig. 4 Distributions of cloud top temperature in the calibration data and observed in the tropical zone, 30^oN to 30^oS.

Based on our rain rate algorithm, yet to be justified, we can tentatively estimate the distribution of mean rain rates in the tropical zone. Using the observed distribution of temperature (dashed curve from Fig. 4) we obtain the dashed curve of Fig. 5. This may be compared to the solid curve in Fig. 5, which is a similar estimate for the calibration data. If our algorithm is even qualitatively correct, it is readily seen that the ranges of temperature (and therefore rain rate) are similar, but that the distributions, or relative numbers differ somewhat. This is so because our data selection procedure emphasized cases for which rain was expected. Therefore the relative numbers of both rain and the cloud top IR temperatures most often associated with rain are enhanced. This was the objective of the data selection method.

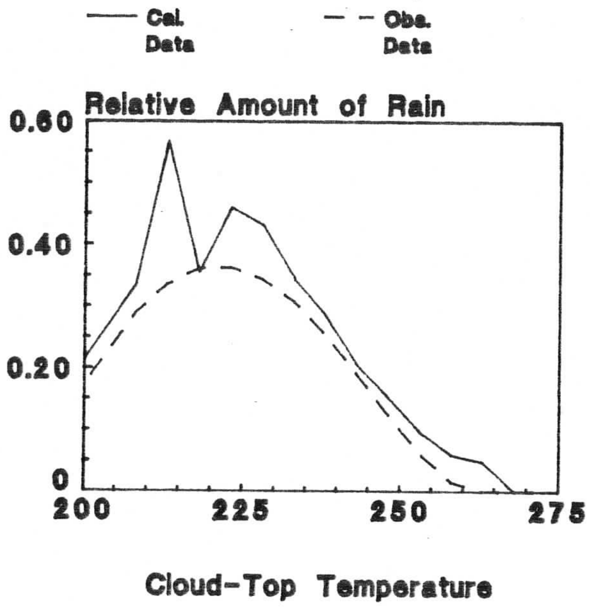

Fig. 5 Relative amounts of rain associated with various cloud top temperatures in the calibration data and which would be observed in the tropical zone, assuming the calibration to be discussed below is correct.

Due to the discrete nature of the z and R values in the calibration data, it is natural to consider the distribution of T_{ir} for the data grouped by z value. Table 3 showed parameters of these distributions. However, the distribution parameters for rain rate, *given a range of temperatures,* is more directly relevant. Table 2, which showed these, suggests that there is a rain rate distribution similar to Fig. 6 at a given temperature. In calibration, we are essentially replacing this distribution by its mean value.

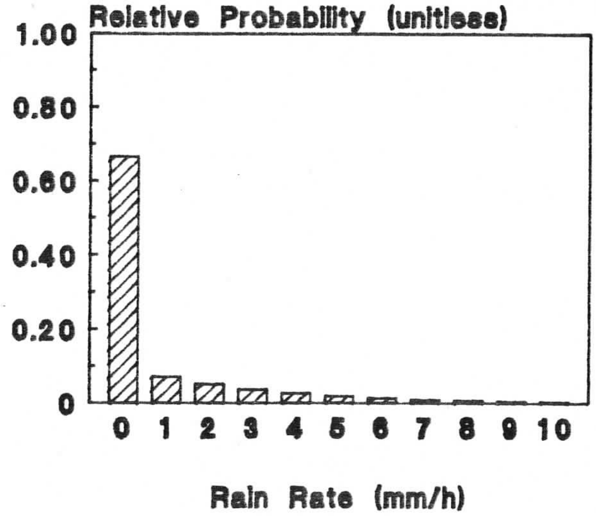

Fig. 6 Hypothetical distribution of rain rates for clouds at a fixed cloud top temperature.

Therefore, one possible calibration method would be to connect the mean rain rates from the table by a smooth curve. More precisely, it would be to fit the mean rain rates to a polynomial in T_{ir} by least squares. Based on abundant evidence that significant rain is rare for cloud top temperatures above ~0°C (273°K), the curve is forced through 0-rain rate there and is defined to be 0 at any warmer temperature. The results of this procedure are illustrated in Table 4 and Fig. 7. To distinguish this function we denote it by R_m. (Note, that the fitting parameters shown in the table refer to the eight means of the binned data, *not* the original observations.)

Table 4. Model fitting results for R_m.

Ind. Variable	Coeff.	Std. Error.	t-value	Sig. Lev.
Const.	298.425	71.240	4.21	0.008
T_{ir}	-2.116	0.558	-3.79	0.013
T_{ir}^2	0.00374	0.00108	3.46	0.018

Square of the Correlation Coeff.: 0.9185 Std. Err.: 0.230

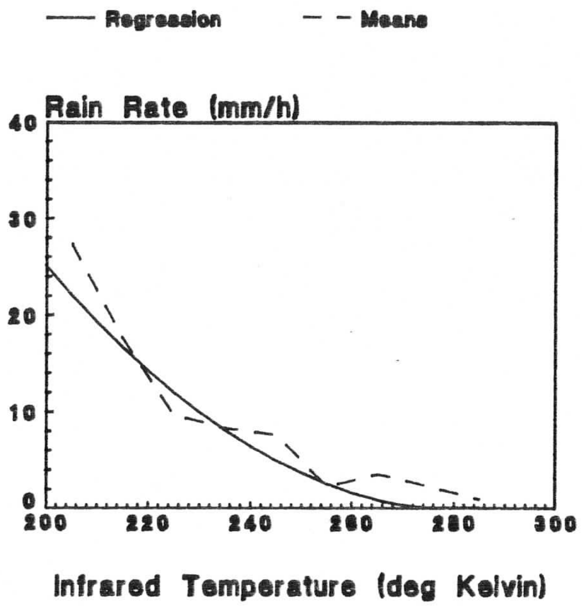

Fig. 7 R_m as a function of cloud top temperature. The dashed polygonal line connects the means from Table 2. The solid line is the regression curve.

An alternative method is to use least squares fitting on the data set directly, without the temperature binning. If the distribution of temperature were uniform there would be no practical difference between the two procedures--no difference at all if the temperature bins were narrow enough. In effect, this second method is weighted by the distribution of Table 2. This second function is expressed in terms of R_m (regarded as a trial function, or first approximation). The resulting function is denoted by $\tilde{R}$. See Table 5 and Fig 8.

Table 5. Model fitting results for $\tilde{R}$.

Ind. Variable	Coeff.	Std. Error.	t-value	Sig. Lev.
Constant Included				
Const.	0.8691	1.312	0.66	0.508
R_m	0.9680	0.120	8.08	3 E-8
Square of the Correlation Coeff.:		0.2298	Std. Err.:	12.230
Constant Excluded				
R_m	1.029	0.075	13.73	0.000
Square of the Correlation Coeff.:		0.4614	Std. Err.:	12.213

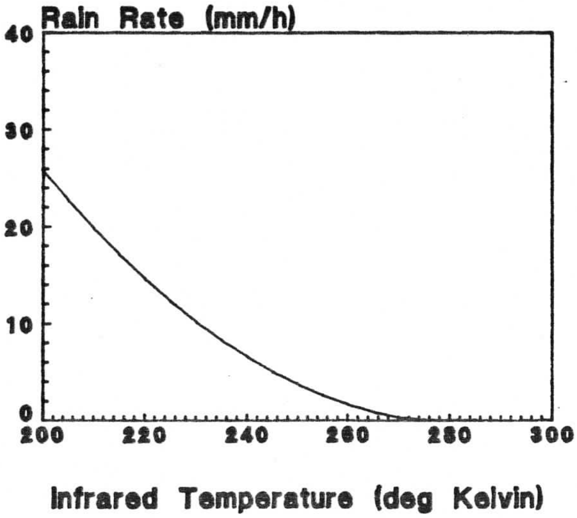

Fig. 8 Linear regression fit of calibration dataset to the cloud top temperature function R_m.

Because of the discrete nature of z, and the consequent spread of R values for a given value of z, a third method was considered. Let R_z, [z=0,1,2,3] be a randomly variable rain rate whose mean value corresponds to z. The mean values are: $\hat{R}_z$=0, 4, 17, 44 [for z= 0, 1, 2, 3]. Thus, for example, R_1 is a random variable rain rate for which the radar exhibits z=1, and which therefore has a mean value of 4 $mm{\cdot}h^{-1}$. Now the temperature ranges of th R_z overlap, as we can infer from Table 3, if we assume that the probability densities of the R_z's are at least approximately Gaussian or "normally" distributed. Schematically, this would be as illustrated in Fig. 9.

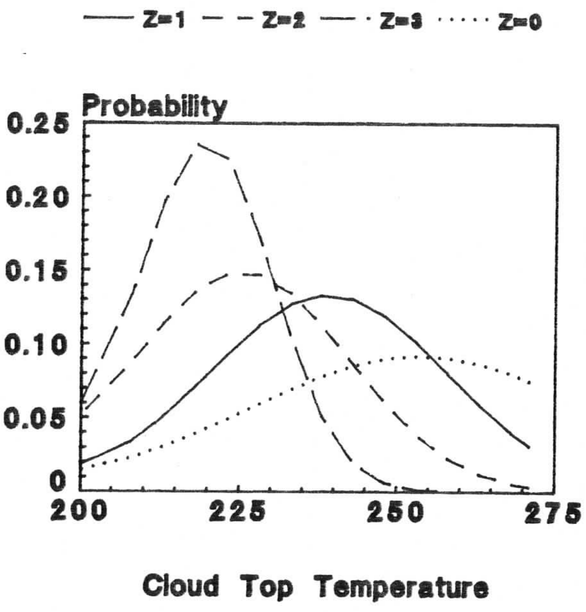

Fig. 9 Normal distribution models of cloud top temperature for z-values zero through four.

Suppose we observe a specific cloud top temperature, *e.g.* 250°K. What value of z (or R_z) do we expect to observe? The expected values, $\hat{R}(T_{ir})$, could be modelled as,

$$\hat{R} = \{ \sum_{z=1}^{3} R_z \cdot w_z \,/\, (\sum_{z=0}^{3} w_z) \} \qquad (2)$$

In (2) w_z is the probability of z, *given* T_{ir}, as shown in the figure referred to above. Note that the sum $w_0 + \ldots + w_\infty$ must be unity. Unfortunately, the magnitude of the z=0 probability curve relative to the others is quite unrealistic. *This is because we systematically excluded cases from the calibration data which were not associated with precipitation.* Even for the R=0 data, there is rain nearby. Nevertheless, because w_0 only occurs in the denominator of (2) the shape is probably well described by the data we have obtained when inserted into (2). The neglect of z > 3 terms is based on the supposed rarity of these values which can (in fact) be justified *a posteriori.*

The functional form generated by (2) was fit to the calibration data (by redefining a multiplicative constant) with the result denoted by $\hat{R}$. See Table 6. below.

Table 6. Results of fitting $\hat{R}$ to calibration data.

Ind. Variable	Coeff.[1]	Std. Error	t-value	Signif.
Function·Const.	1	7.42 (%)	13.47	0.000

Square of the Correlation Coeff.: 0.4521 Std. Err.: 12.31

[1] Pre-normalization coefficient is 1 by definition.

For convenience we show our three preliminary functions R_m, $\tilde{R}$,

and $\hat{R}$ together in Fig. 12. It is readily seen that the curves are similar in character, and that R_m and $\tilde{R}$ are practically identical.
Nor do the results differ significantly in terms of the square of the correlation coefficient or the standard error for fitting the calibration data. Specifically, all have a squared correlation of about 0.46, referred to the variance about zero rain rate, rather than the mean rain rate of the calibration data. This is appropriate, since the *a priori* mean tropical rain rate is only 0.1 to 0.2 $mm \cdot h^{-1}$. Somewhat arbitrarily then, we decided to formulate our algorithm in terms of $\hat{R}$.

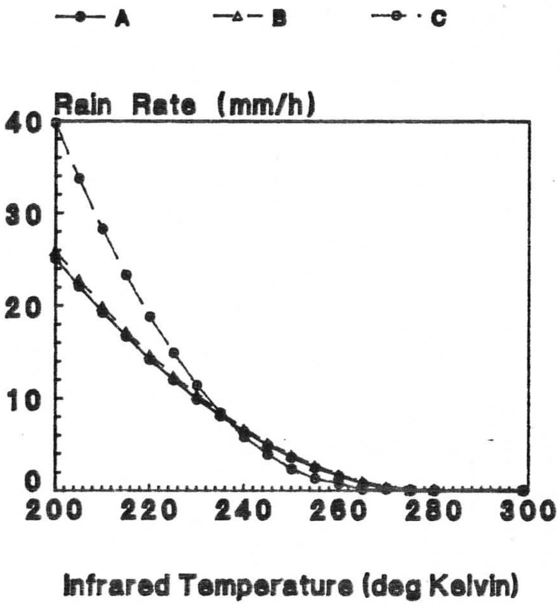

Fig. 10 Three candidate calibration curves. Curve A (long dashed line, dots) is R_m, B (short dashed line, triangles) is $\tilde{R}$, and curve C (dashed-dotted line, dots) is $\hat{R}$.

We have plotted the GPI curve (divided by 24 to give hourly rate) and $\hat{R}$ in Fig.11. The great disparity in the areas under these curves illustrates the relative enrichment of out calibration data set in rain cases. Therefore, we normalized our curve by requiring the globally averaged rain rate in the tropical band to agree with the GPI.,

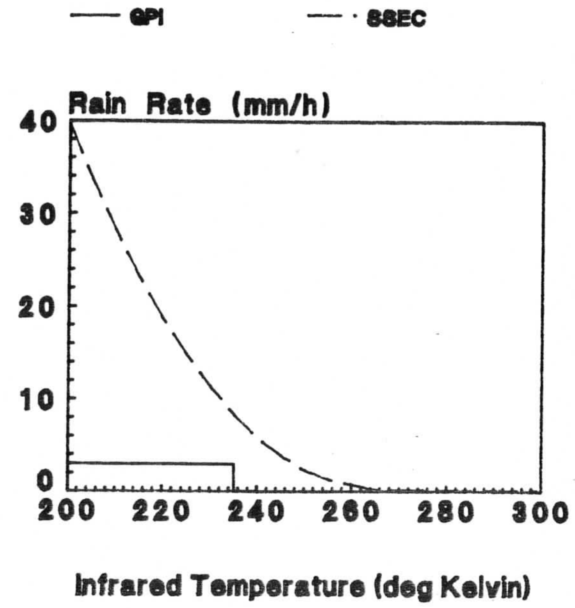

Fig. 11 Comparison of the non-normalized $\hat{R}$ and the rain rate as a function of cloud top temperature used in the GPI. $\hat{R}$ is the dashed curve labeled SSEC. The GPI is the solid curve.

Fig. 12 is a comparison of the $\hat{R}$ algorithm with several others.

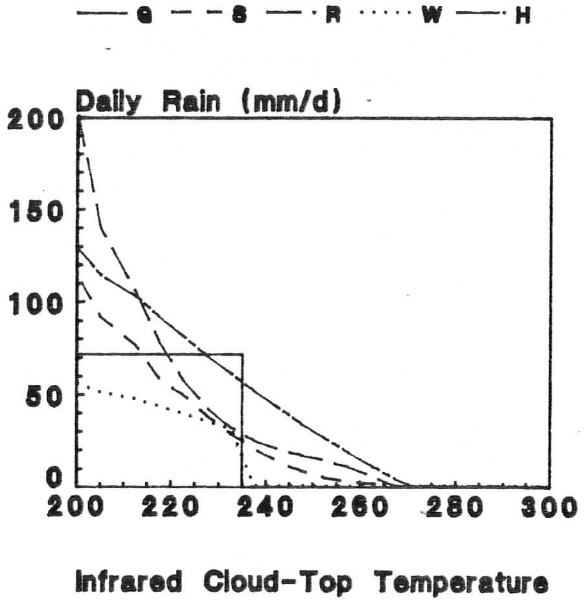

Fig. 12 Calibration comparison. The normalized version of The $\hat{R}$ algorithm, is denoted by S, the one by Robertson [1986] is denoted by R, the one by Wylie and Laitsch [1983], W and the one by Hinton and Martin [1986] is denoted by H, and the GPI is denoted by G. The H- and W-curves were derived from data over land.

Fig. 13 and Fig. 14 compare the latitude-longitude distributions of rainfall produced by the GPI, the SSEC and Robertson's algorithm. It is readily seen that, in spite of the extreme difference between the shape of the GPI and the other two algorithms as a function of cloud top temperature, the latitude-longitude maps of rainfall are rather similar. The most noticeable differences are the maxima in the regions of higher rain rate. This further suggests that the shape of the rain rate *vs* T_{ir} relation is of secondary practical importance. One concludes that the mixture of cloud top temperatures has roughly constant properties over the tropical region. In keeping with the success of the GPI, it appears that the existence of cold (*e.g.* T_{ir}<235°K) cloud alone is the more significant factor

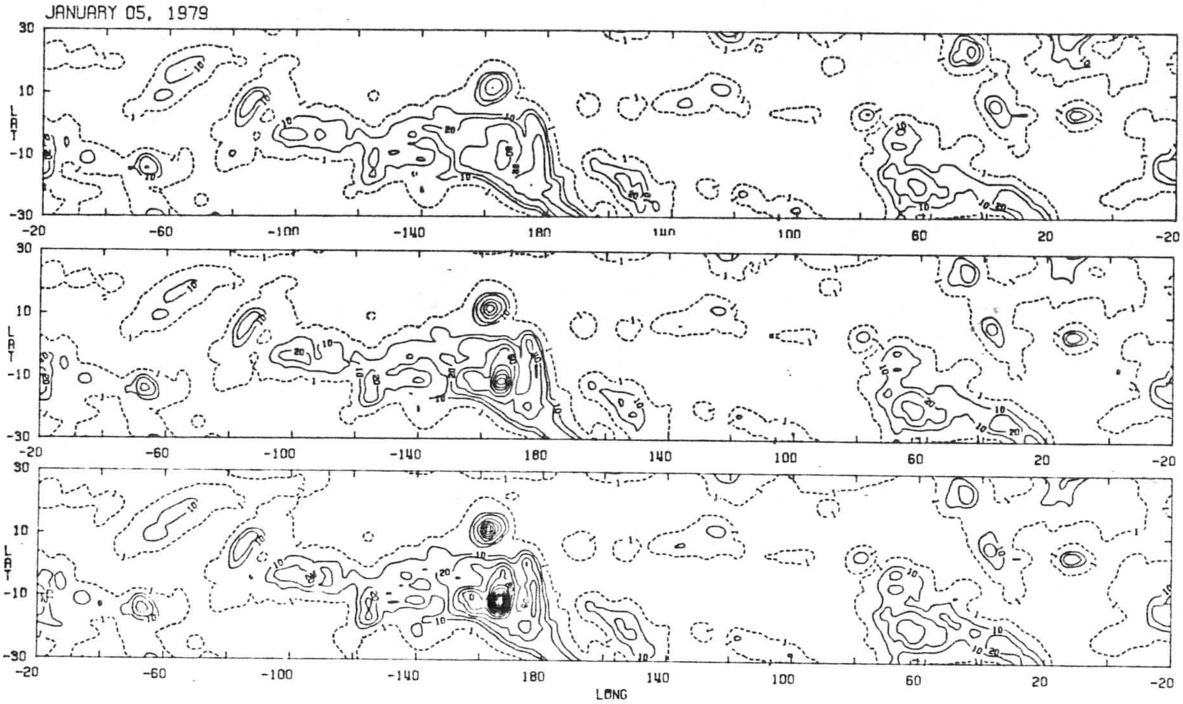

Fig. 13 Tropical rainfall on 5 January 1979 according to three algorithms. Top to bottom: GPI, SSEC($\hat{R}$), & Robertson's algorithms.

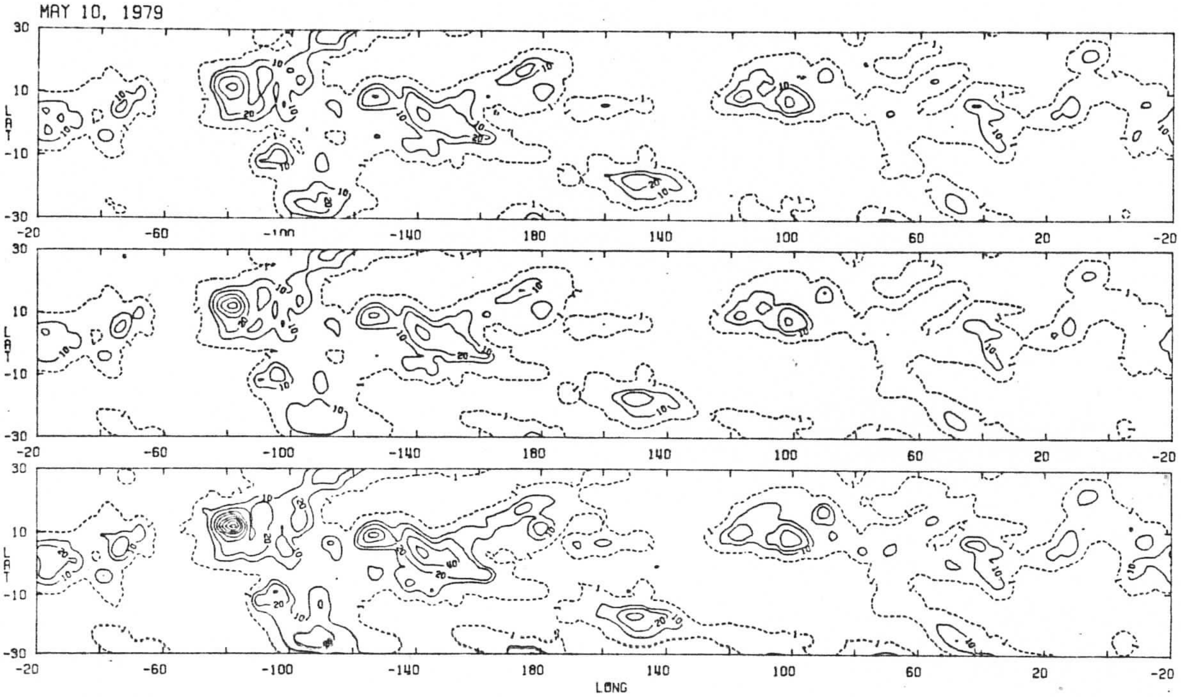

Fig. 14 Tropical rainfall on 10 May 1979 according to three algorithms. Top to bottom: GPI, SSEC($\hat{R}$), & Robertson's algorithms.

3.2 Production Software

There two "phases" to the production software. First, the IR data for a given time of observation within a given 2.5^o latitude by 2.5^o longitude grid cell are collected from the satellite data tapes and their distribution, the relative number in 16 specific brightness temperature intervals, summarized in the tabular equivalent of histograms. The brightness temperature intervals are given in Table 7. Second, the histograms are converted to rain rate as described above in connection with calibration.

We chose to make the first phase identical in all essential respects to the processing used for the GPI. In order to do this we acquired and modified the computer code [Arkin, 1986] for the GPI binning. The significant changes required to complete the software for this phase all were to integrate it into our specific hardware (IBM 4381) and software environment (McIDAS low level subroutines), or with adapting it to Meteosat and GMS.

This choice of processing system had several advantages. Most importantly, through McIDAS we could access the extensive library of digital image processors for navigating and efficiently manipulating large quantities of satellite data. The two phase aspect allowed most of the data handling and compaction to be independent of a specific calibration algorithm, so it is possible to rapidly up-date, or reprocess, the results *a posteriori* if a new calibration is selected

The GOES data were archived on modified video cassette tape recorders. Before these data could be used, they had to be converted to computer compatible tape (CCT), specifically 9-track 6250 bits per inch (bpi) tapes. The Meteosat data are available at our facility on 6250 bpi tapes, but unlike GOES, or GMS, the navigation information is often on a different tape than the images. In the GMS case, also available on 6250 bpi, the operational navigations supplied by the data producer

(JMA) were often unsatisfactory and had to be redone. Fortunately, many had been revised for previous research done at SSEC.

Navigation, calculated independently for each satellite based on its daily orbital characteristics, had a nominal accuracy of several kilometers at the equator, although errors in the navigation data file could lead to considerably worse results. For this reason, each image was visually checked for gross accuracy (to insure errors somewhat less than one degree) by viewing the actual continental outlines visible in a TV display of the image in relation to those retrieved from a base map file using the navigation data from the navigation file.

In almost all cases there was sufficient contrast and unobscured detail in the images to allow this determination. In addition, significant errors in navigation would show up as distortions on the number of non-zero brightness temperature pixels in a given grid cell. Since the expected numbers of pixels can be calculated quite accurately, the difference indicates (among other things, as will be discussed further below) a possible navigation problem.

McIDAS routines performed the task of counting the number of pixels in each of the 16 temperature classes and sorting the histograms by box location, time of day and day. Where coverage for different satellites overlapped, the results from the two sources were averaged. In addition, in each geographical box or cell, these routines counted the usable (non-zero) pixels in each box and compared it with the expected number as mentioned above.

If the total number of valid pixels fell below 25% of the minimum number of pixels expected for that box, the box received a quality control flag value 2, for a major data loss, since pixels with a digital value of zero were deemed noise. These boxes were subsequently excluded from the analysis. A complete lack of data within a box was assigned a quality control flag value of 9, whether due to a missing image of a missing section of data within an image.

For each satellite image, the grid of quality control flags was printed and examined. In this way, a record of missing and/or mis-navigated data are maintained for each grid box.

Table 7. Cloud class definitions.

Class No.	Temperature
1	> 270
2	266-270
3	261-265
4	256-260
5	251-255
6	246-250
7	241-245
8	236-240
9	231-235
10	226-230
11	221-225
12	216-220
13	211-215
14	201-210
15	191-200
16	< 191

For the final analysis the histogram data in the McIDAS files was downloaded to a Bernoulli Box flexible disk cartridge attached to an IBM PC/AT[1]. The downloading is accomplished via a dial-access port. The data were averaged over four the time intervals for that day and the

---

[1] Bernoulli Box™ IOMEGA Corp. IBM PC/AT denotes a Personal Computer AT manufactured by the IBM Corp. Specific product names in this report are for convenient reference, not endorsement

absolute numbers of pixels in a given class converted to percents of the total number of valid pixels in each box.[1] In addition, the quality control flags were packed into one array for each satellite and day.

On the PC/AT, the quality flags were printed out and the histogram percentages multiplied by the appropriate calibration weights to produce files of daily rainfall totals. The latter were used with a mainframe-type plotting program to generate daily contour maps of rain.

3.3 Data Processed

Plots and a list of data processed, detailing missing data sectors for each day, are given in an appendix to this report.

3.4 Data Export and Auxiliary Processing

The rain files are readily exportable via 1.2 MB floppy diskette or 9-track tapes. We can also provide small hard copy plots of specific days or time periods.

By means of additional software, the rain files have been processed to present summarizing information in several presentations. These include:

Daily values of global tropical average rain rate

Rain rates in 360^{o} longitude by 2.5^{o} latitude "zones"

Phase and amplitude of longitudinal wave numbers 1-15

---

[1] After tests showed only minor differences between four and eight samples per day, we processed only four per day to reduce costs. (Four and eight samples correlated >0.95).

Composites of rain for longer time intervals

Samples of daily rain rates were shown in Fig. 13 and Fig. 14. An example of zonal average rain rates is shown in Fig. 15. Figures 16 and 17 show the phases and amplitudes of zonal wave numbers one and two. Figures 18 and 19 show "monthly" averages for January and June, 1979. (These are pseudo-averages since, due to missing data, not all days of the month are present in every sector.)

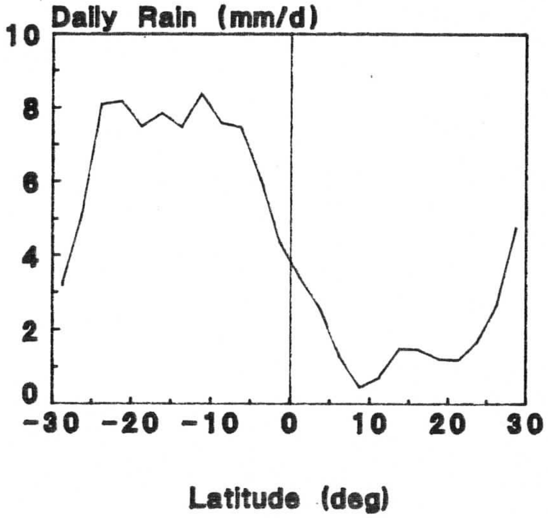

Fig. 15 Zonally averaged rainrates for 05 January 1979.

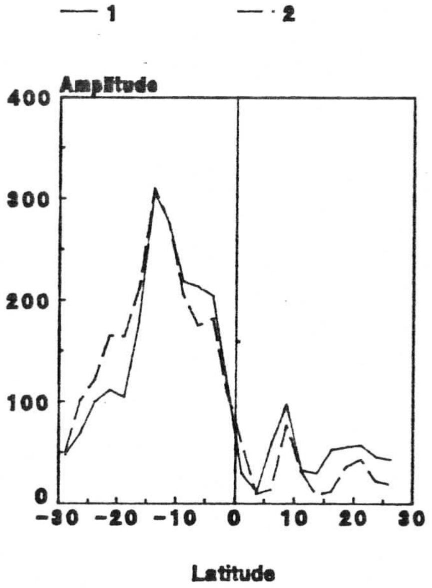

Fig. 16 Amplitudes of zonal waves number one and two as functions of latitude for 05 Jan. 79.

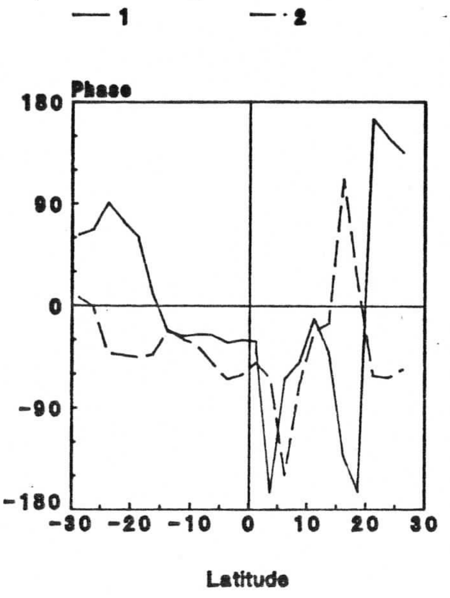

Fig. 17 Phases of zonal waves number one and two as functions of latitude for 05 Jan. 79.

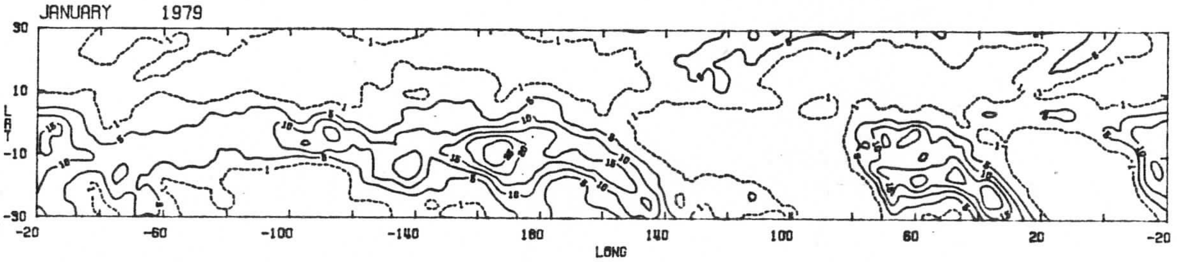

Fig. 18 Approximate average daily rainfall for January 1979.

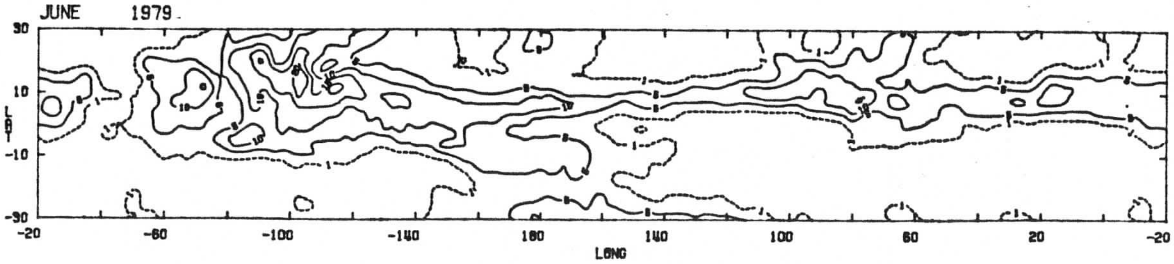

Fig. 19 Approximate average daily rainfall for June 1979.

4. CONCLUSIONS

Calibration and verification data remains the bane of those of us doggedly pursuing rainfall remote sensing methods. We expended considerable effort on it in this program, arriving at an algorithm resembling Robertson's more than the GPI in shape. A higher quality data set is required. For example, it would be desirable to observe (doppler) fall speeds as an adjunct to reflectivity as a means of inferring the "true" rain rate. Also, the (operational) radars available are more representative of the littoral zone than mid-ocean conditions. The data set has to be systematic as well. Research radars are often turned on only during "intersting" conditions. A long term dedicated data set representative of mid-ocean conditions is needed.

Because the GATE radar record seems less afflicted by bias effects, we ultimately normalized our algorithm with this data set (which is the basis of the GPI). Since our algorithm differs in shape from the GPI--lighter rains from relatively warm clouds and more intense rains from relatively cold clouds--it produces a different distribution of rain than the GPI. In practice, however, it emerged that the differences are "second order". Evidently this has to do with some persistent features of the height distribution of tropical clouds.

LIST OF ILLUSTRATIONS

Figures

Tables

REFERENCES

Arkin, P.A., 1983: A Diagnostic Precipitation Index from Infrared Satellite Imagery. *Tropcal Ocean-Atmosphere Newsletter*, 17, 5-7.

Arkin, P.A., and B.A. Meisner, 1985: The Relationship between Large Scale Convective Rainfall and Cold Cloud over the Americas during 1982-1984. *Personal Communication*

Barrett, E.C., and D.W. Martin, 1981: *The Use of Satellite Data in Rainfall Monitoring.*. Academic Press, 340 pp.

Cooper, N.S., 1986: The Importance of Salinity in the Tropics. *Tropical Ocean-Atmosphere Newsletter*, 36, 6-7.

Hinton, B.B., and D.W. Martin, 1986: *Microwave-Infrared Rain Algorithms for the SSM/I, Final Report to NOAA on Contract NA-84-DGC-00240 by the University of Wisconsin-Madison Space Science and Engineering Center.*. SSEC, U. Wisconsin-Madison.

Levitus, S., 1986: Annual Cycle of Salinity and Salt Storage in the World Ocean. *J. Phys. Oceanogr.*, 16, 322-343.

Richards, F., and P. Arkin, 1981: On the Relationship Between Satellite-Observed Cloud Cover and Precipitation. *Mon. Wea. Rev.*, 109, 1081-1093.

Robertson, F.R., 1985: IR Precipitation Estimates in the South Pacific during FGGE SOP-1. *Sixteenth Conference on Hurricanes and Tropical Meteorology.*, 16, 48-49.

Wylie, D.P., and D. Laitsch, 1983: The Impacts of Different Satellite Data on Rain Estimation Schemes. *J. Clim. Appl. Meteor.*, 22, 1270-1281.

APPENDIX A: RAIN CHARTS AND QUALITY TABLES

A.1 Introduction to Charts and Quality Table

The charts are given in two sequences. The first is for Special Observing Period I, or Day 006 through Day 064, while the second which begins on Day 130 and extends through Day 181, is for Special Observing Period II. Each chart represents daily accumulated rainfall contoured in mm. Contour intervals are 10 mm, with a supplemental (dashed) contour at 1 mm. There is no contour for the value 0 mm. The first sequence of charts is preceded by an orientation map. No geographical outlines are shown on the rain charts.

Approximate areas of missing or unusable data are blocked out on each chart. These blocked out areas can be correlated with the entries in the quality table. Note, however, that the blocked out areas only show cases for which an entire day's data could not be used. The table contains entries on an image-by-image basis for data which are missing (no entry in comments column), or of questionable quality (appropriate

A.2 Rain Charts for Special Observing Period I

Charts for Days 79006-79064 (5 Jan 79 through 5 Mar 79) begin on the following page.

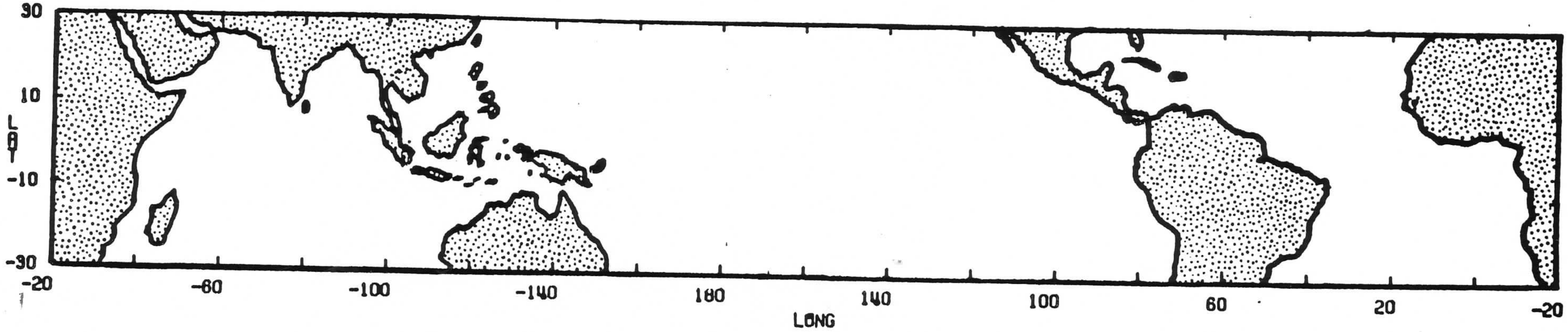
30
10
-10
-30
LAT
-20
-60
-100
-140
180
140
100
60
20
-20
LONG

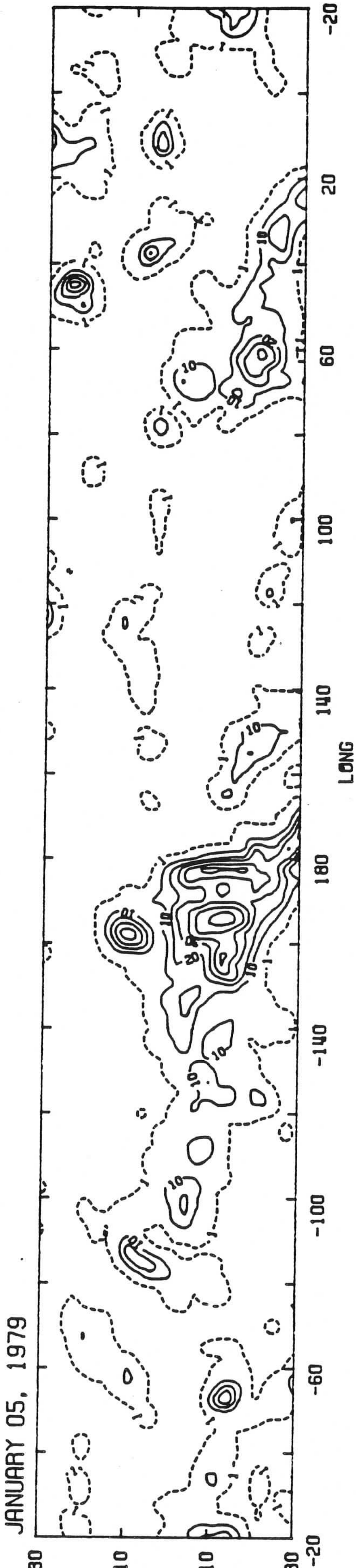
JANUARY 05, 1979

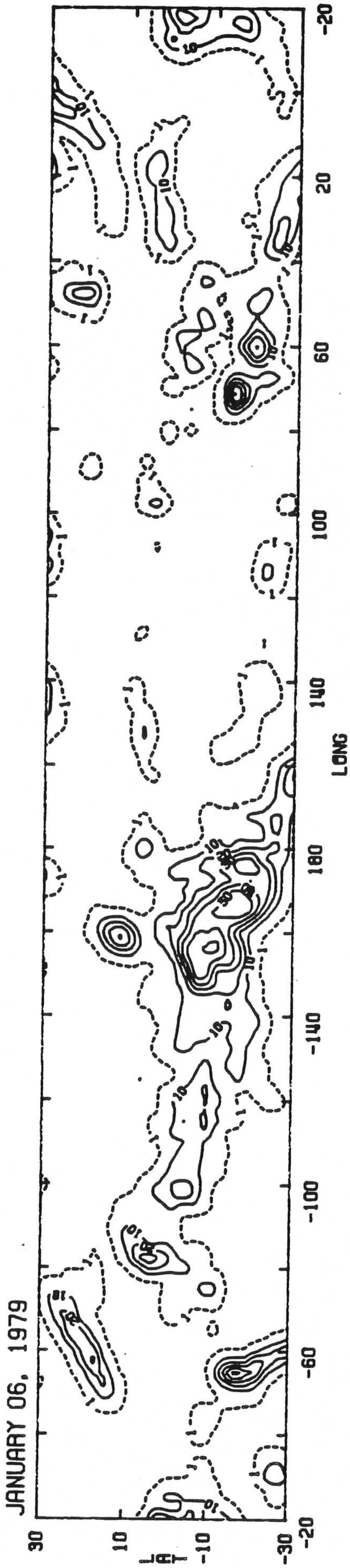
JANUARY 06, 1979

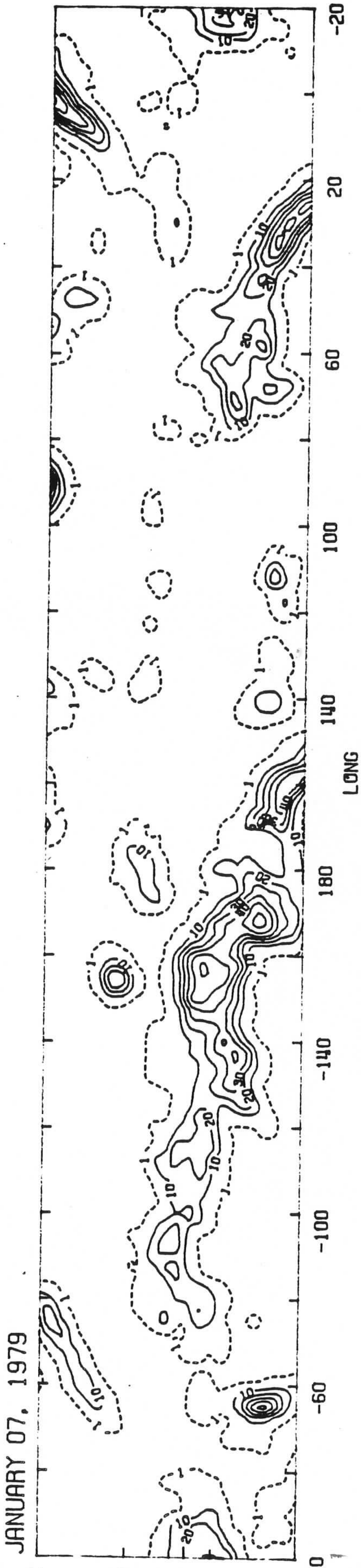
JANUARY 07, 1979

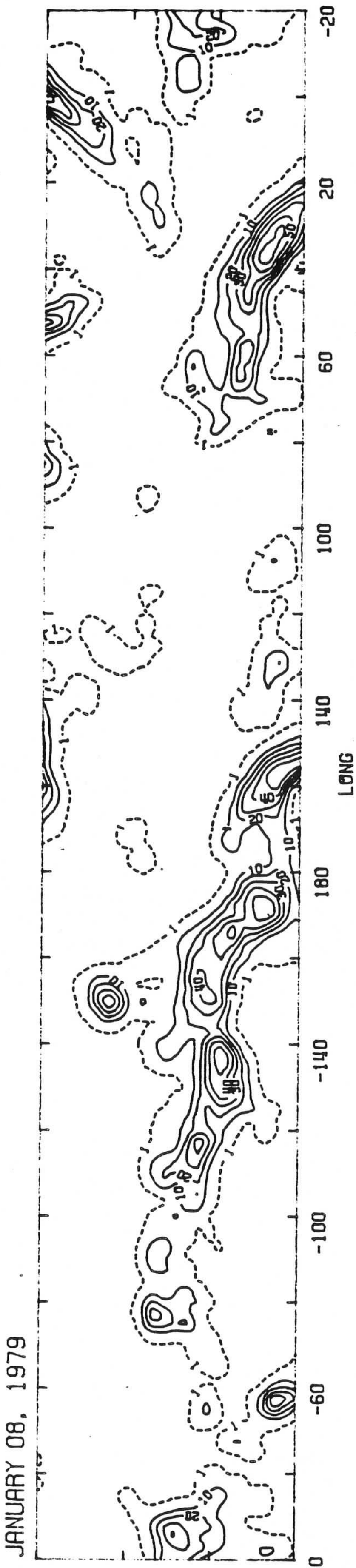
JANUARY 08, 1979

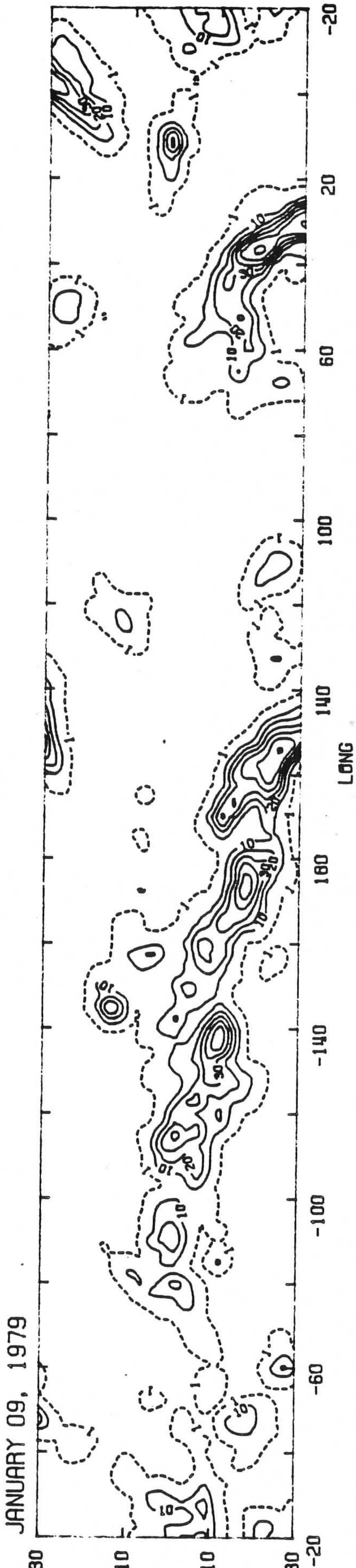
JANUARY 09, 1979

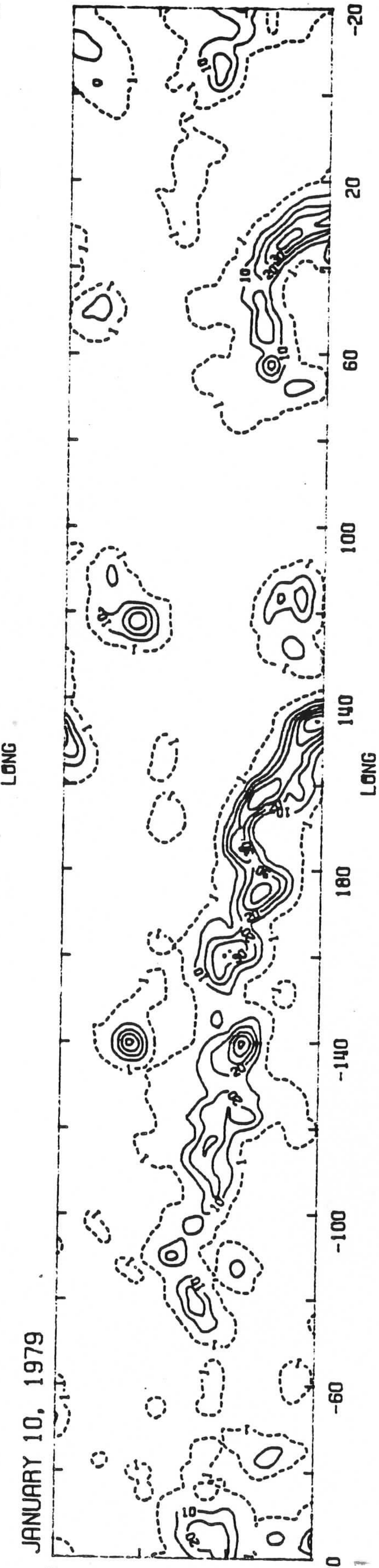
JANUARY 10, 1979

JANUARY 11, 1979

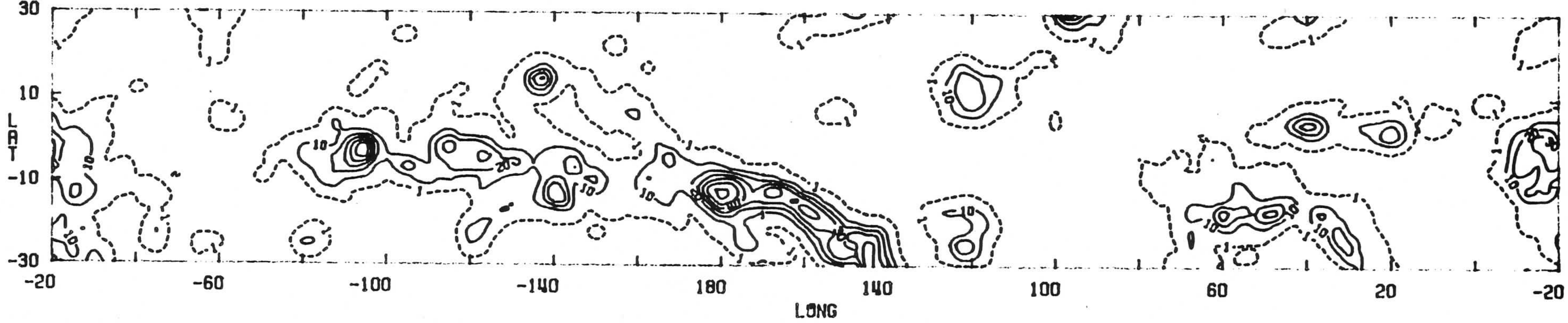

JANUARY 12, 1979

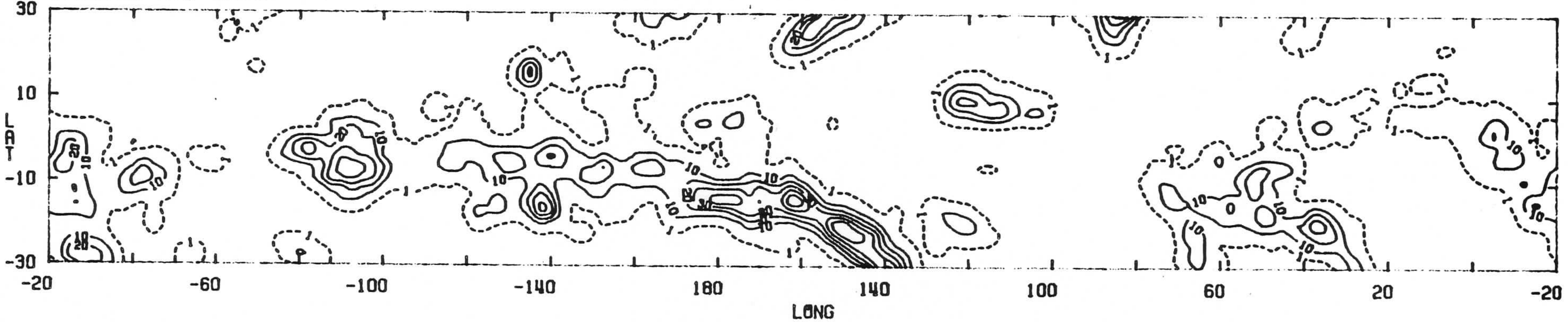

JANUARY 13, 1979

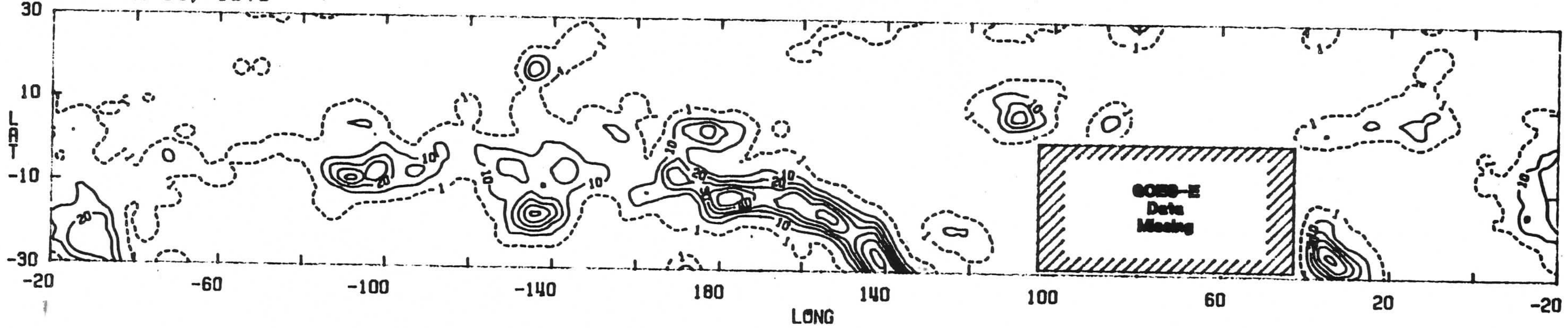

JANUARY 14, 1979

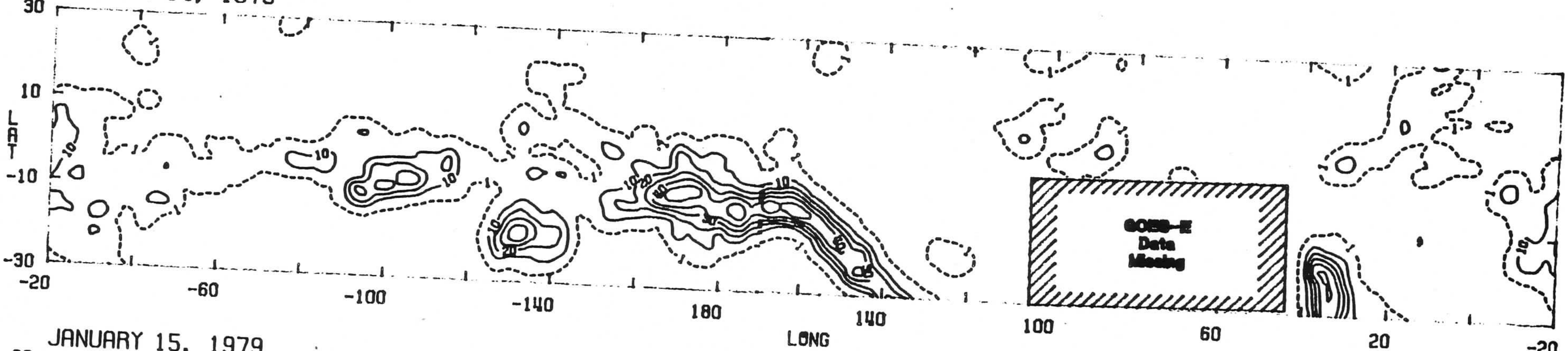

JANUARY 15, 1979

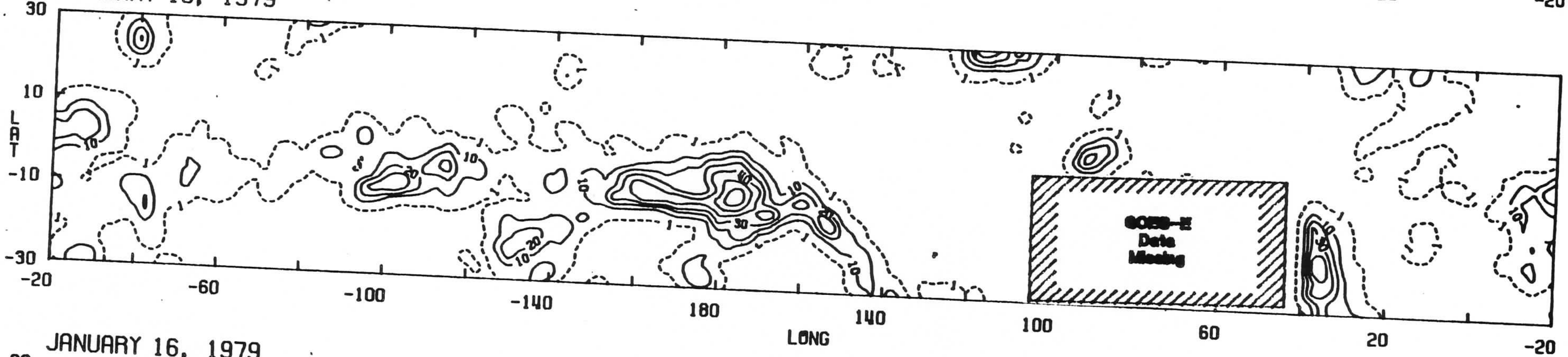

JANUARY 16, 1979

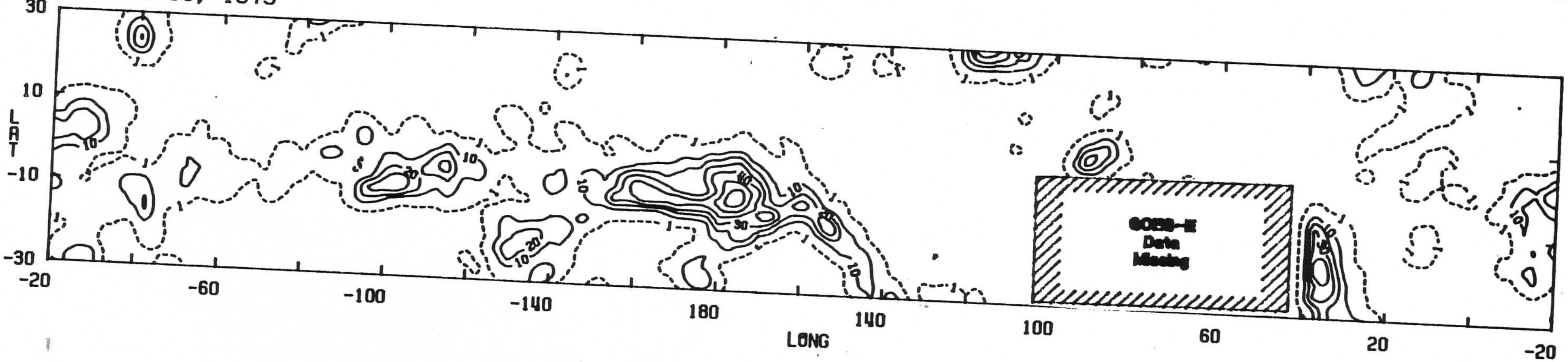

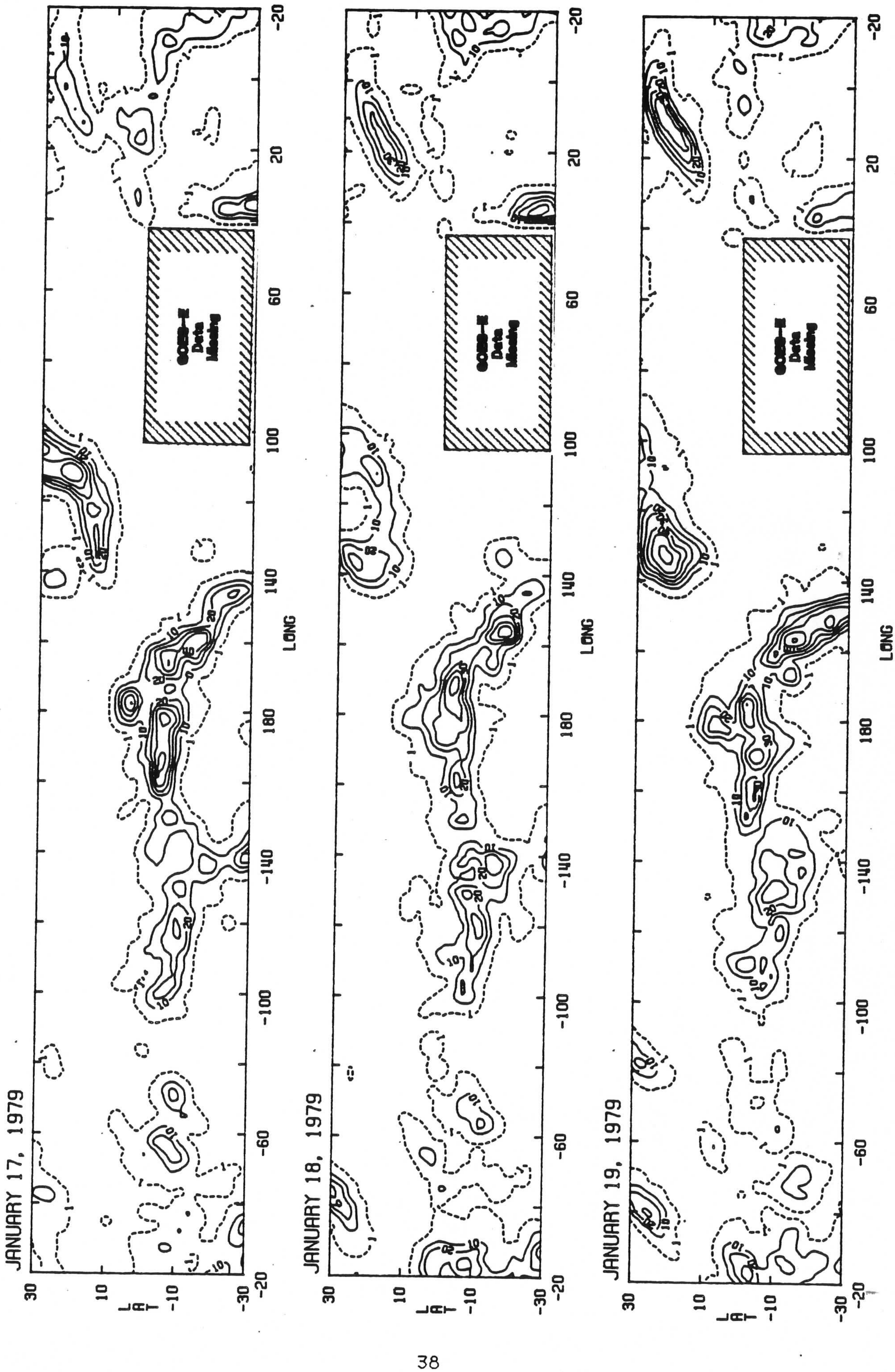
JANUARY 17, 1979
JANUARY 18, 1979
JANUARY 19, 1979
LAT
30
10
-10
-30
LONG
-20
-60
-100
-140
180
140
100
60
20
-20
GOES-I Data Missing
10
20

JANUARY 20, 1979

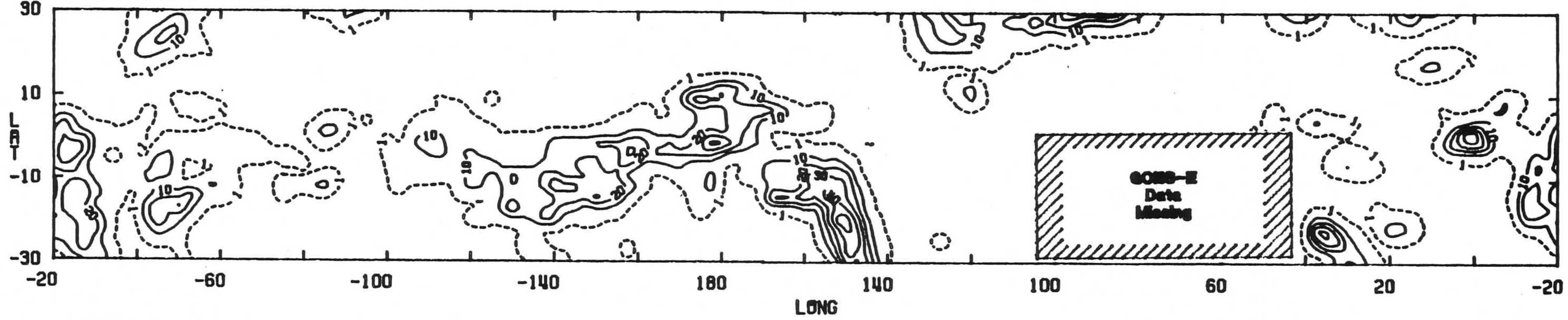

JANUARY 21, 1979

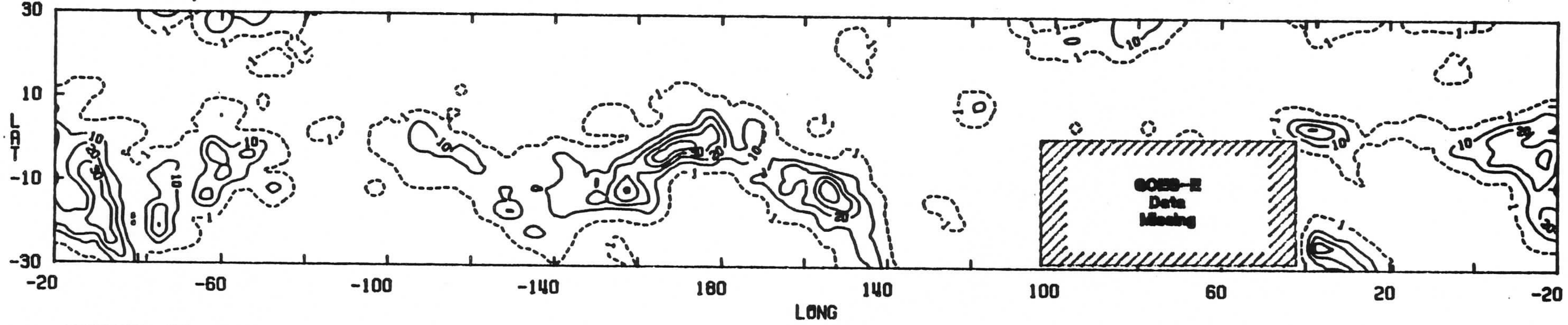

JANUARY 22, 1979

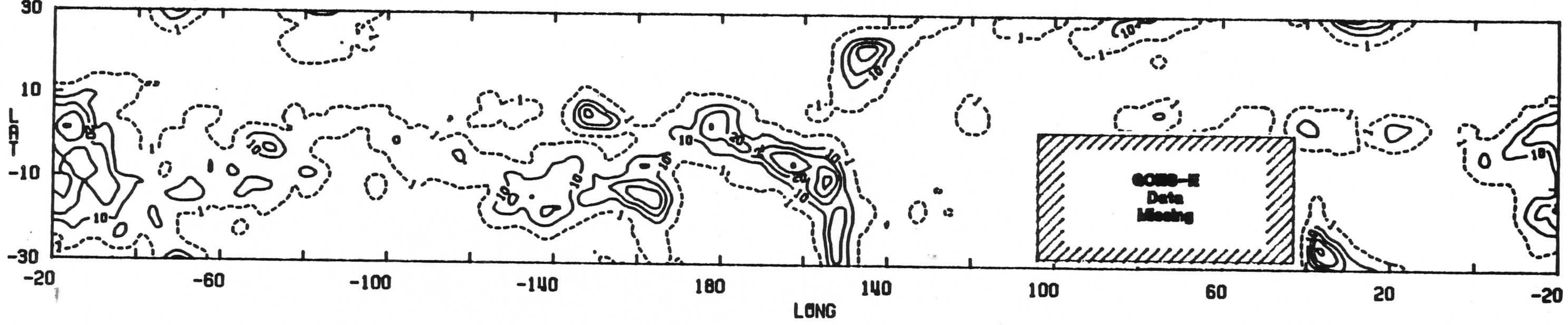

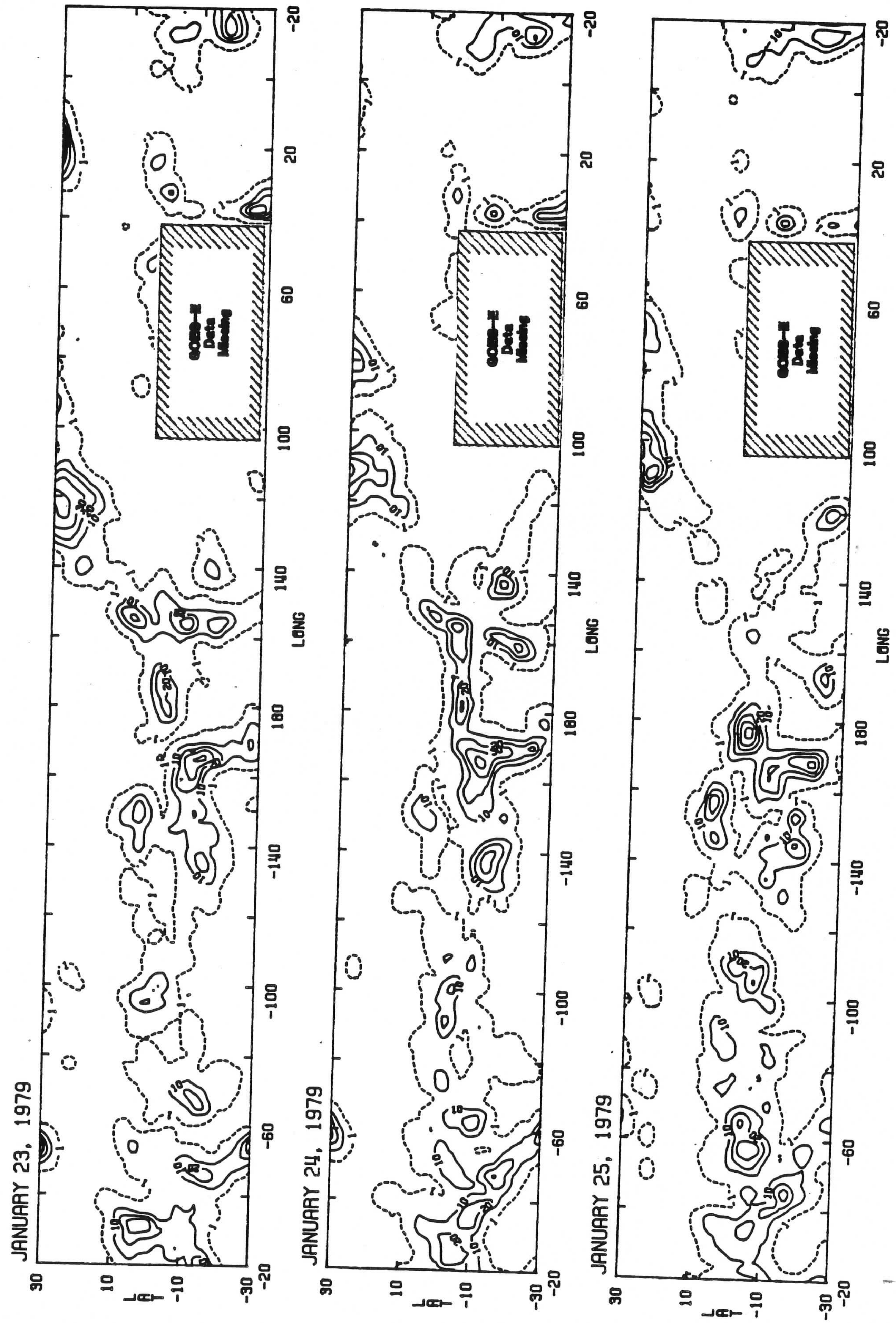
JANUARY 23, 1979
JANUARY 24, 1979
JANUARY 25, 1979
GOES-I Data Missing
LAT
LONG
30
10
-10
-30
-20
20
60
100
140
180
-140
-100
-60
-20
10
20

JANUARY 26, 1979

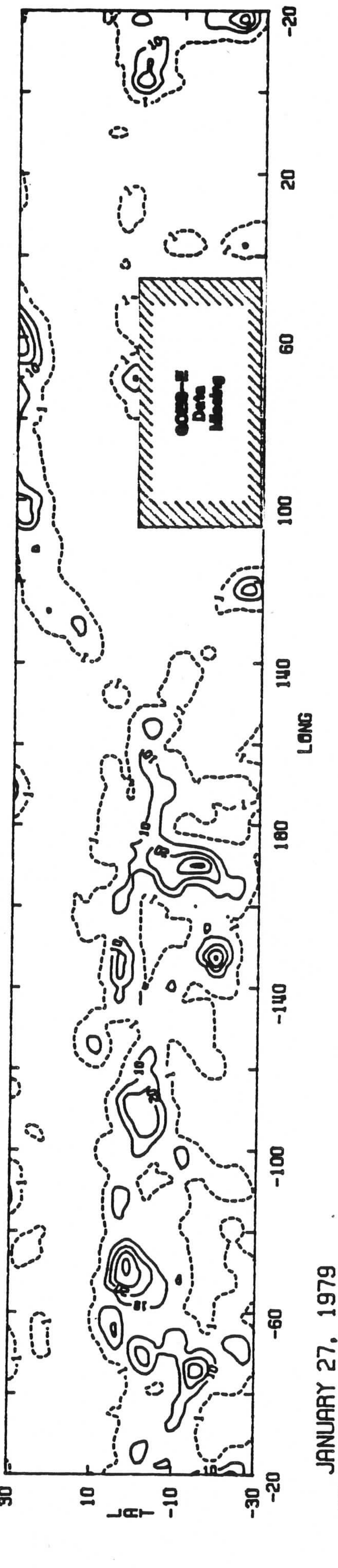

JANUARY 27, 1979

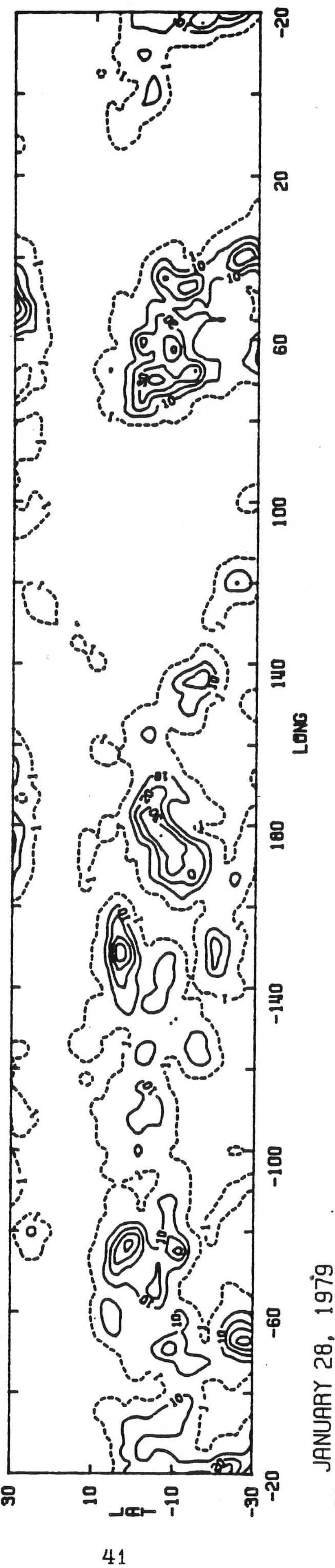

JANUARY 28, 1979

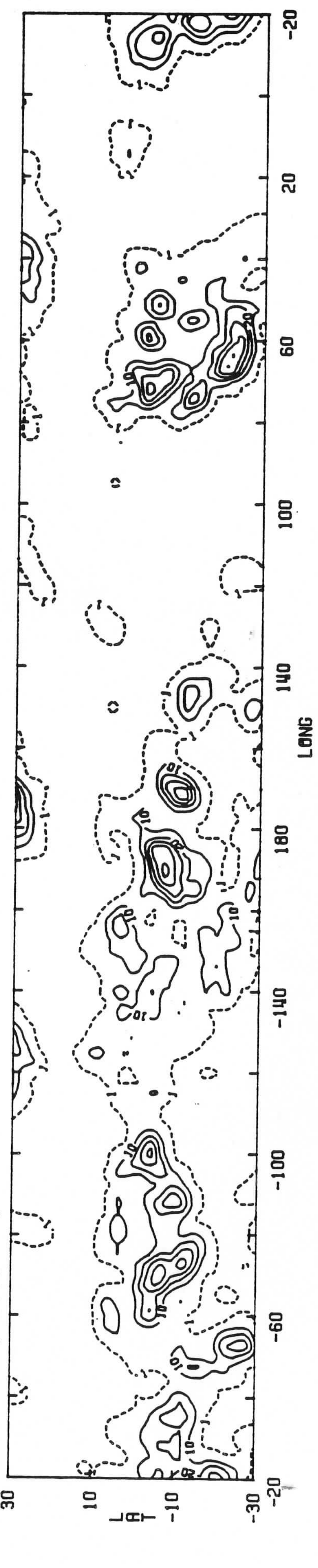

JANUARY 29, 1979

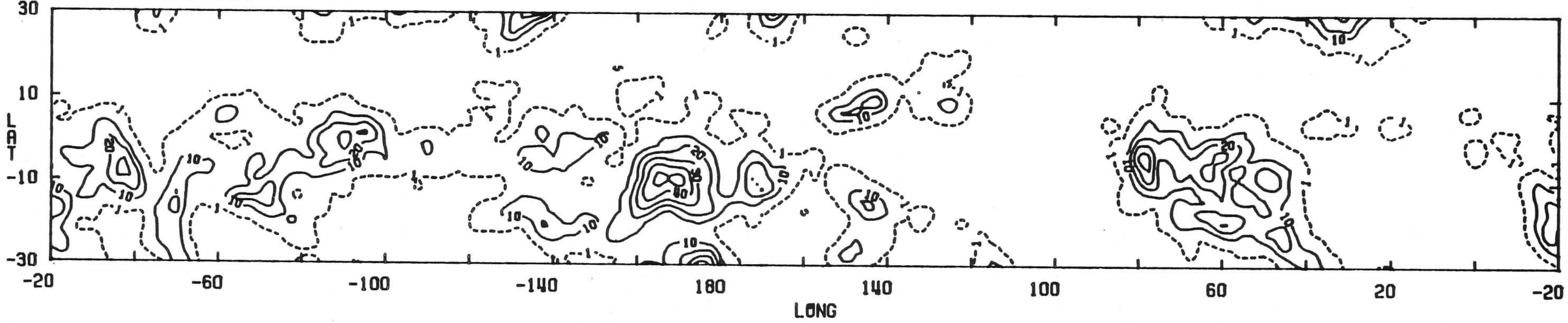

JANUARY 30, 1979

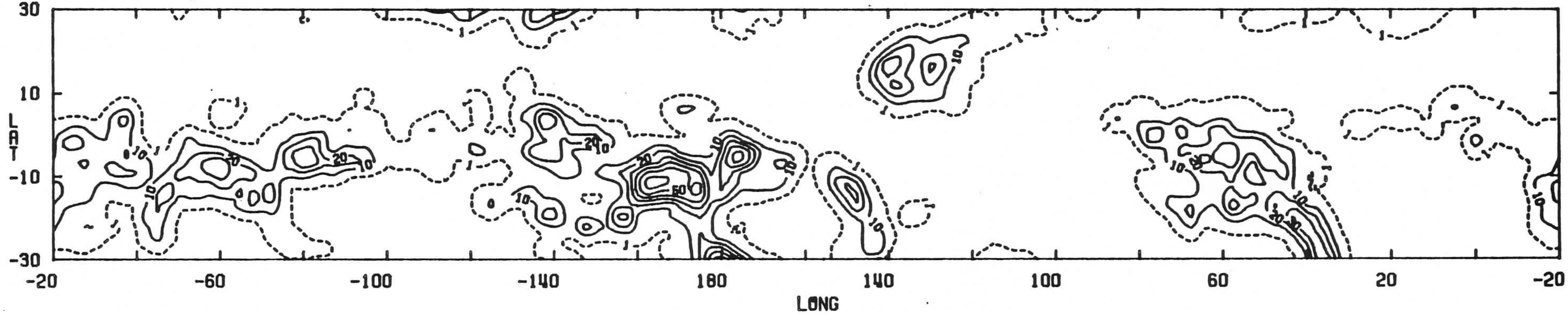

JANUARY 31, 1979

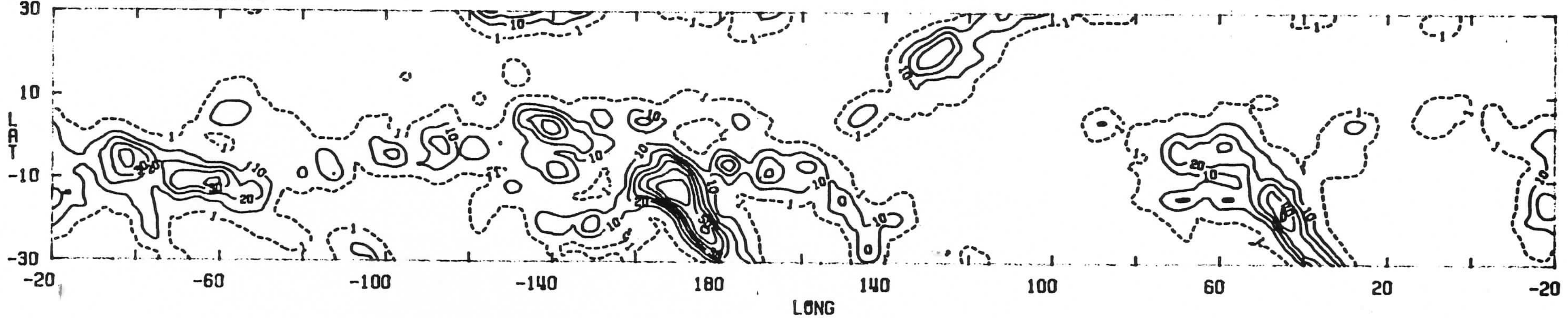

FEBRUARY 01, 1979

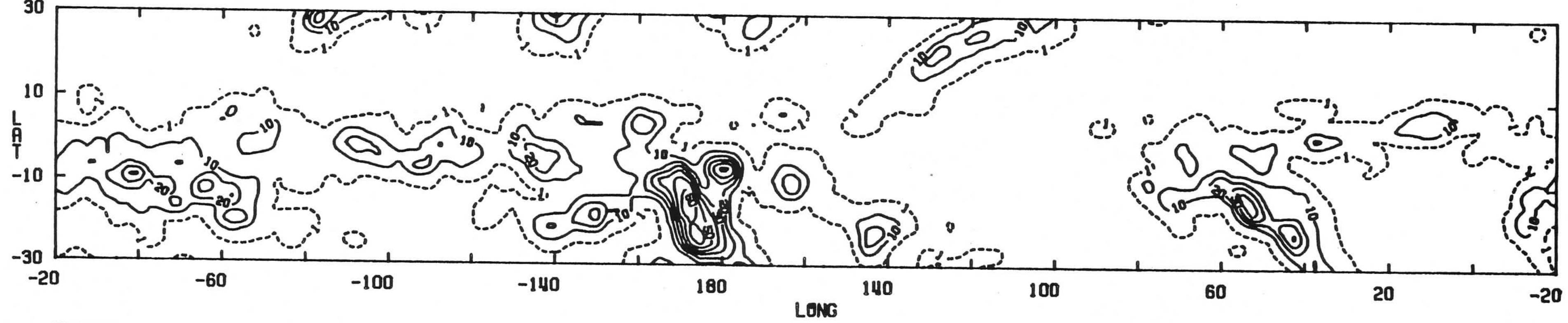

FEBRUARY 02, 1979

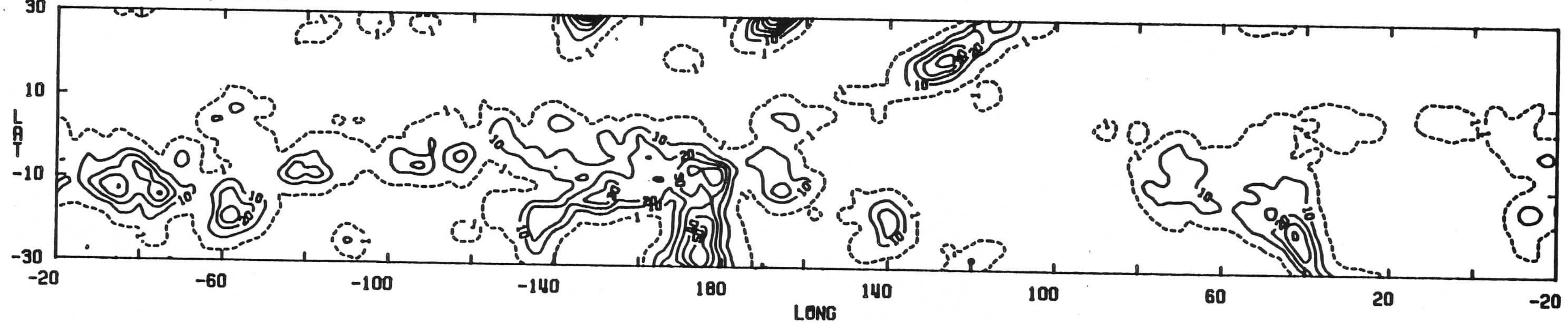

FEBRUARY 03, 1979

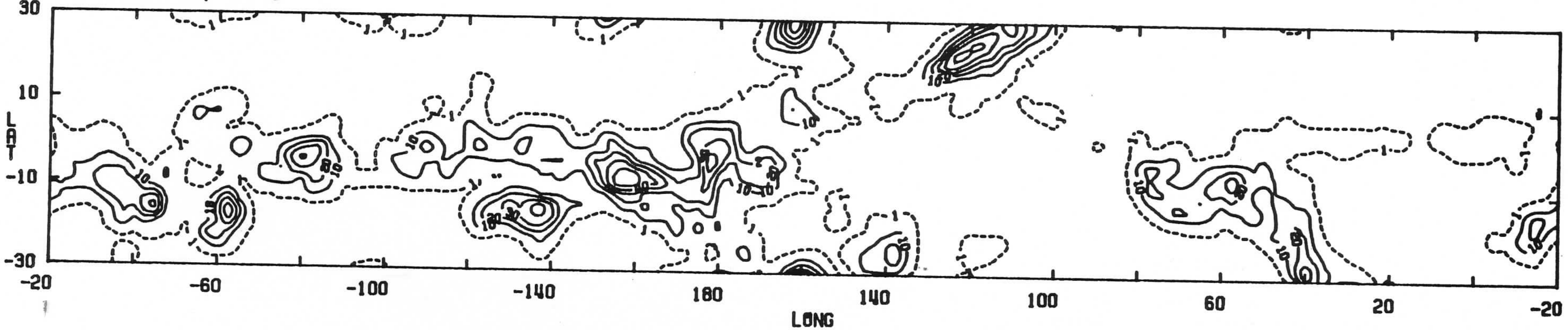

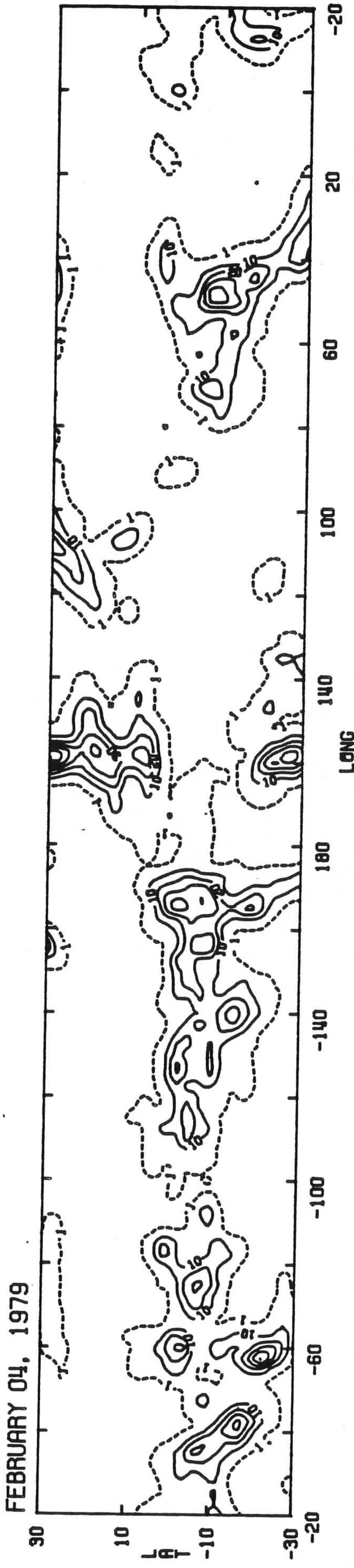
FEBRUARY 04, 1979

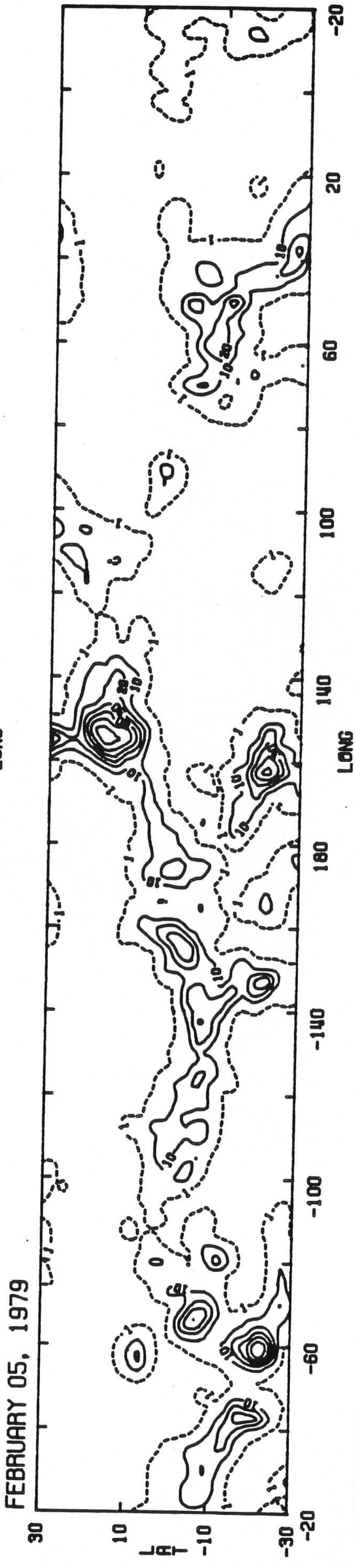
FEBRUARY 05, 1979

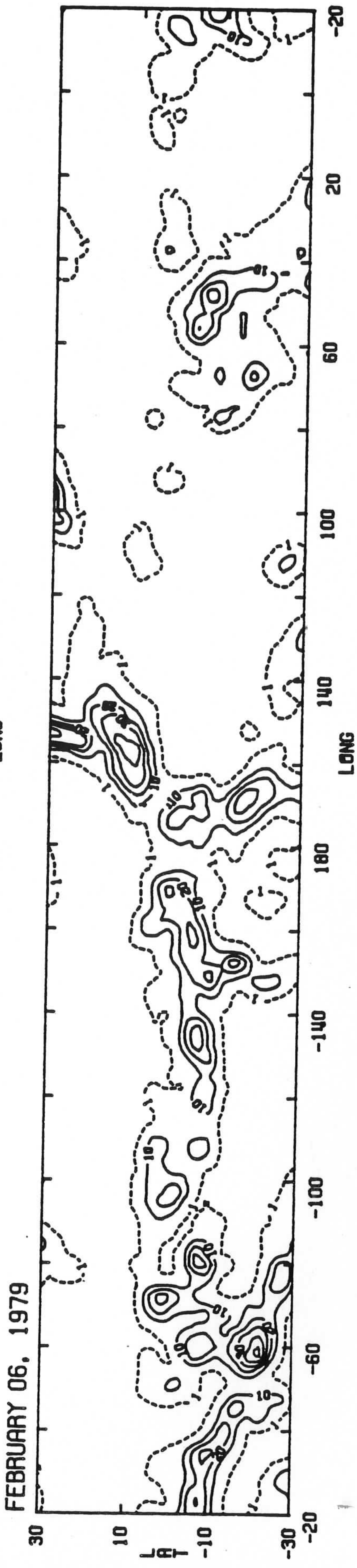
FEBRUARY 06, 1979

FEBRUARY 07, 1979

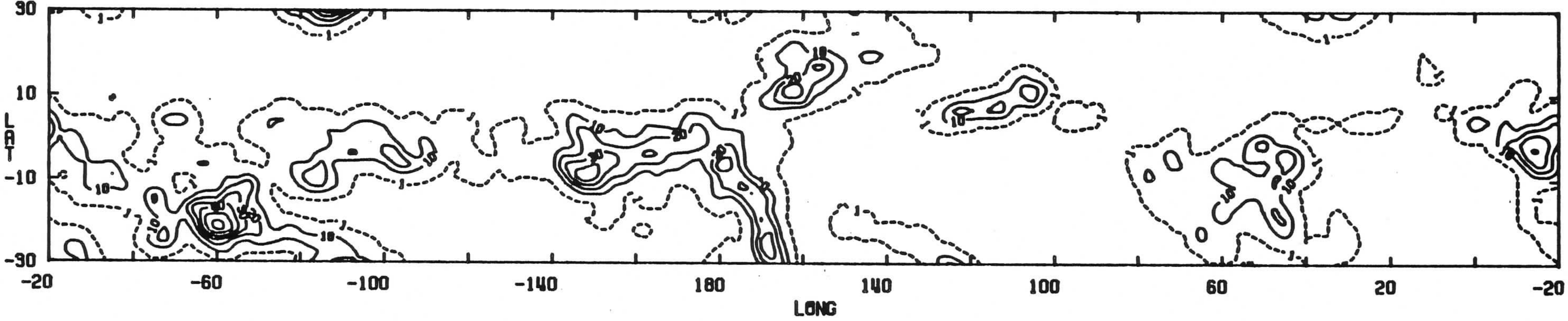

FEBRUARY 08, 1979

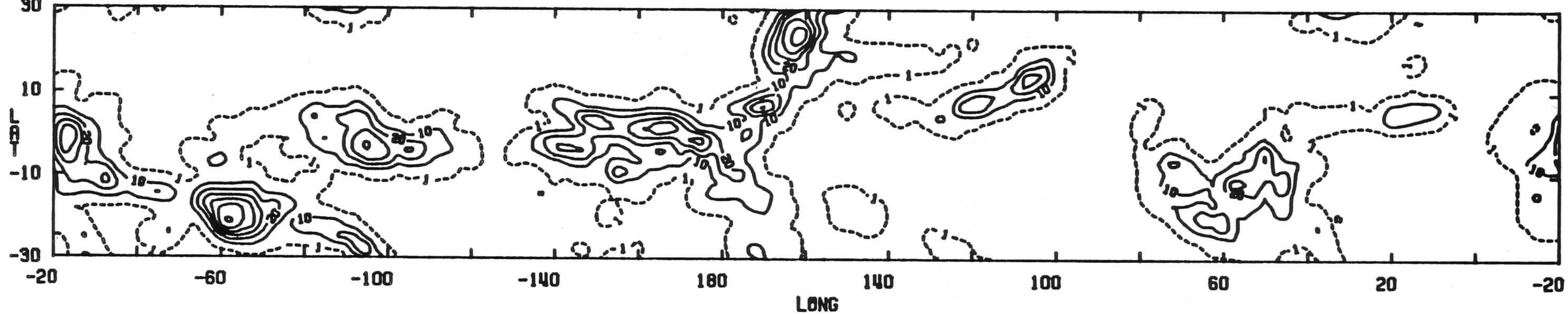

FEBRUARY 09, 1979

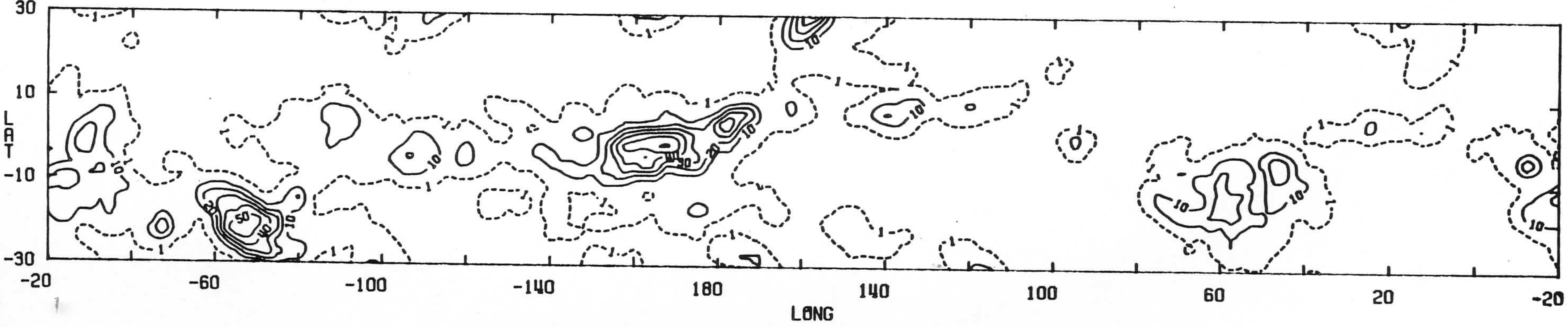

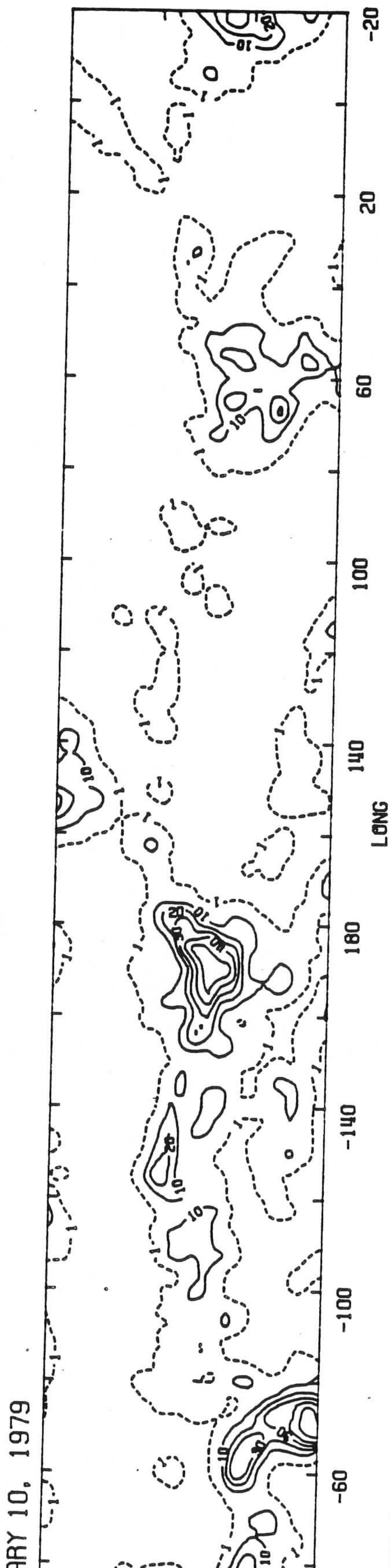
FEBRUARY 10, 1979

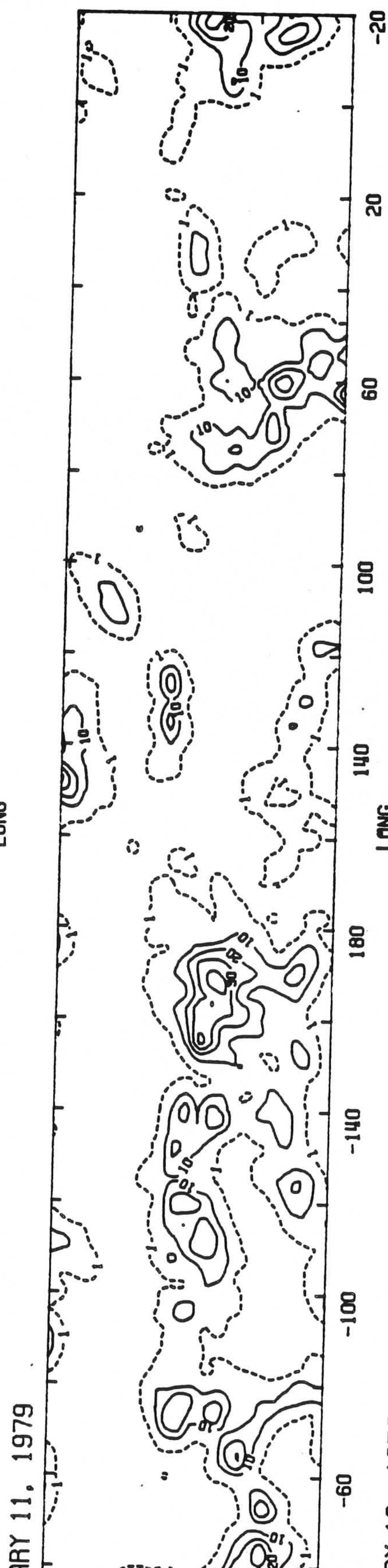
FEBRUARY 11, 1979

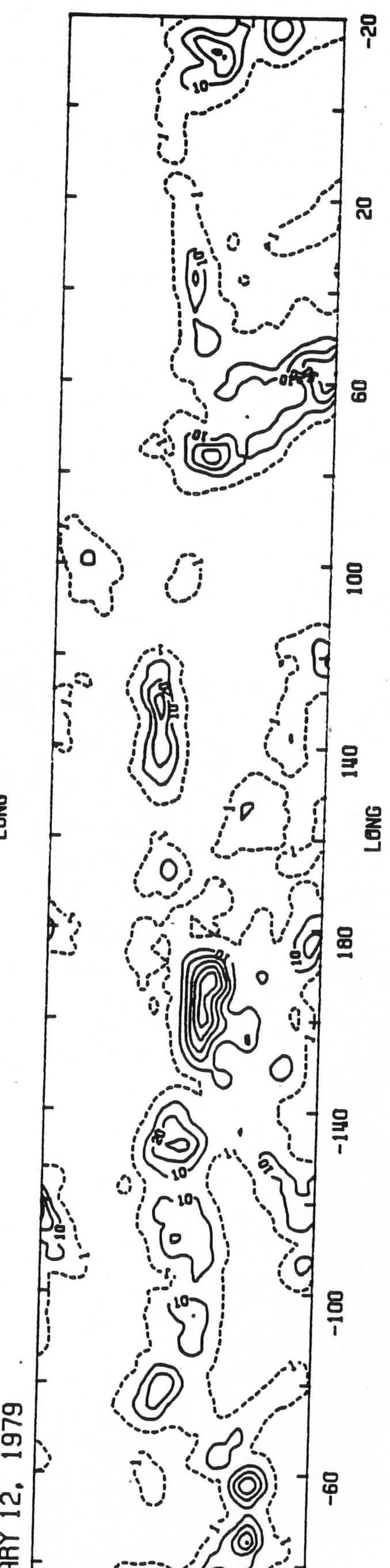
FEBRUARY 12, 1979

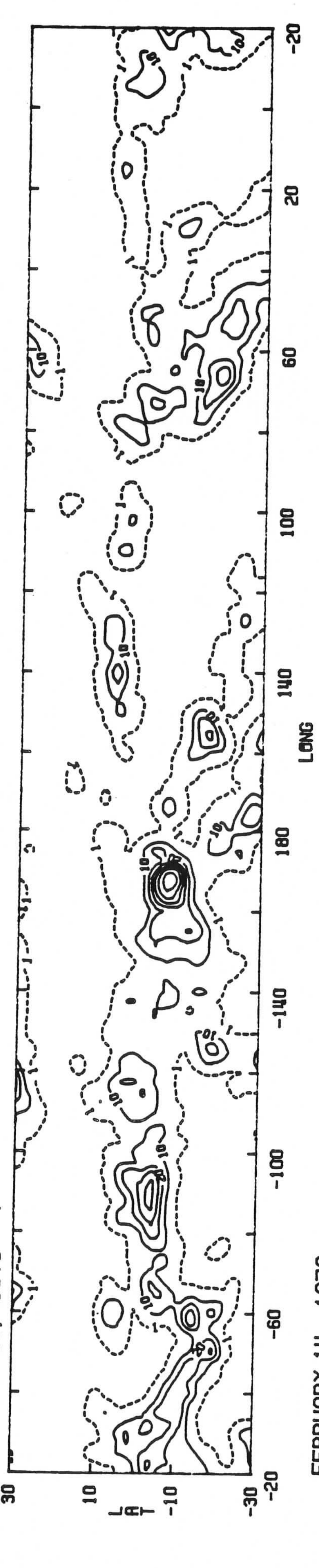
FEBRUARY 13, 1979

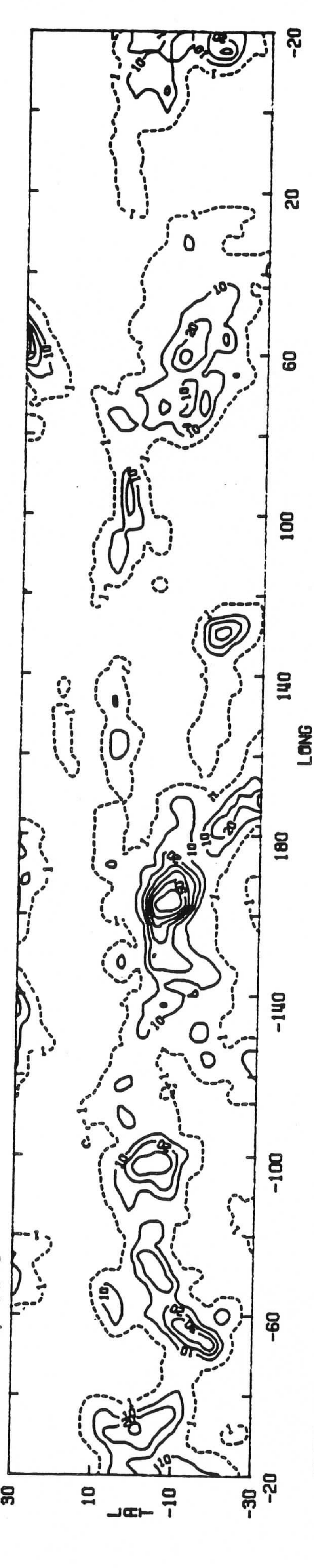
FEBRUARY 14, 1979

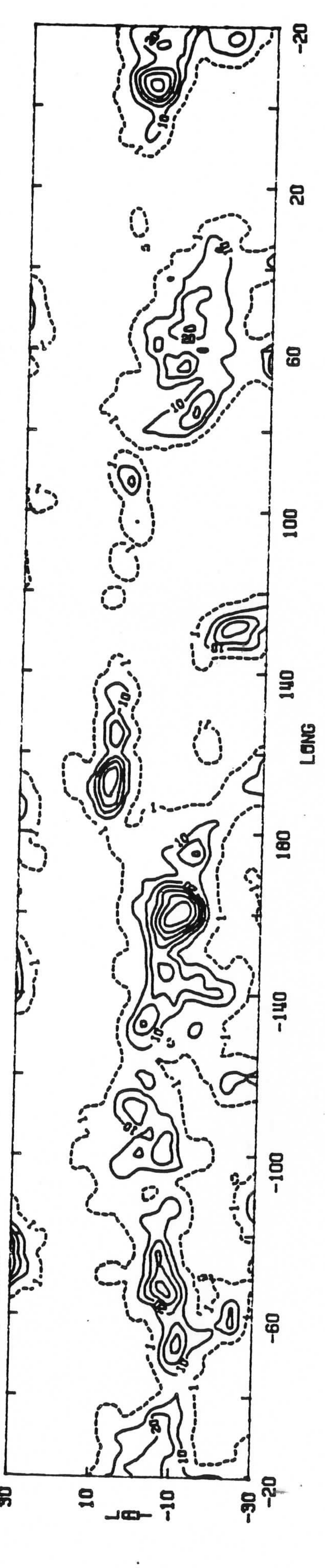
FEBRUARY 15, 1979

FEBRUARY 16, 1979

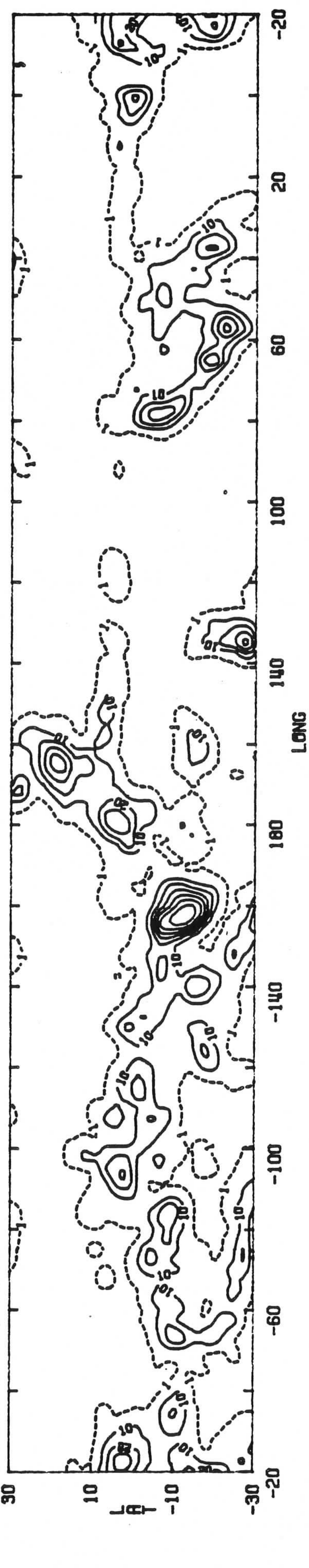

FEBRUARY 17, 1979

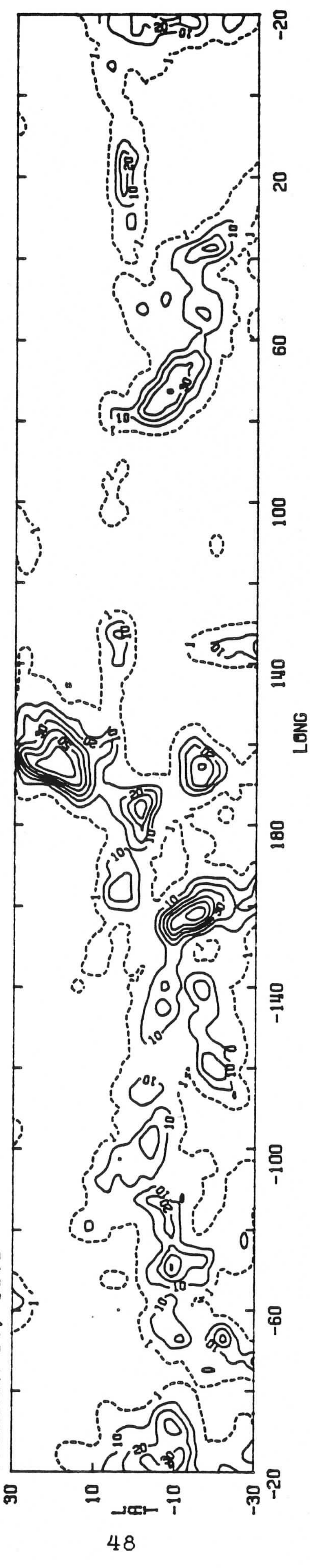

FEBRUARY 18, 1979

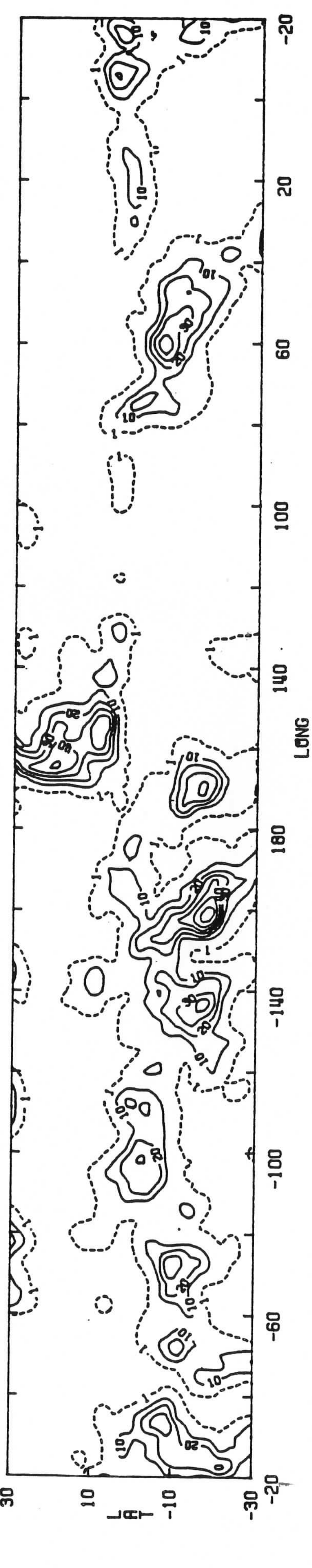

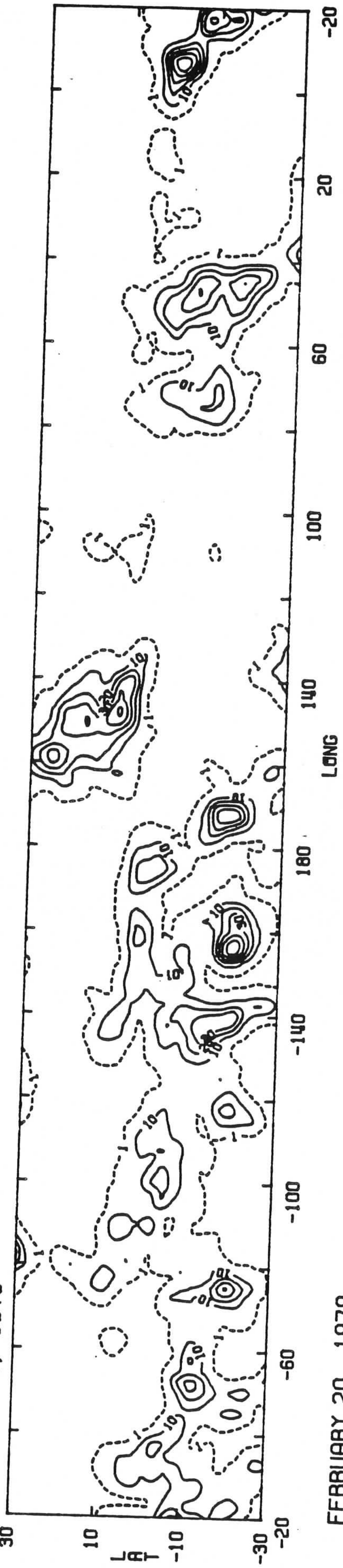

FEBRUARY 19, 1979

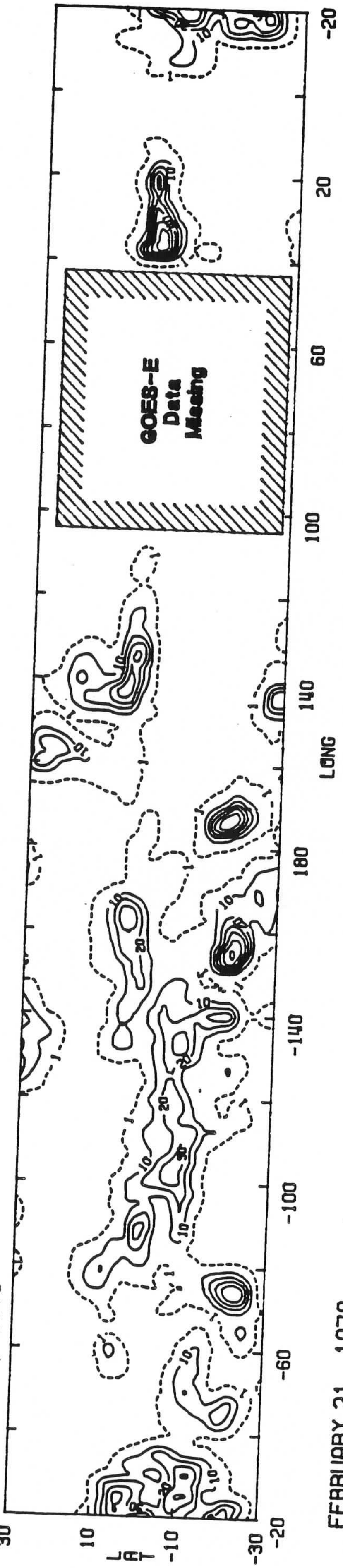

FEBRUARY 20, 1979

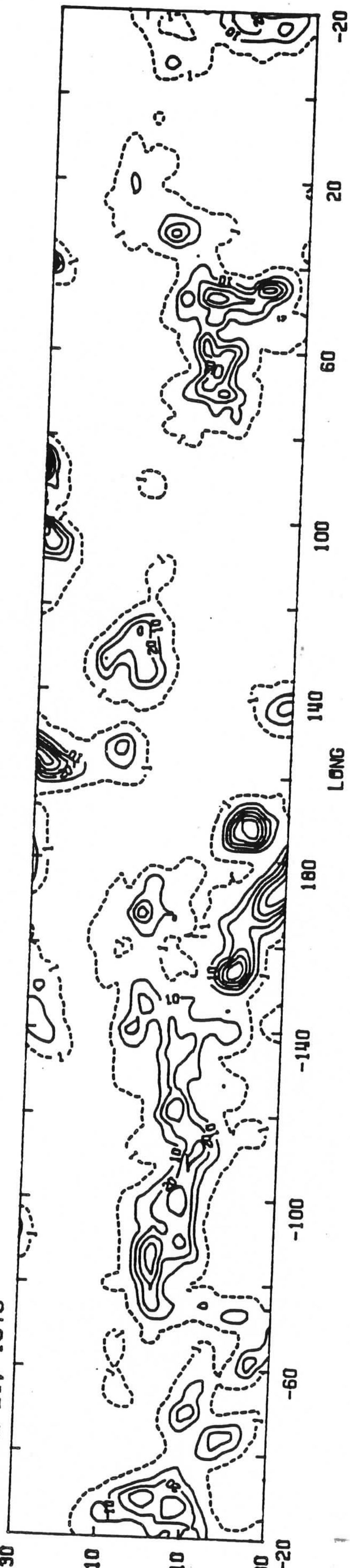

FEBRUARY 21, 1979

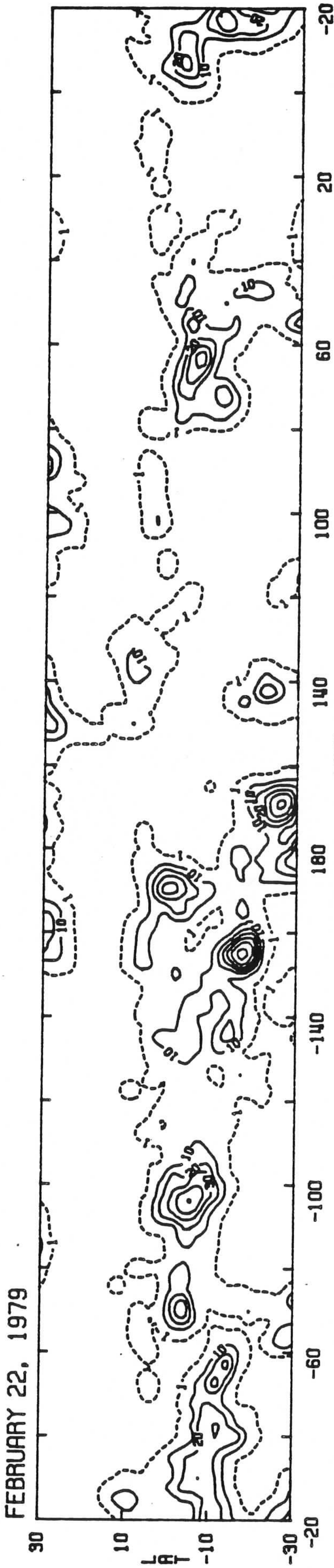

FEBRUARY 22, 1979

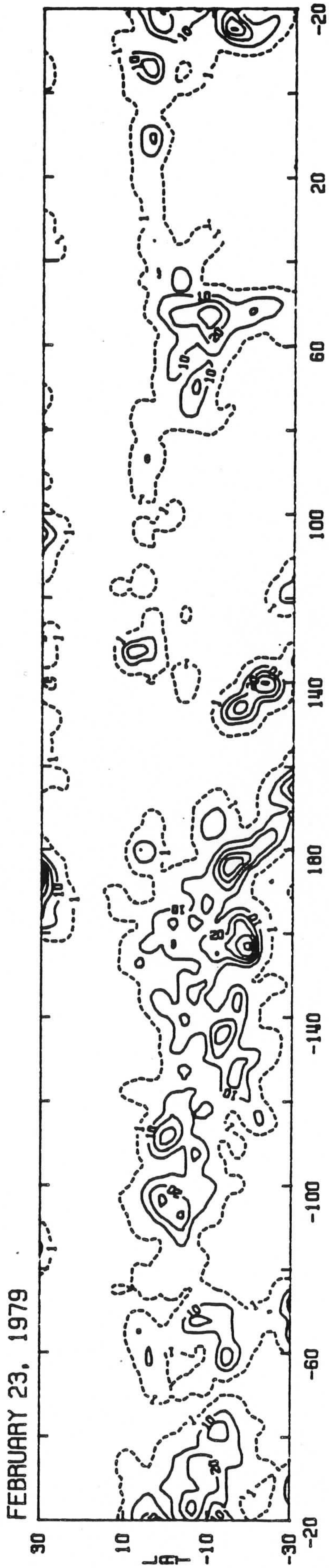

FEBRUARY 23, 1979

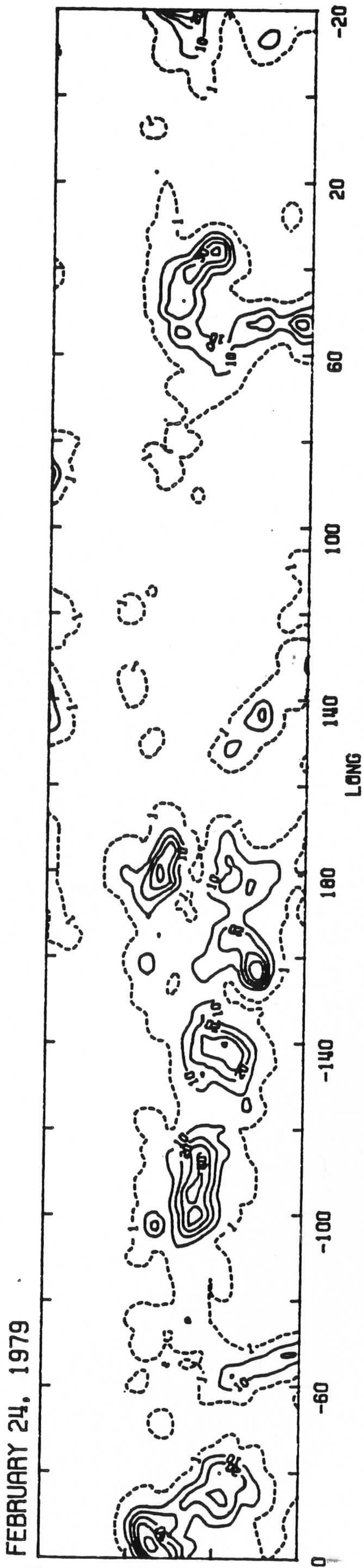

FEBRUARY 24, 1979

FEBRUARY 25, 1979

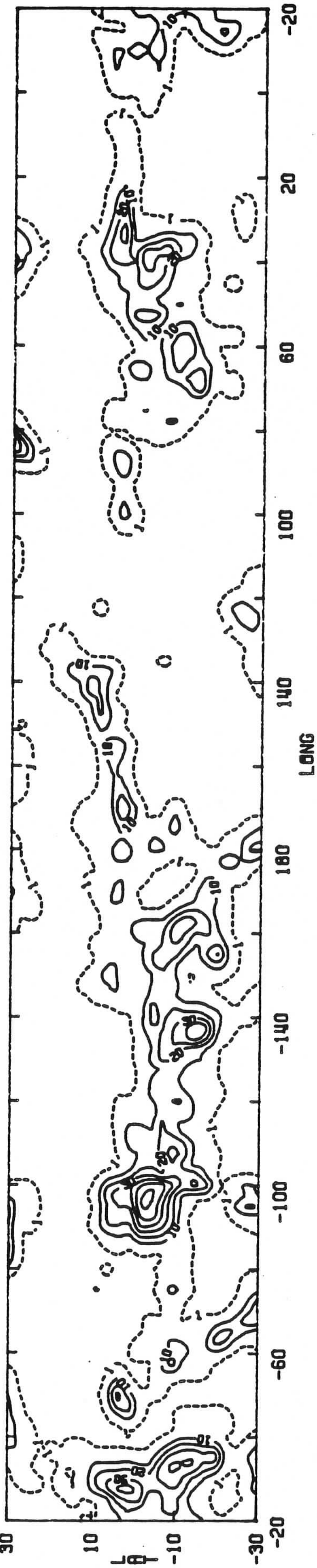

FEBRUARY 26, 1979

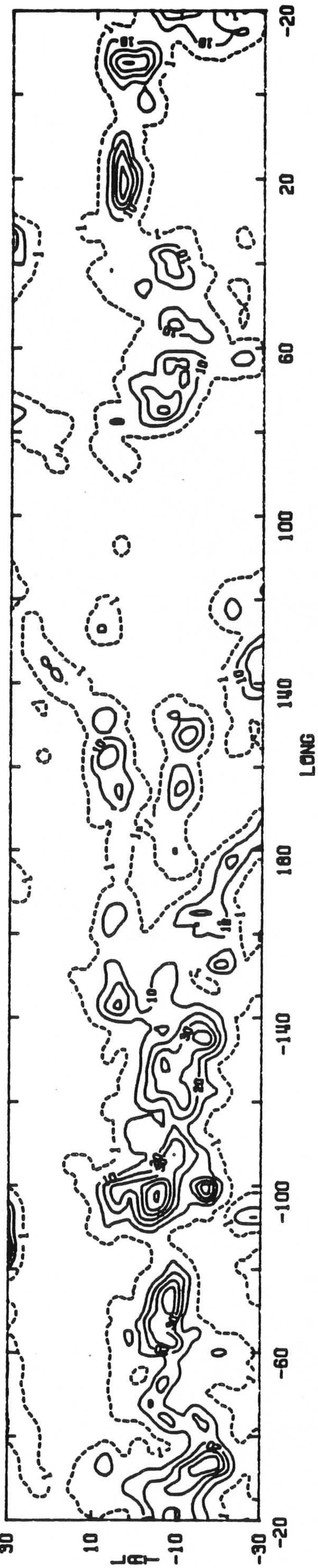

FEBRUARY 27, 1979

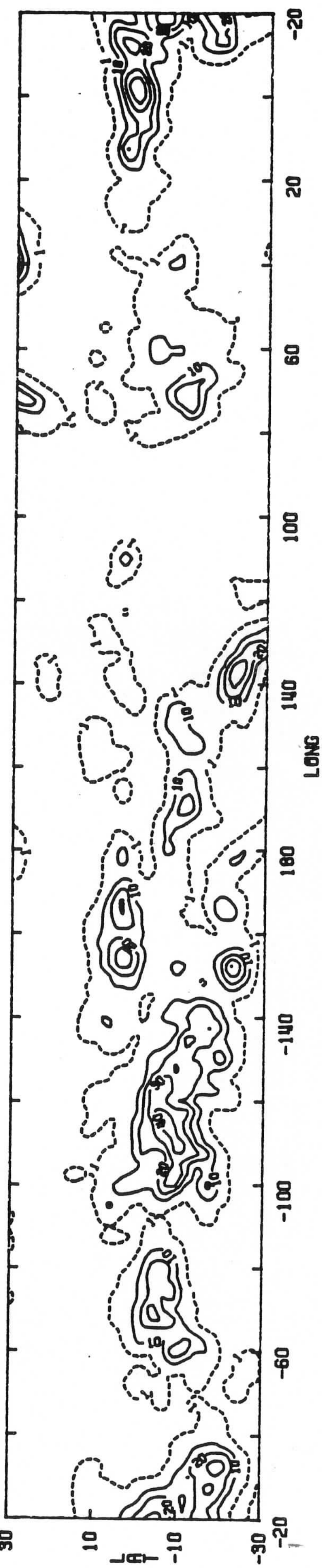

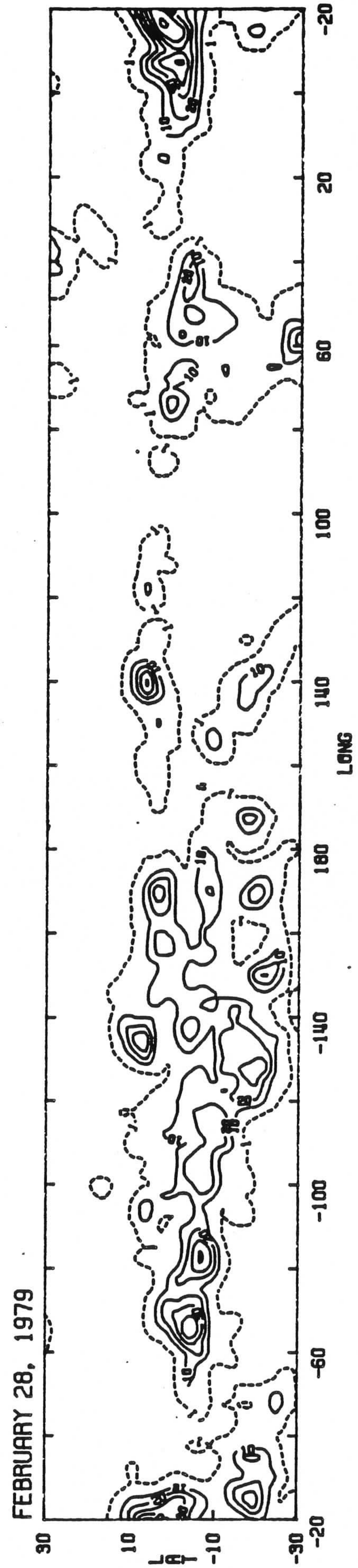
FEBRUARY 28, 1979

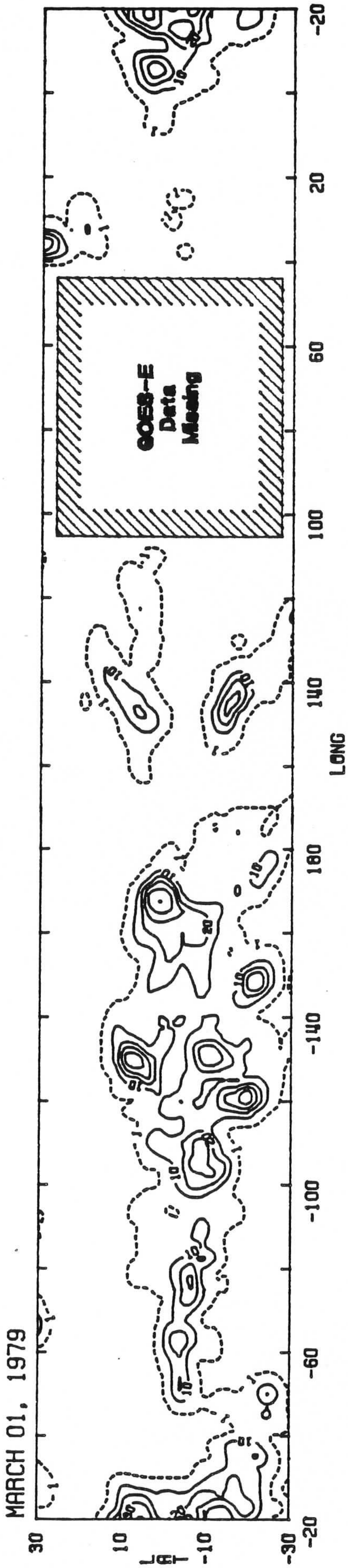
MARCH 01, 1979

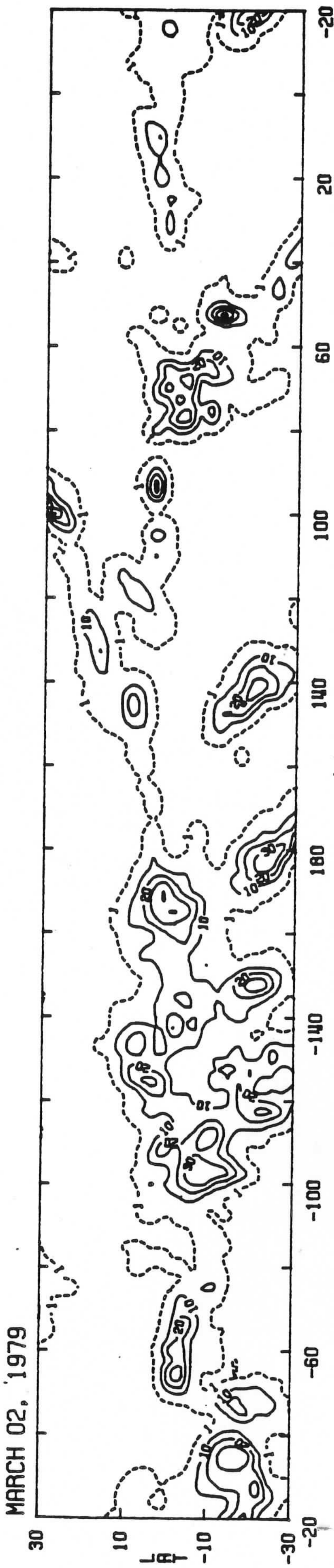
MARCH 02, 1979

MARCH 03, 1979

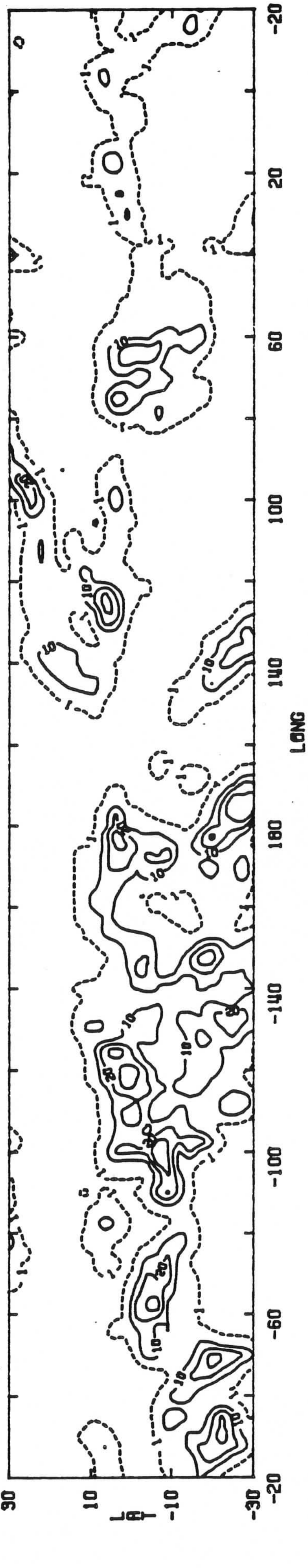

MARCH 04, 1979

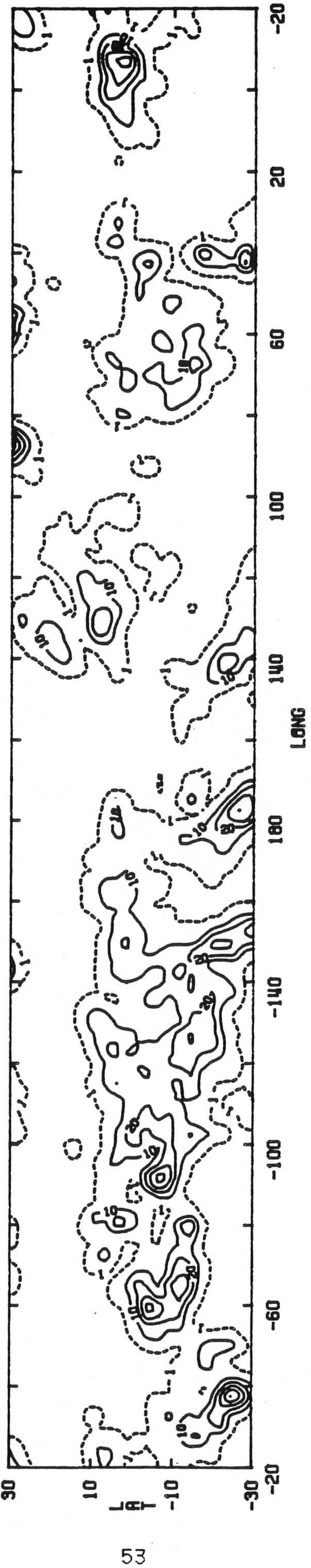

MARCH 05, 1979

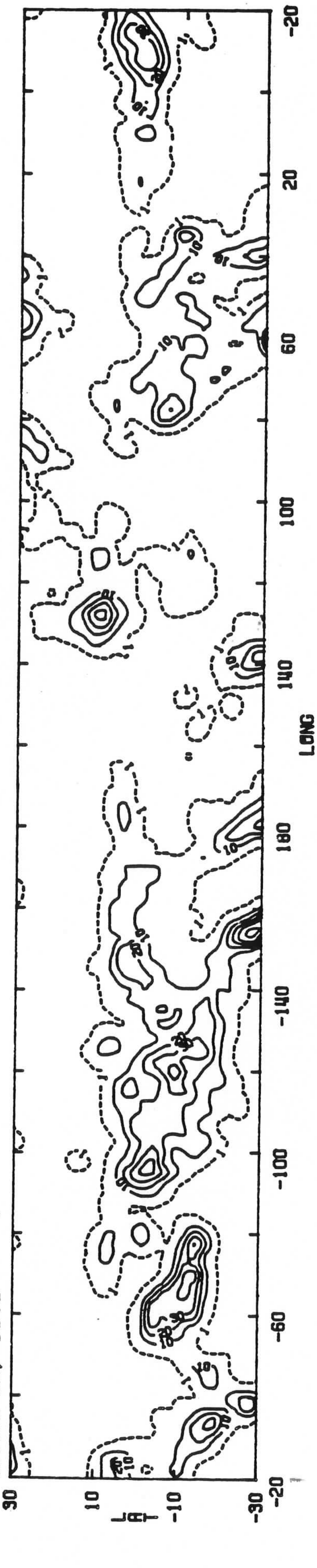

A.3 Rain Charts for Special Observing Period II

Charts for Days 79121-79181 (1 May 79 through 30 Jun 79) begin on the following page.

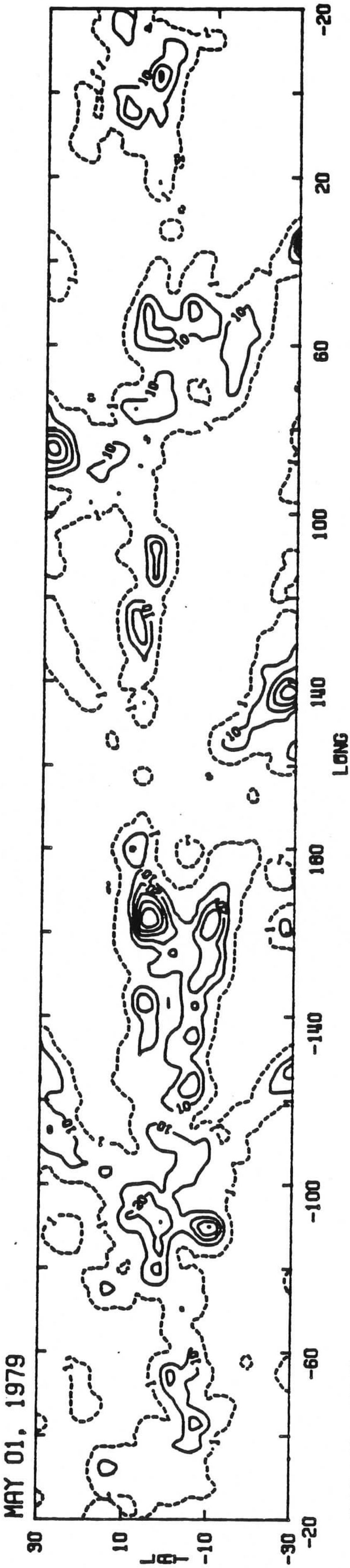
MAY 01, 1979

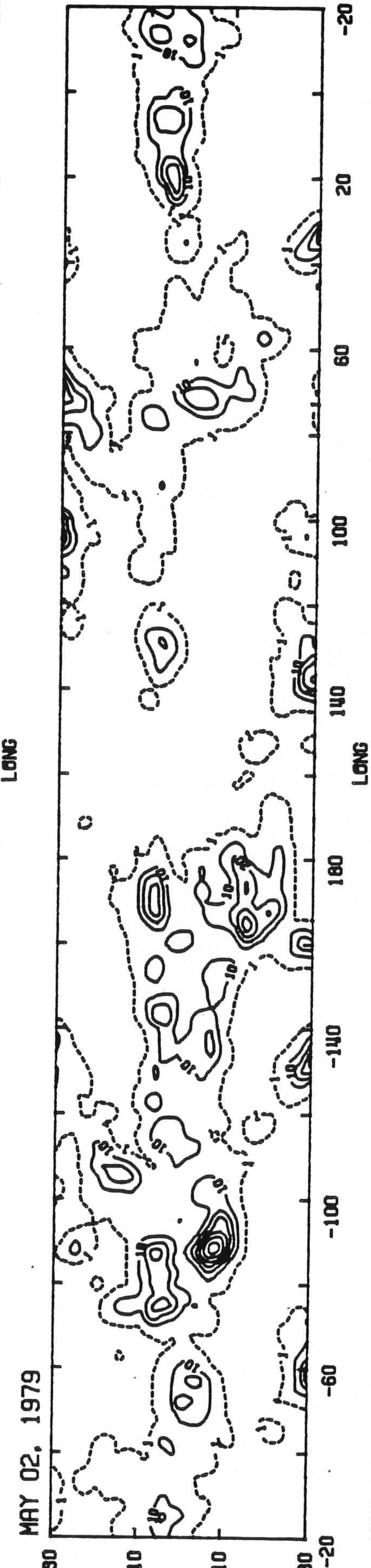
MAY 02, 1979

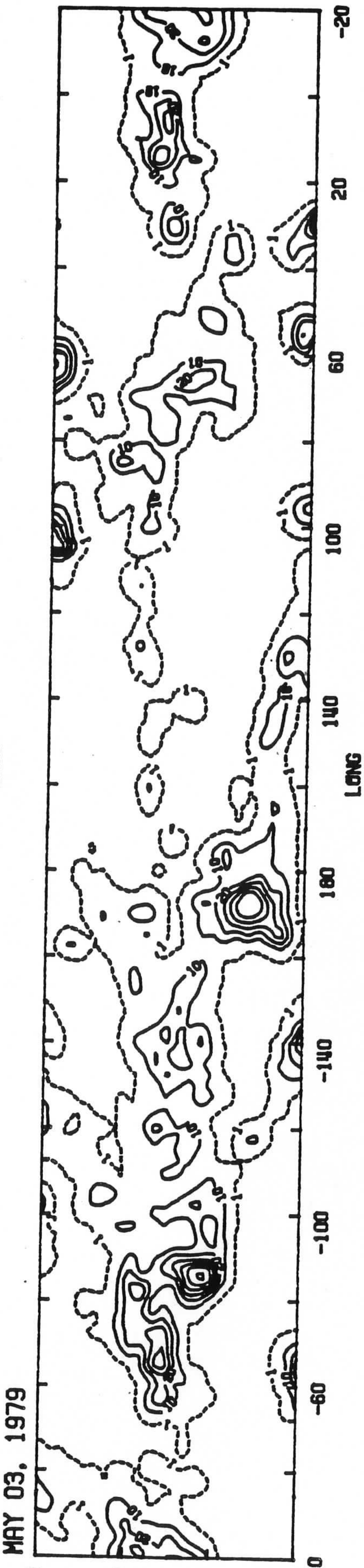
MAY 03, 1979

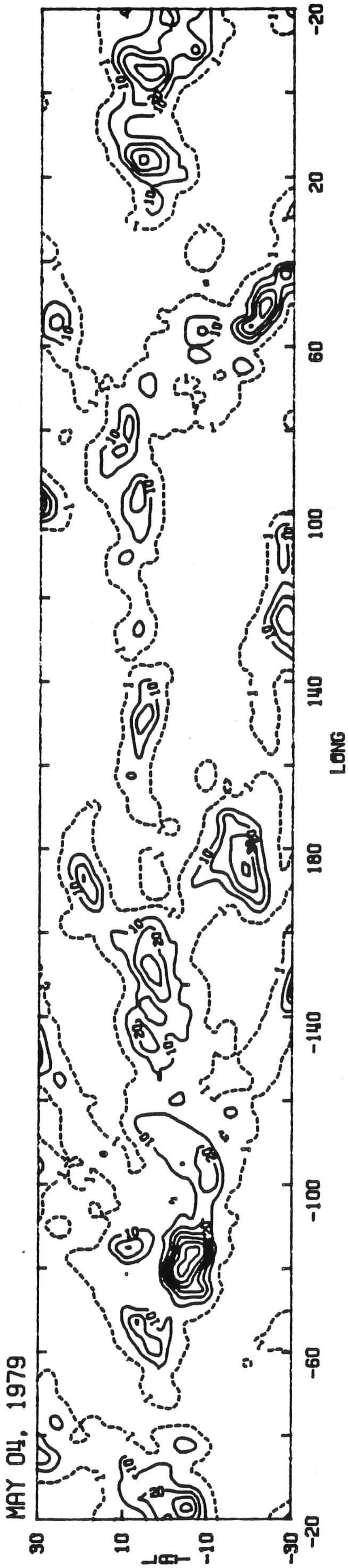
MAY 04, 1979

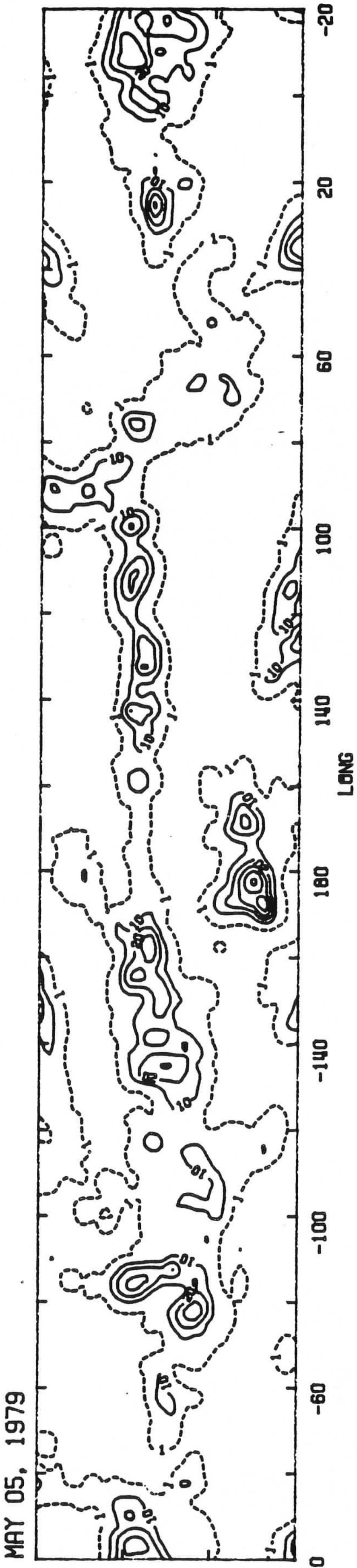
MAY 05, 1979

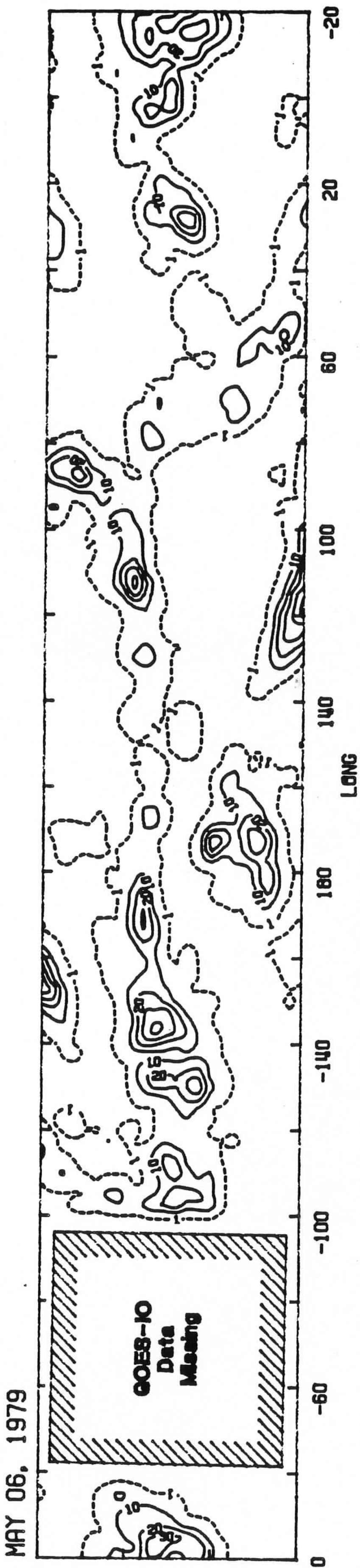
MAY 06, 1979

MAY 07, 1979

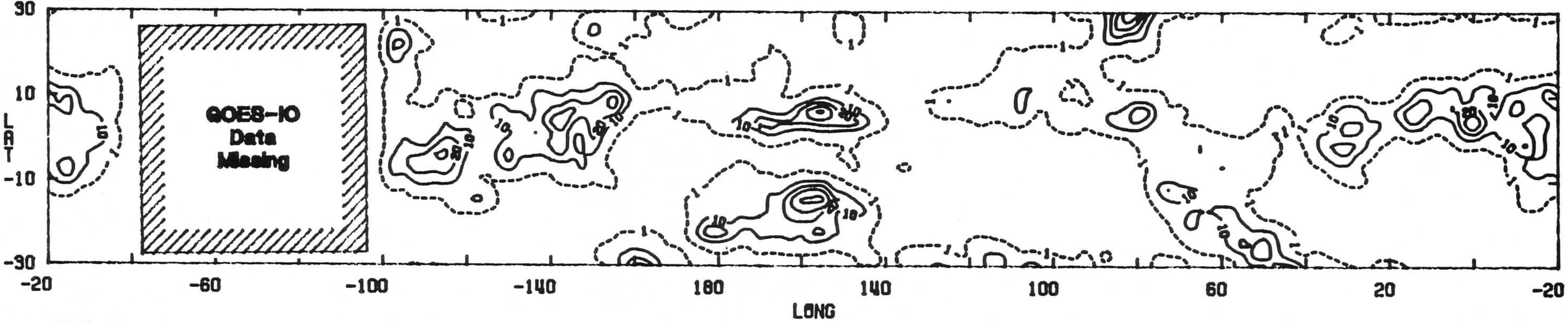

MAY 08, 1979

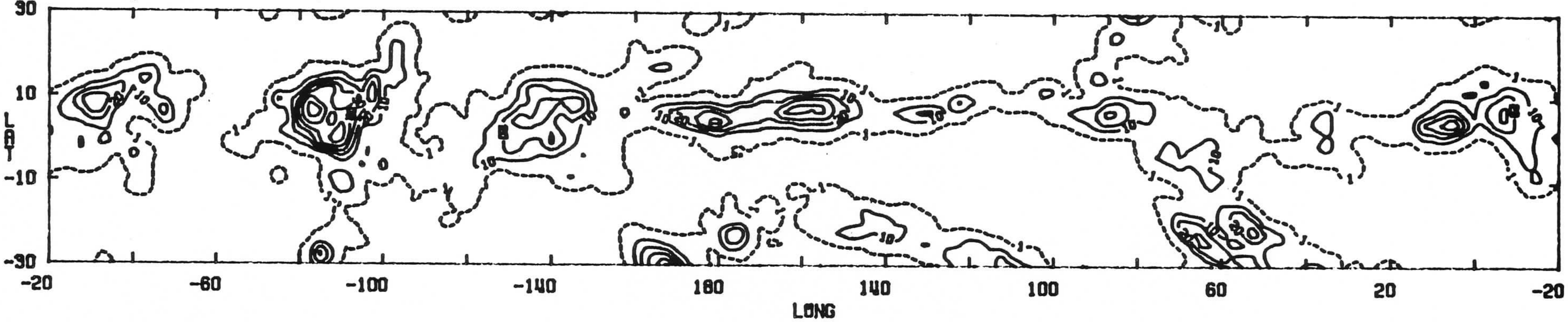

MAY 09, 1979

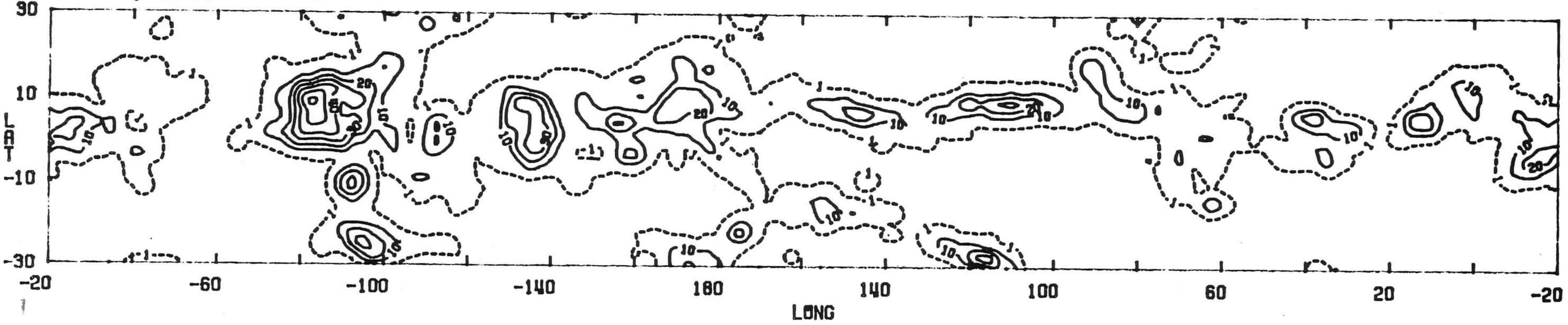

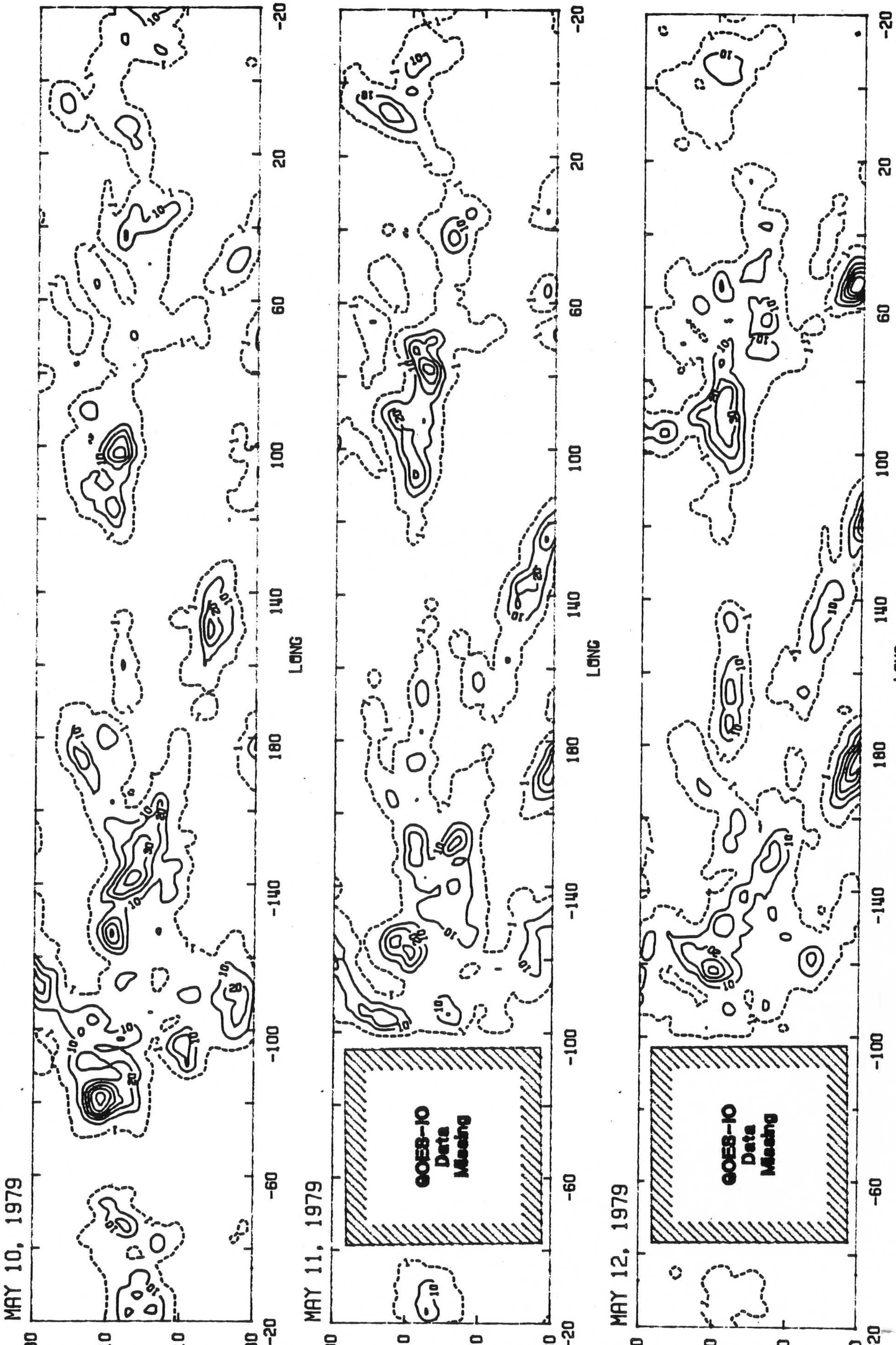
MAY 10, 1979
MAY 11, 1979
MAY 12, 1979
LAT
LONG
30
10
-10
-30
-20
-60
-100
-140
180
140
100
60
20
-20
10
20
30
GOES-IO Data Missing
GOES-IO Data Missing

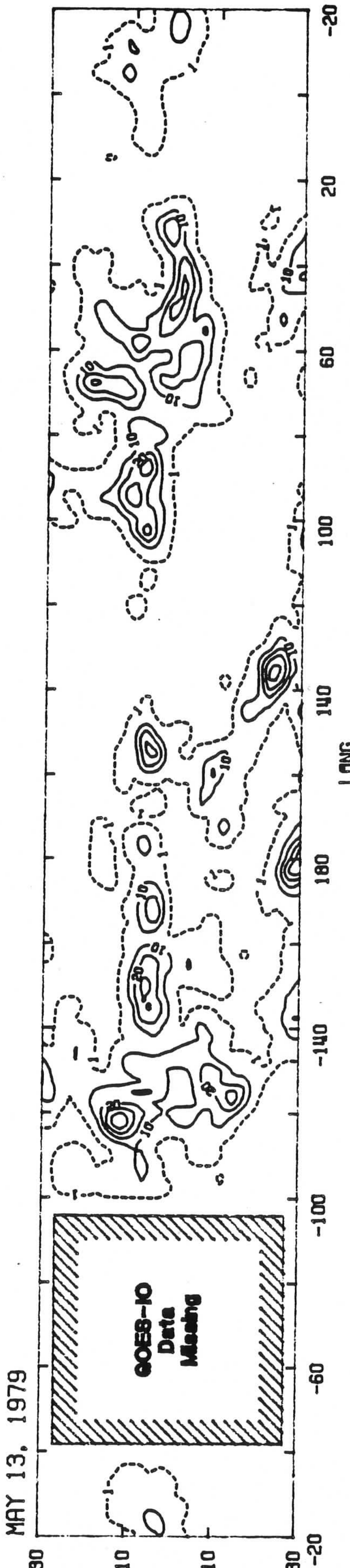
MAY 13, 1979

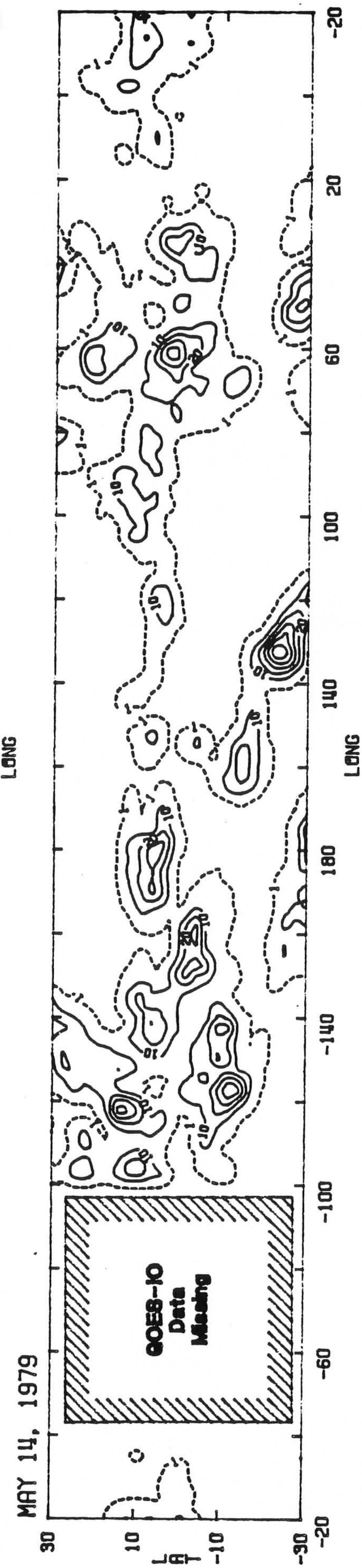
MAY 14, 1979

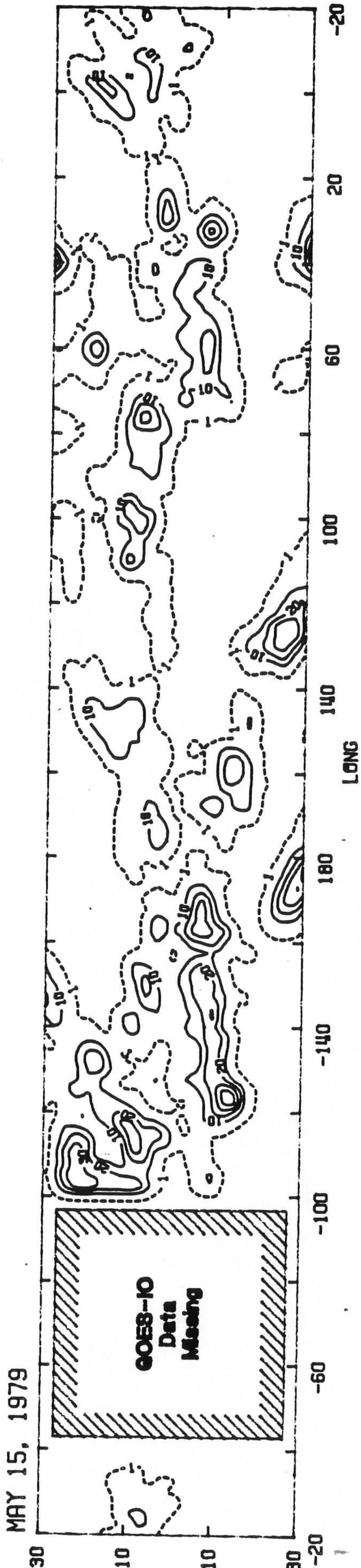
MAY 15, 1979

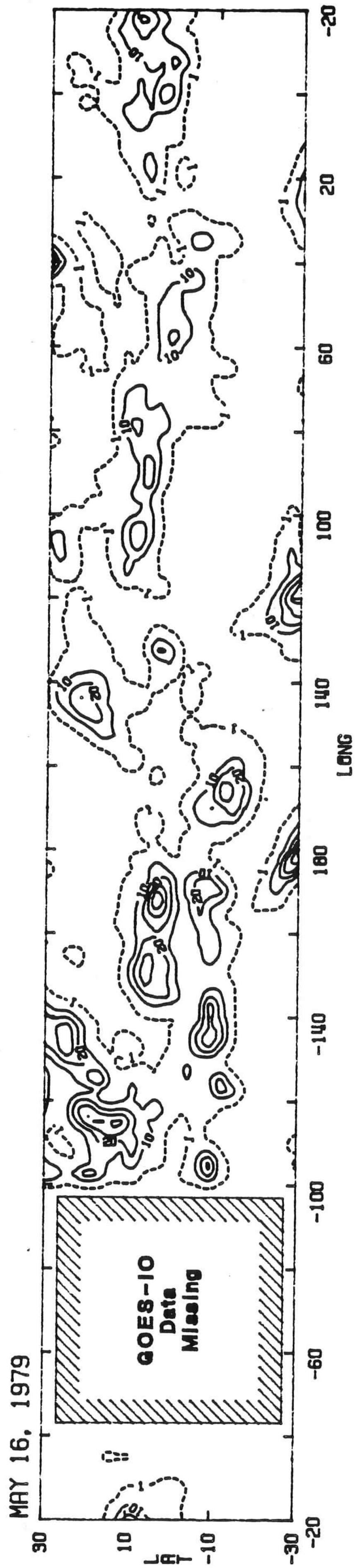

MAY 16, 1979

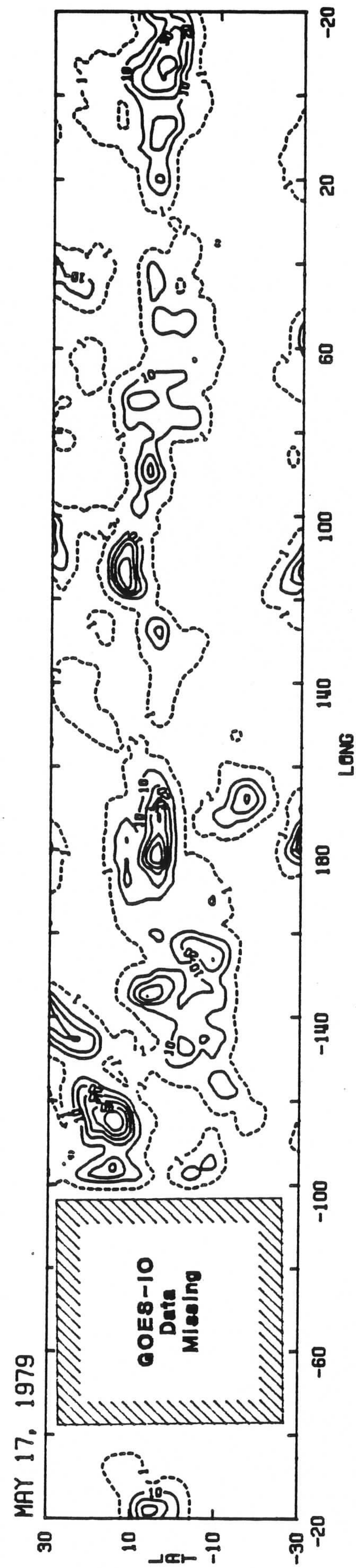

MAY 17, 1979

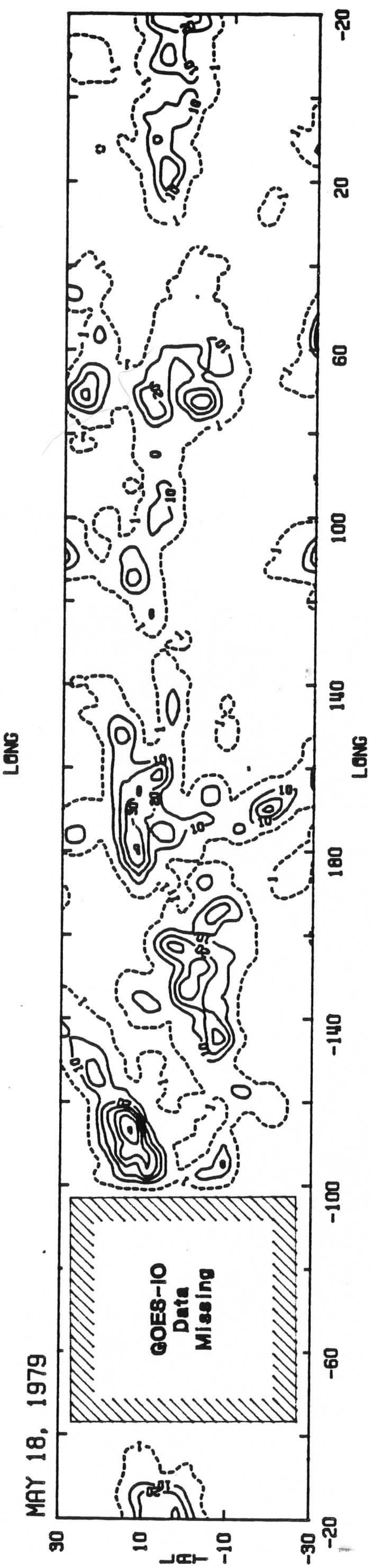

MAY 18, 1979

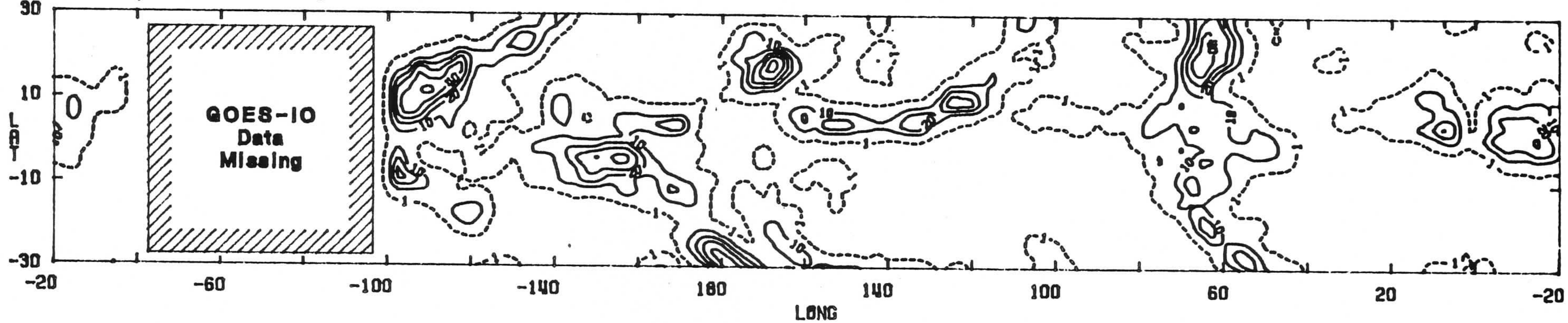
MAY 19, 1979

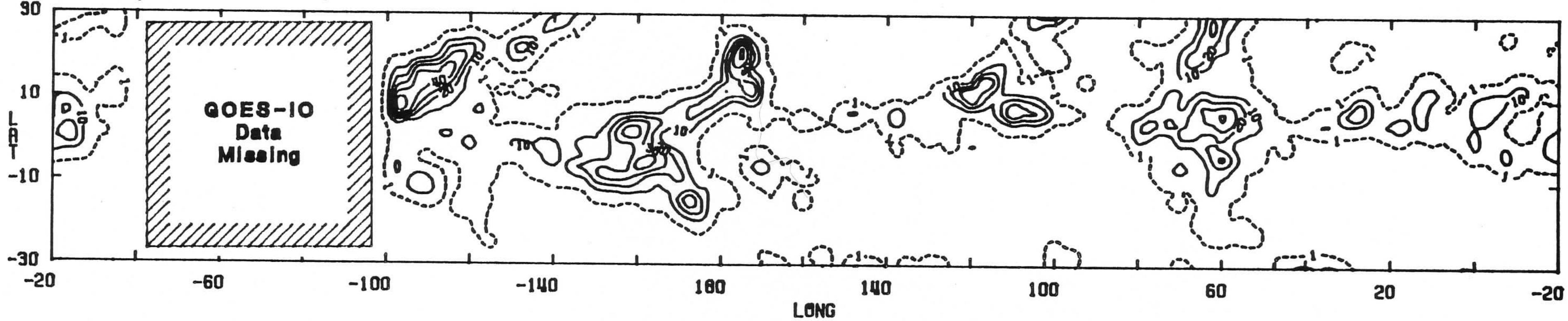
MAY 20, 1979

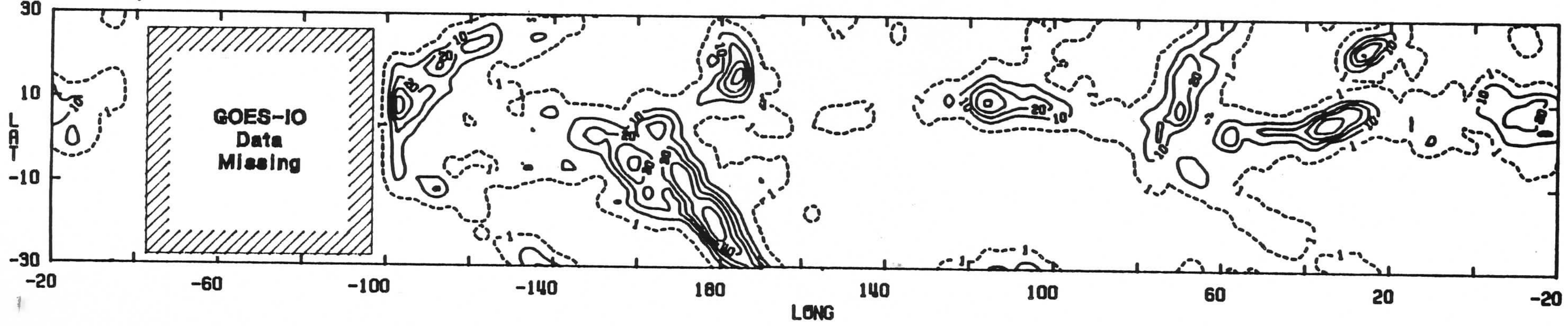
MAY 21, 1979

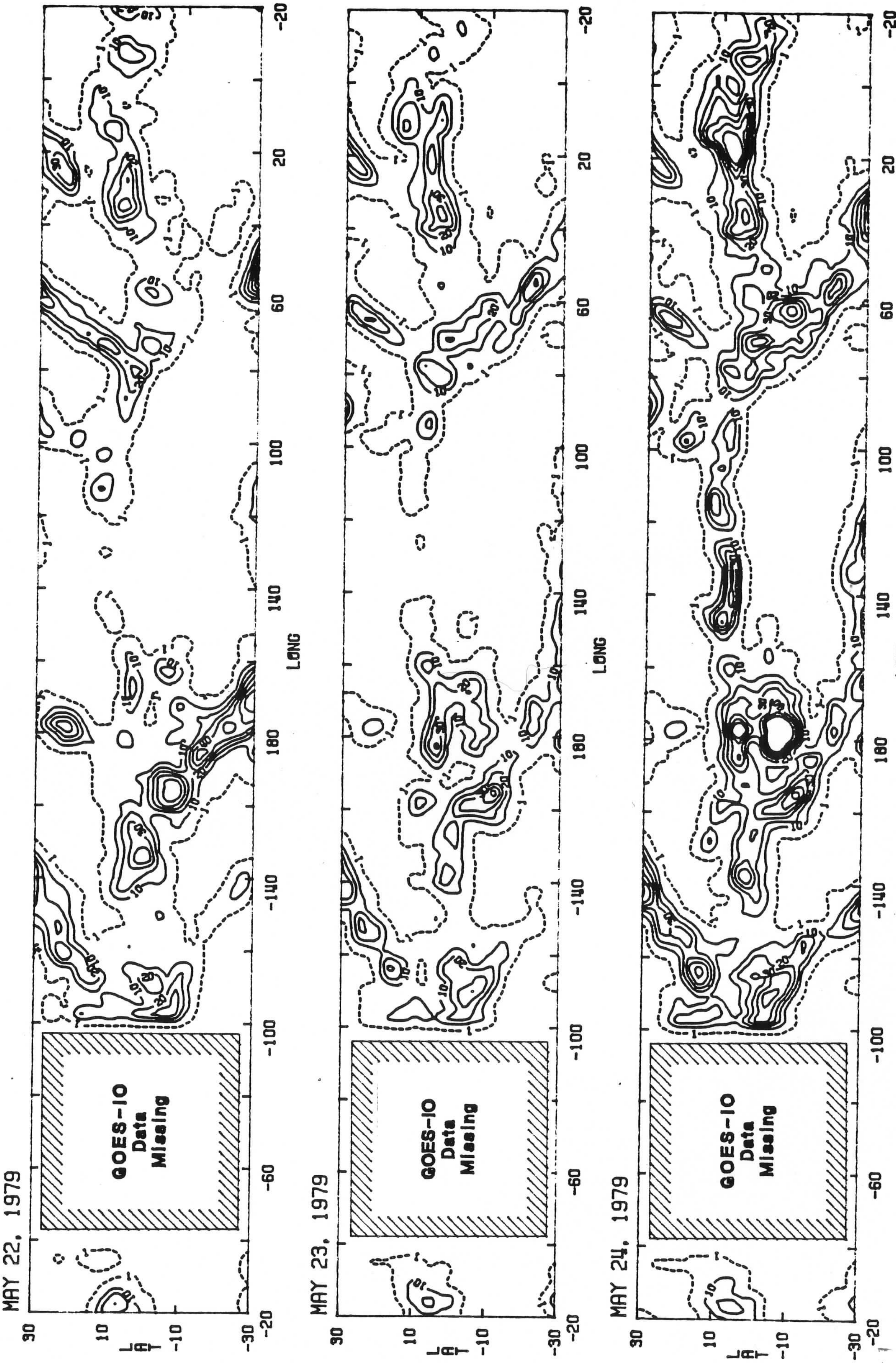
MAY 22, 1979
MAY 23, 1979
MAY 24, 1979
LAT
30
10
-10
-30
LONG
-20
-60
-100
-140
180
140
100
60
20
GOES-10 Data Missing
10
20
30

MAY 25, 1979

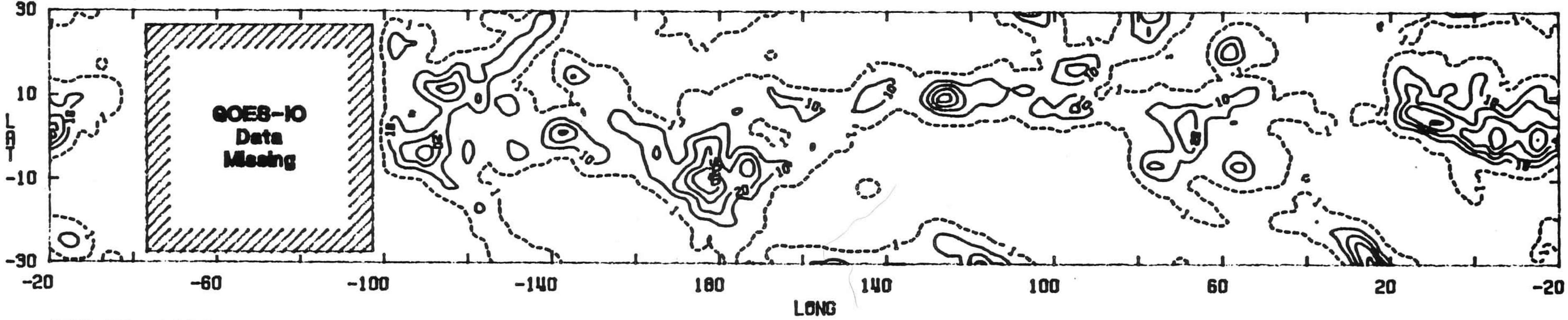

MAY 26, 1979

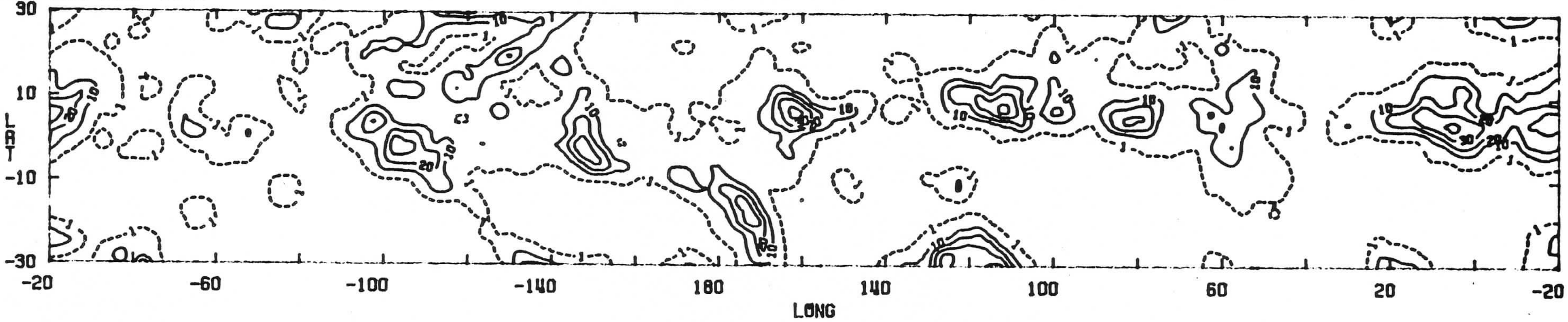

MAY 27, 1979

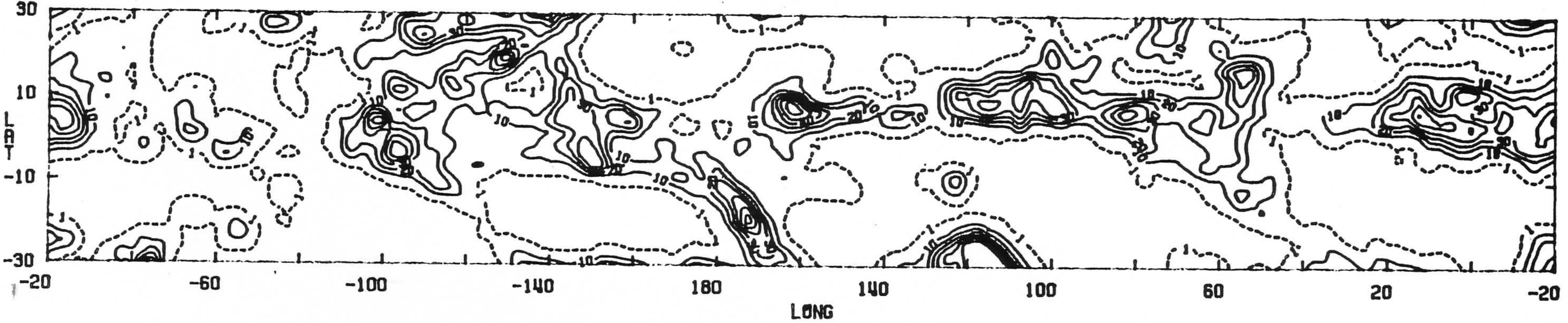

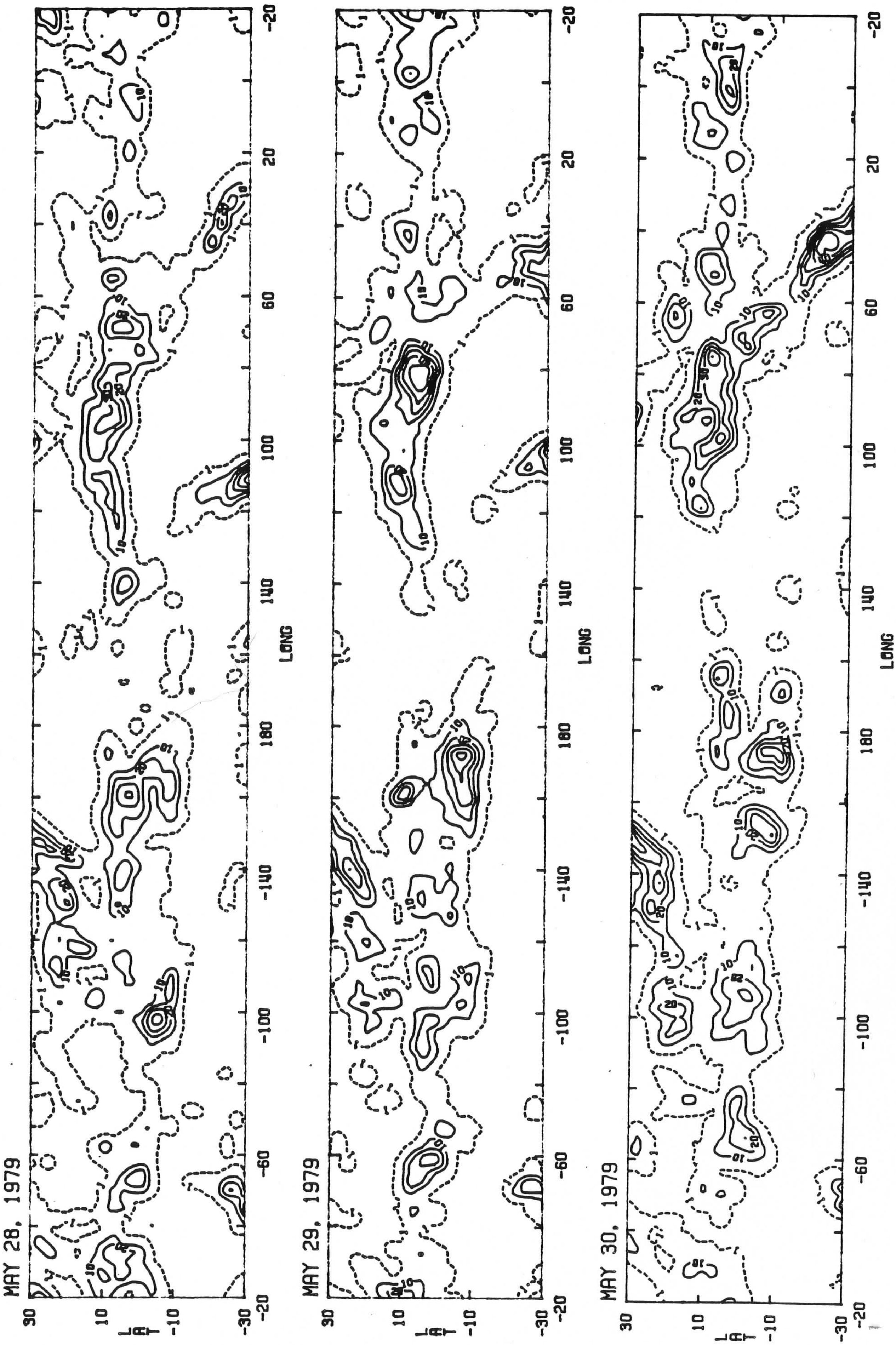
MAY 28, 1979
MAY 29, 1979
MAY 30, 1979
LAT
30
10
-10
-30
LONG
-20
20
60
100
140
180
-140
-100
-60
-20
10
20

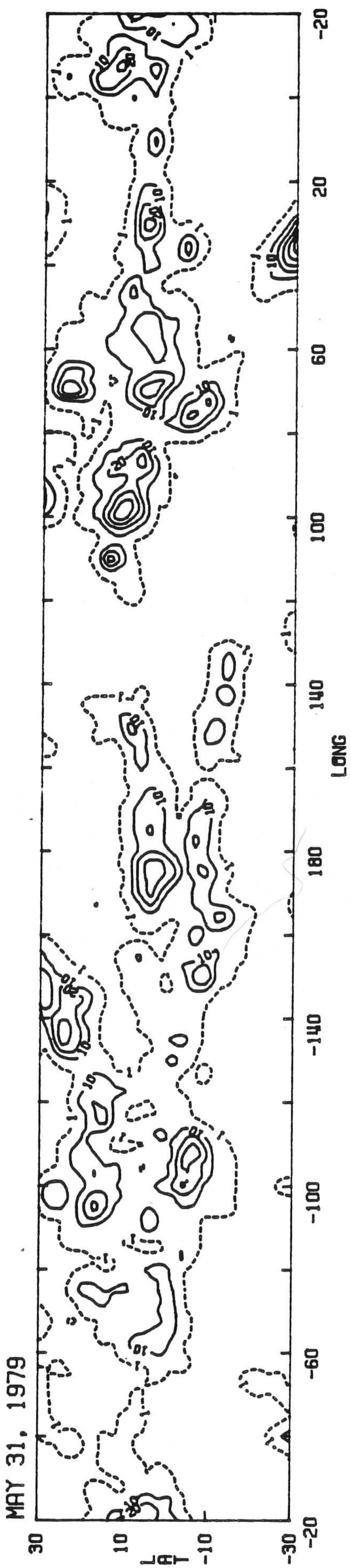
MAY 31, 1979
LAT
30
10
-10
-30
LONG
-20
-60
-100
-140
180
140
100
60
20
-20
10
1

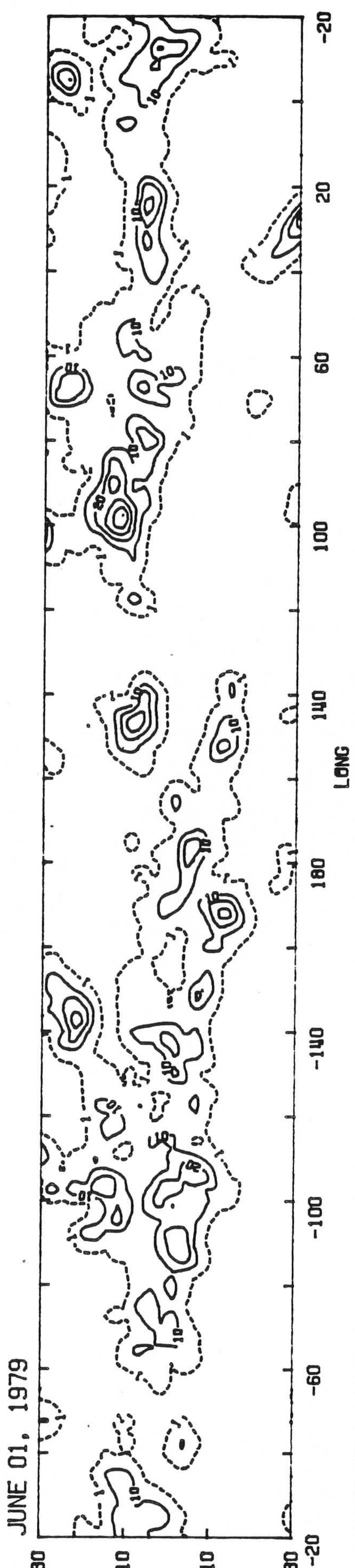
JUNE 01, 1979
LAT
30
10
-10
-30
LONG
-20
-60
-100
-140
180
140
100
60
20
-20
10
1

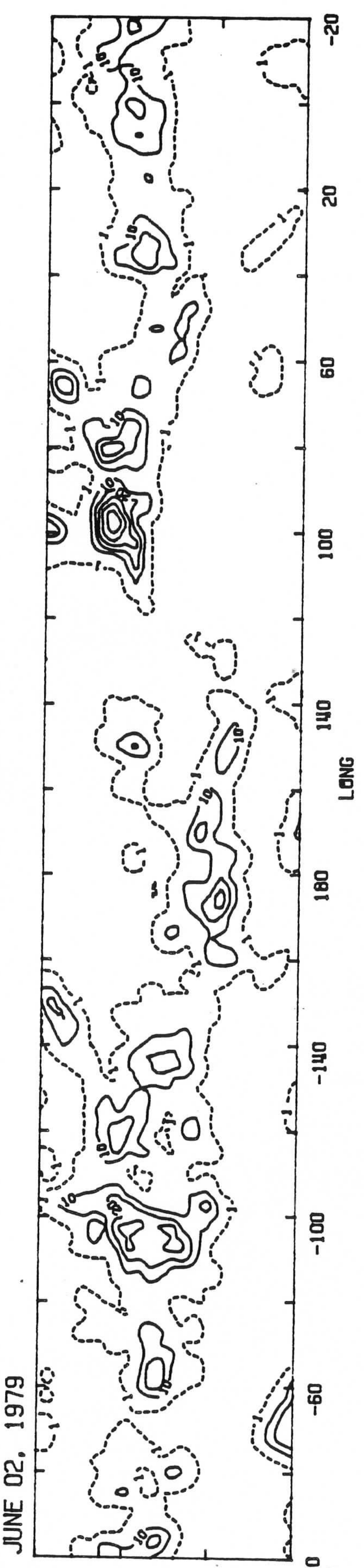
JUNE 02, 1979
LAT
30
10
-10
-30
LONG
-20
-60
-100
-140
180
140
100
60
20
-20
10
1

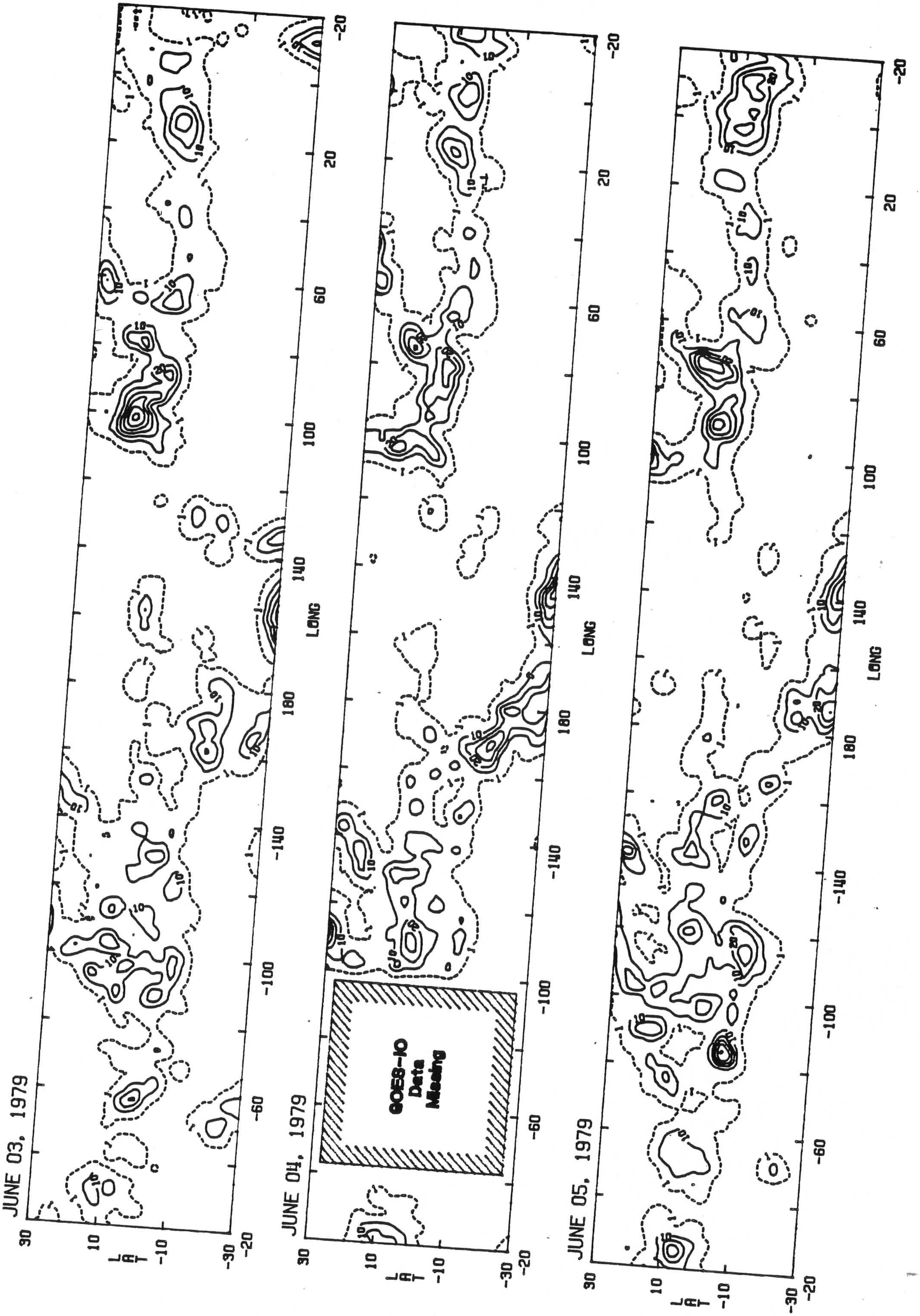
JUNE 03, 1979
JUNE 04, 1979
JUNE 05, 1979
GOES-IO Data Missing
LAT
LONG
30
10
-10
-30
-20
-60
-100
-140
180
140
100
60
20
-20
10
20

JUNE 06, 1979

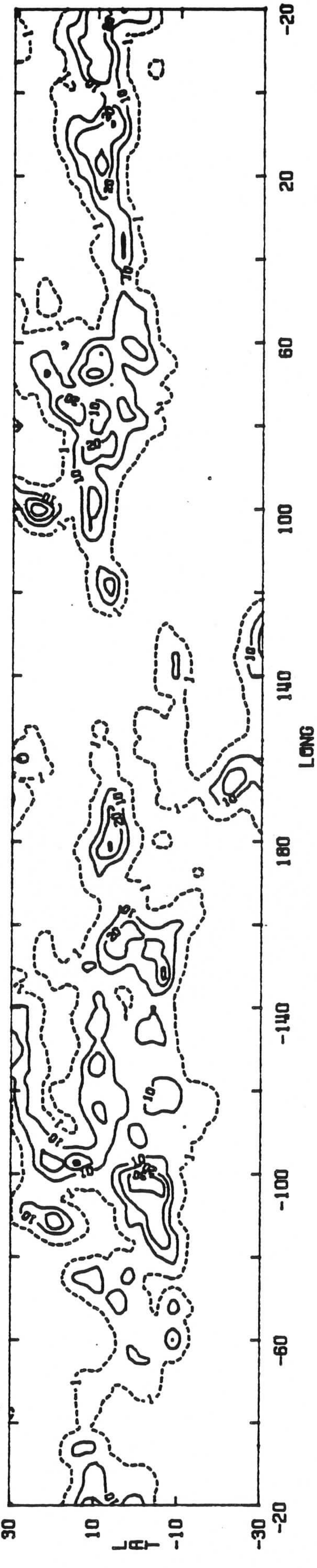

JUNE 07, 1979

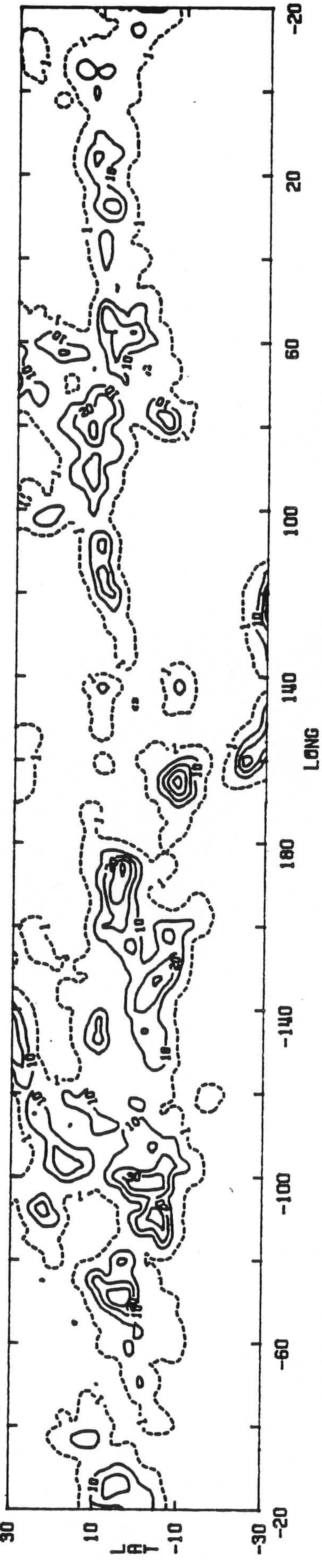

JUNE 08, 1979

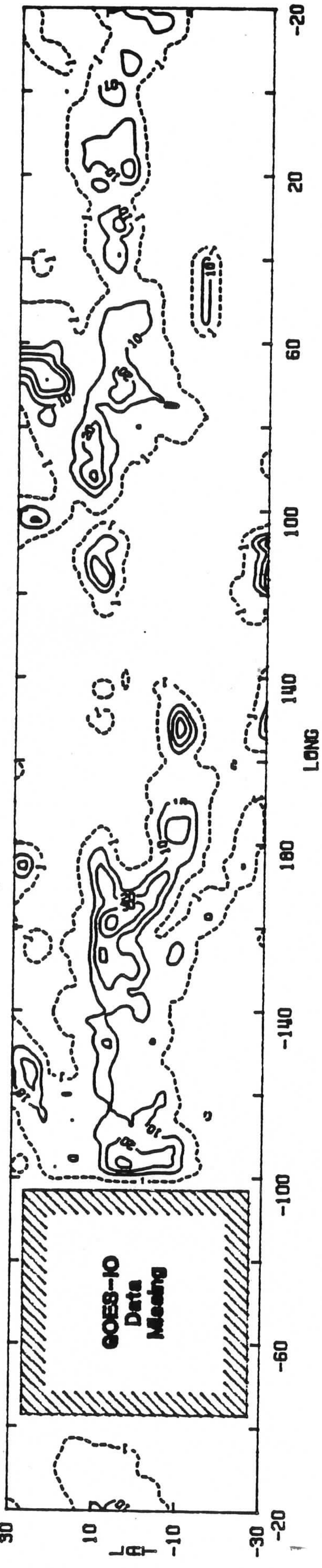

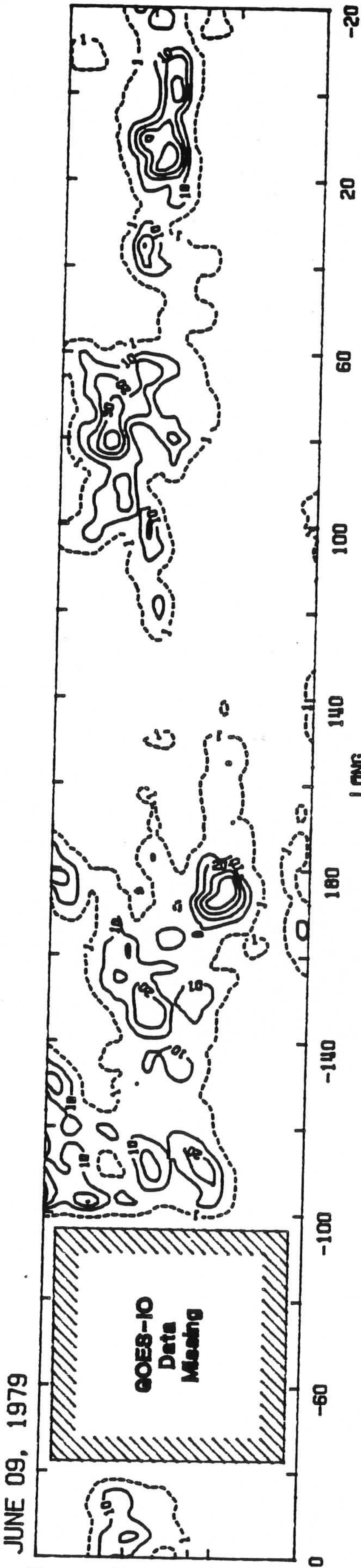

JUNE 09, 1979

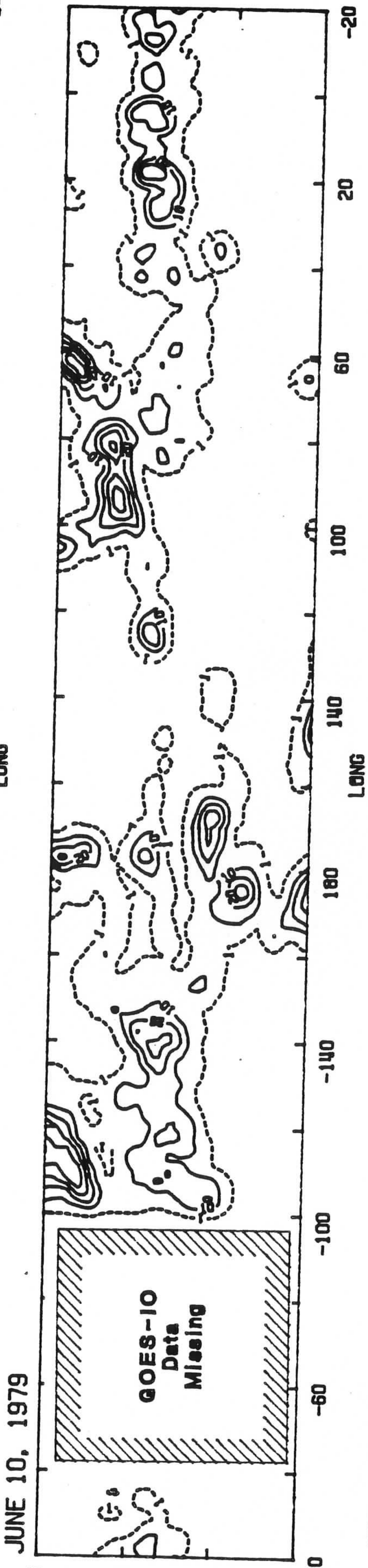

JUNE 10, 1979

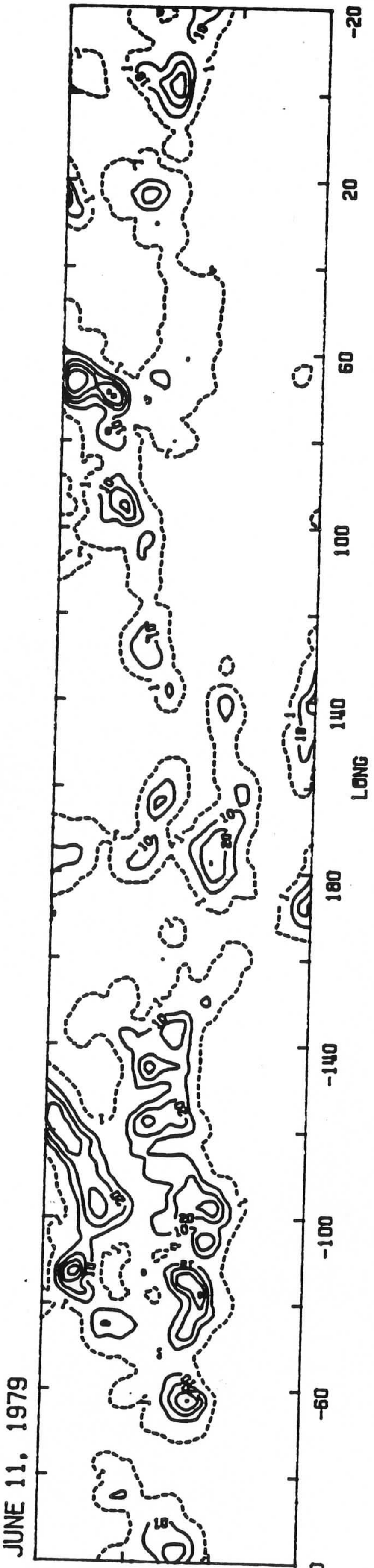

JUNE 11, 1979

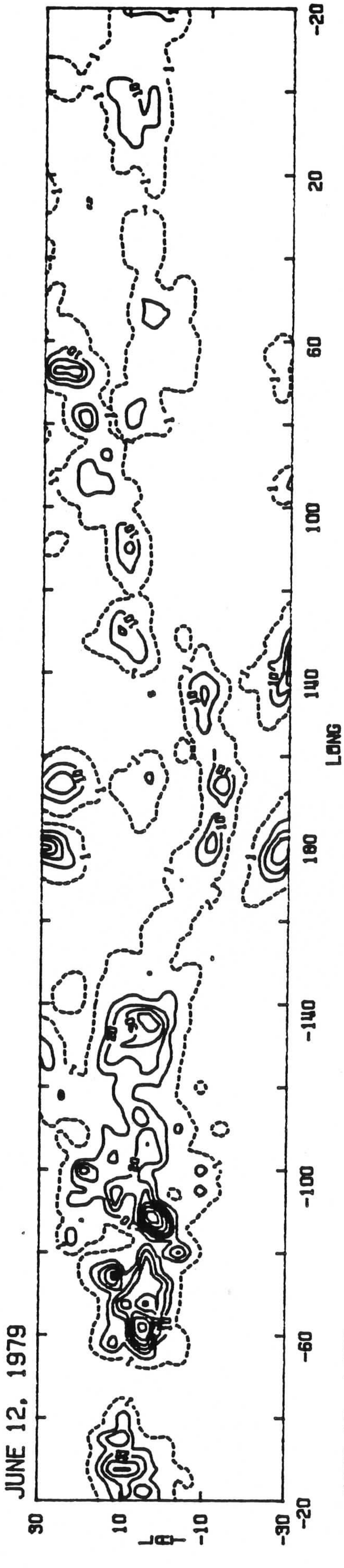
JUNE 12, 1979
LAT
30
10
-10
-30
LONG
-20
20
60
100
140
180
-140
-100
-60
-20
10
20

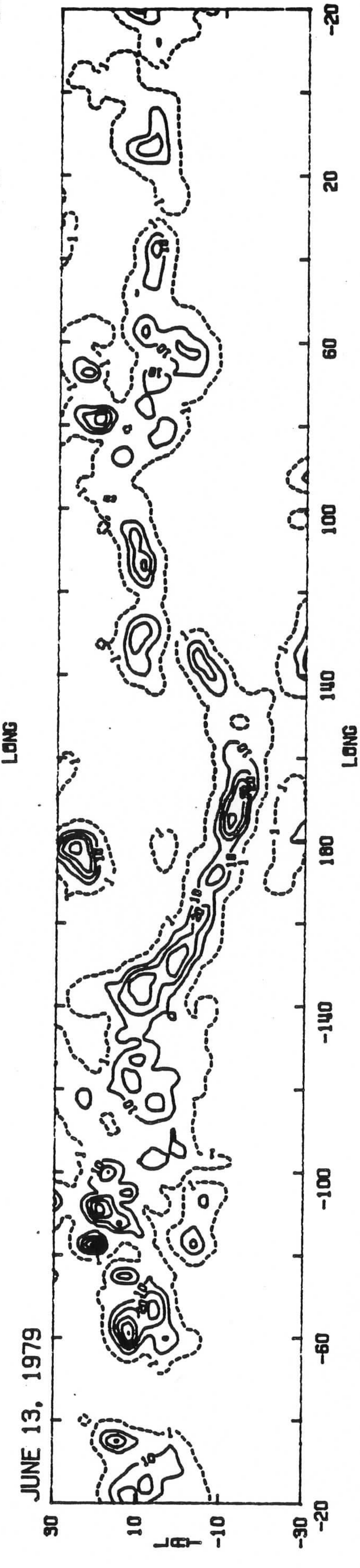
JUNE 13, 1979
LAT
30
10
-10
-30
LONG
-20
20
60
100
140
180
-140
-100
-60
-20
10
20

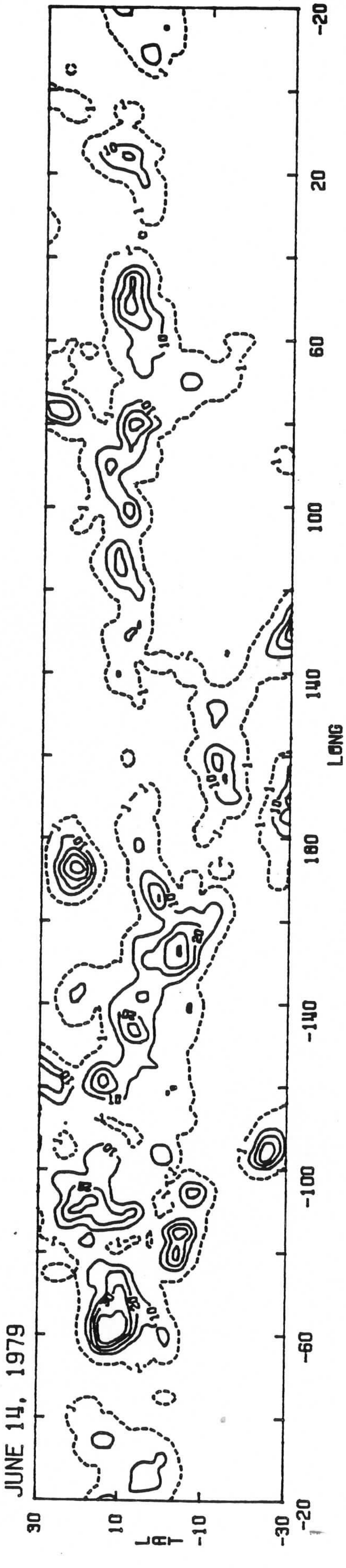
JUNE 14, 1979
LAT
30
10
-10
-30
LONG
-20
20
60
100
140
180
-140
-100
-60
-20
10
20

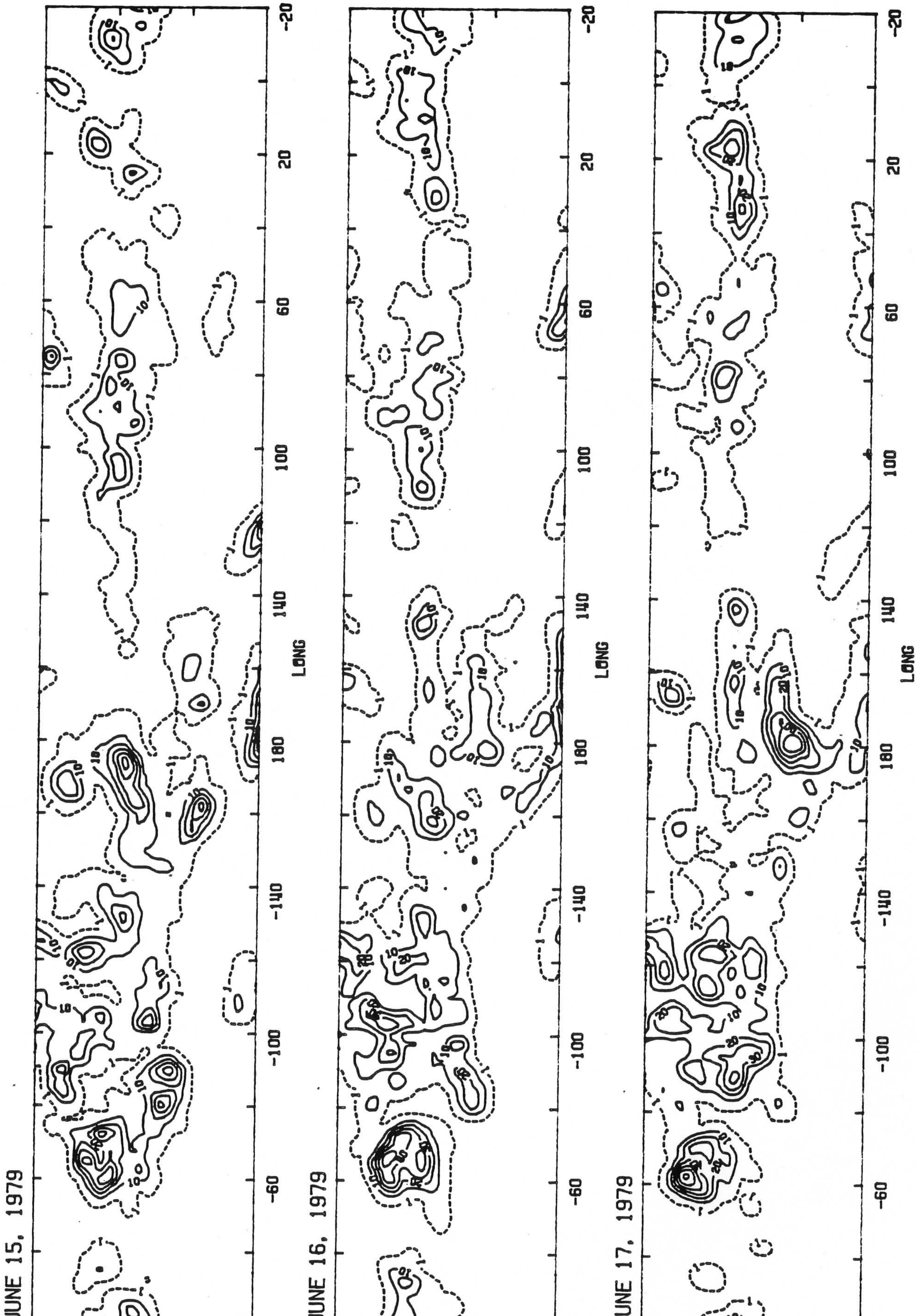
JUNE 15, 1979
JUNE 16, 1979
JUNE 17, 1979
LAT
30
10
-10
-30
LONG
-20
-60
-100
-140
180
140
100
60
20
-20
1
10
20
30

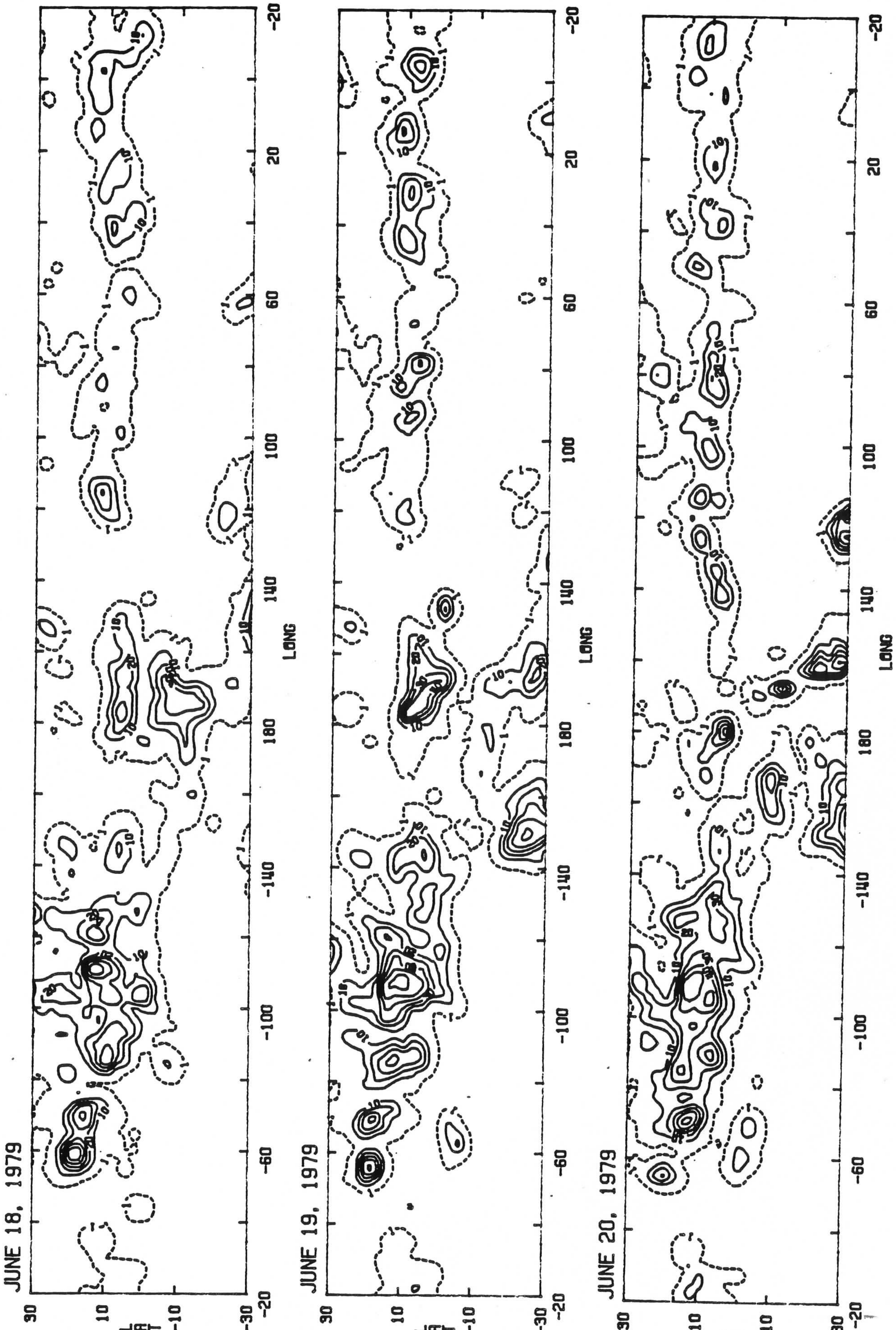
JUNE 18, 1979
JUNE 19, 1979
JUNE 20, 1979
LAT
30
10
-10
-30
LONG
-20
-60
-100
-140
180
140
100
60
20
-20
10
20

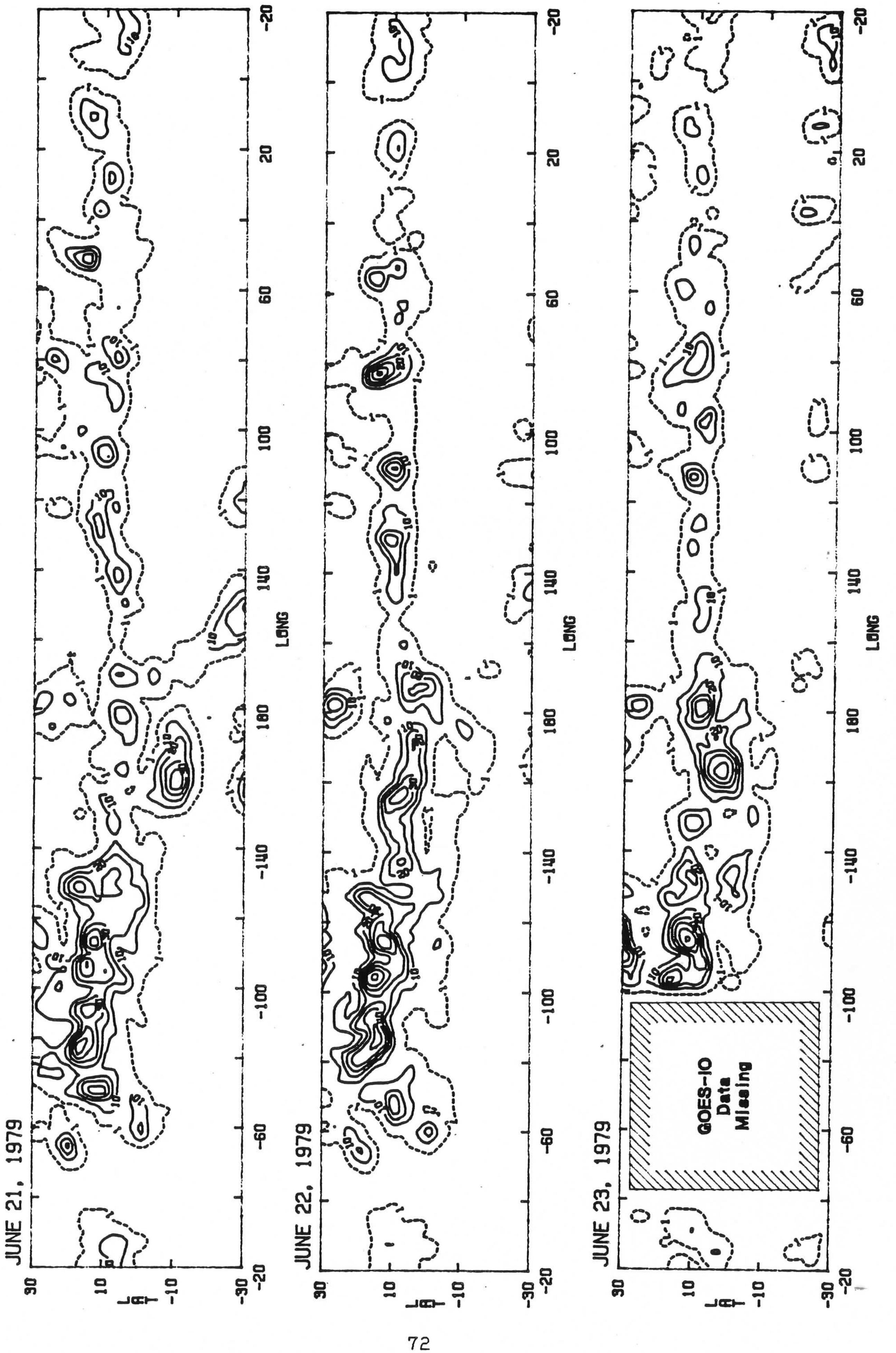
JUNE 21, 1979
JUNE 22, 1979
JUNE 23, 1979
LAT
LONG
30
10
-10
-30
-20
20
60
100
140
180
-140
-100
-60
10
GOES-10
Data
Missing

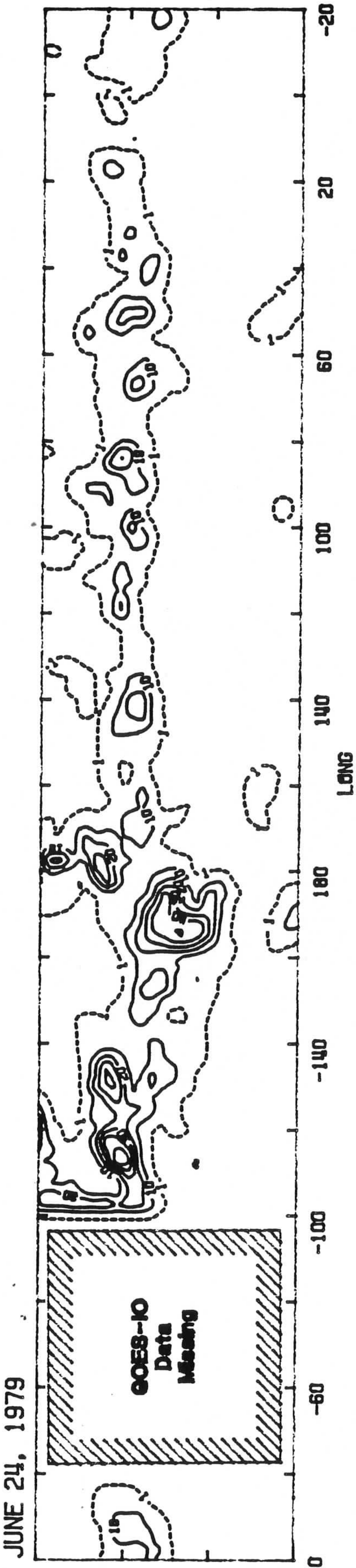

JUNE 24, 1979

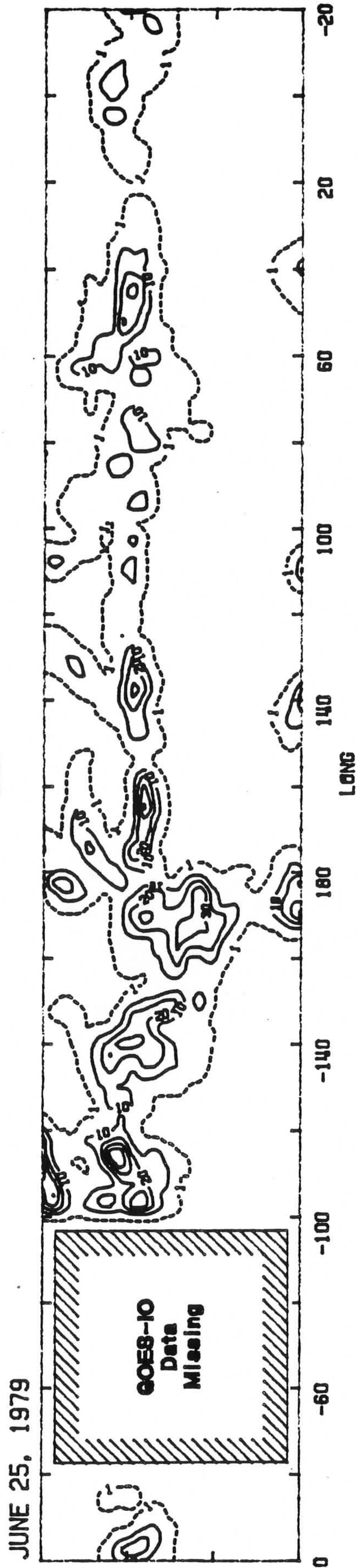

JUNE 25, 1979

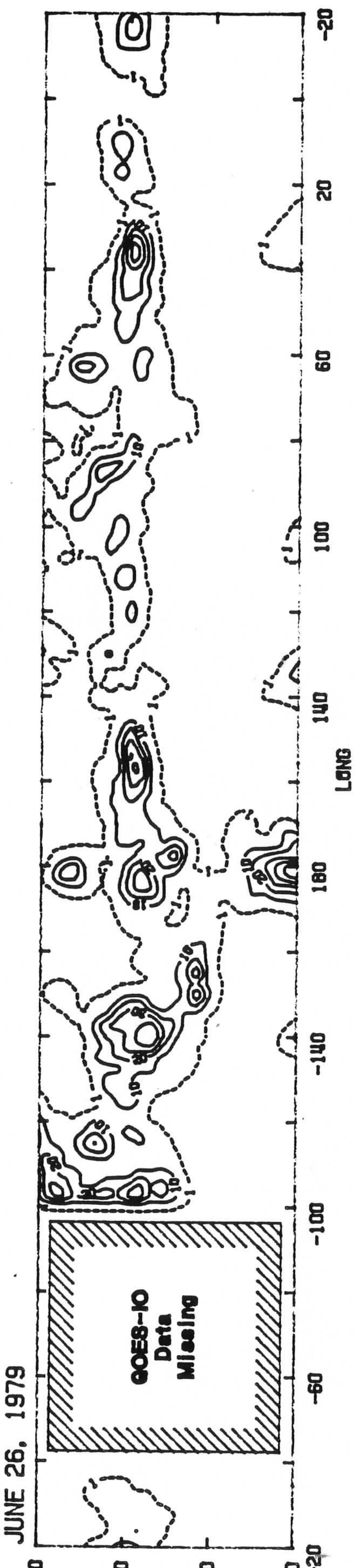

JUNE 26, 1979

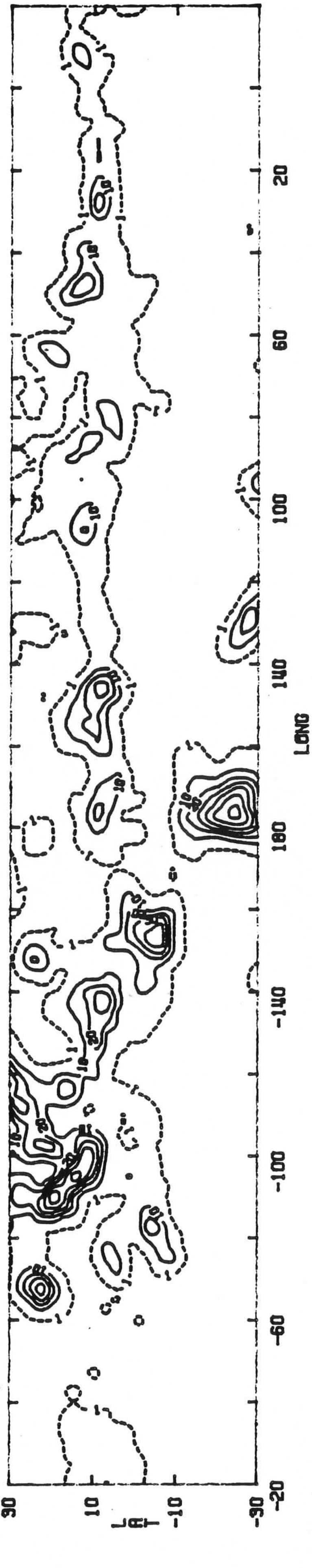
JUNE 27, 1979

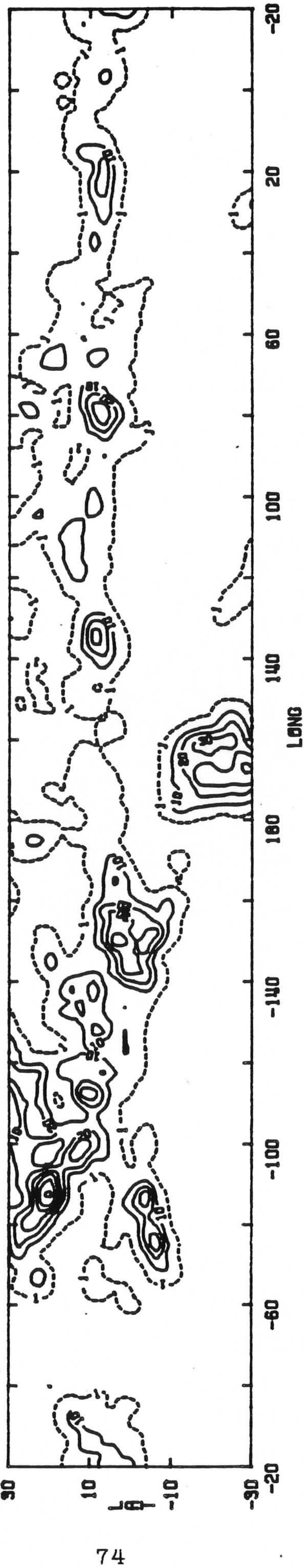
JUNE 28, 1979

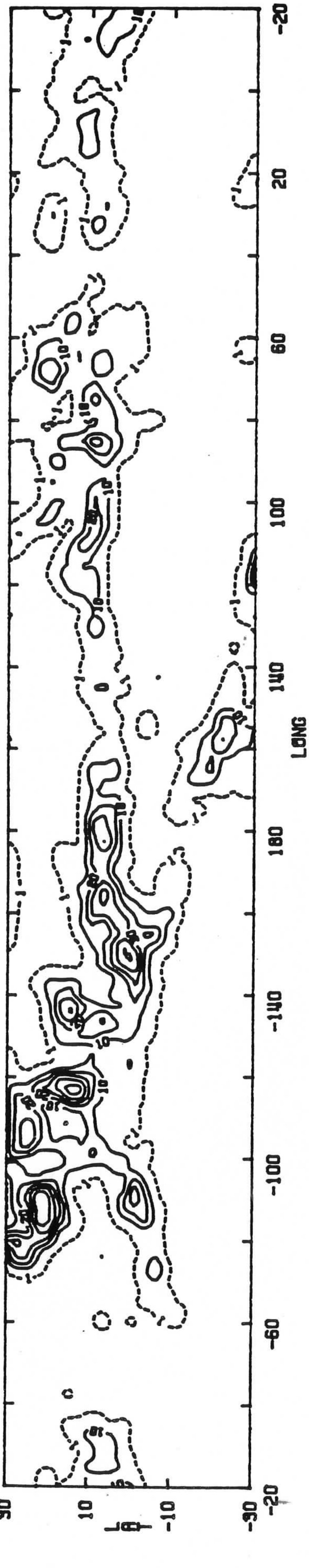
JUNE 29, 1979

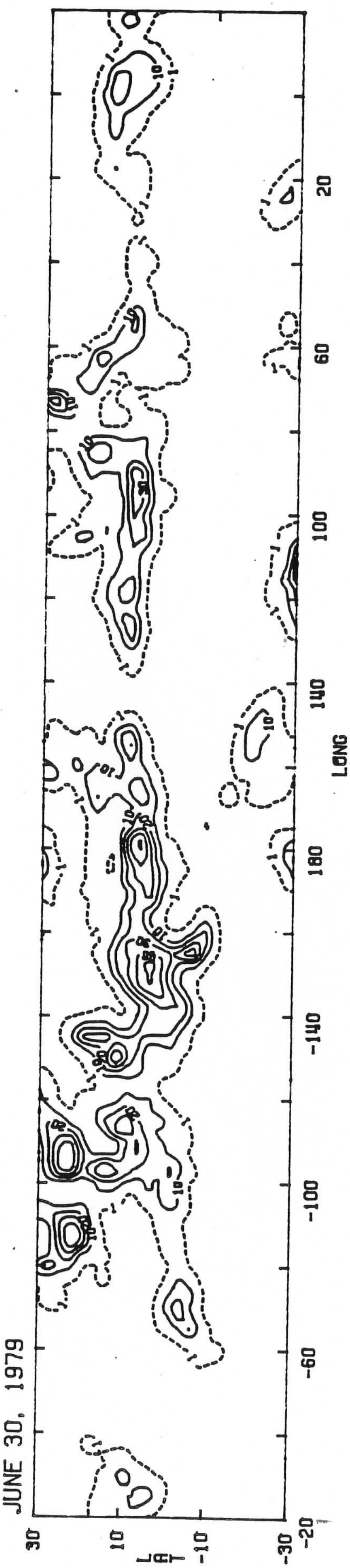
JUNE 30, 1979
LAT
30
10
-10
-30
LONG
-20
-60
-100
-140
180
140
100
60
20
10
30

A.4 Quality Table

The table notes the data not available or unsuitable for use in our study. Most data voids are attributable to the failure of GOES-E (Satellite 23) to scan south of the equator, or to the failure of the infrared sensor on GOES-IO (Satellite 21). On an image-by-image basis just under 16% of the data was lost. Extremely reliable coverage was provided by Meteosat, GMS, and Goes-W (Satellites 5, 13, and 25).

MISSING DATA LOG
FGGE SOP RAINFALL ESTIMATION

Satellite numbers: 5=Meteosat, 13=GMS, 21=GOES-1, 23=GOES-2, 25=GOES-3

Julian Day	Time GMT	Satellite #	Lat. Bounds - = s		Long. Bounds - = w		Comments
79005	0	13	10.0	-27.5	102.5	175.0	
		21					a few bad lines
	12	25	30.0	-27.5	177.5	-110.0	
	18	5	17.5	-27.5	-37.5	35.0	
		25	30.0	-27.5	177.5	-110.0	
79006	18	23	30.0	-27.5	-112.5	-40.0	
79007	0	21					many bad lines
	18	23	0.0	-27.5	-112.5	-40.0	
79009	6	5	30.0	-27.5	-37.5	35.0	
79011	0	23	0.0	-27.5	-112.5	-40.0	
	12	25	-25.0	-27.5	177.5	-110.0	
79012	18	23	0.0	-27.5	-112.5	-40.0	
79013	0	5	22.5	2.5	-37.5	35.0	
		23	0.0	-27.5	-112.5	-40.0	
	6	23	0.0	-27.5	-112.5	-40.0	
	12	23	0.0	-27.5	-112.5	-40.0	
	18	23	0.0	-27.5	-112.5	-40.0	
79014	0	23	0.0	-27.5	-112.5	-40.0	
	6	23	0.0	-27.5	-112.5	-40.0	
	12	23	0.0	-27.5	-112.5	-40.0	
	18	23	0.0	-27.5	-112.5	-40.0	
79015	0	23	0.0	-27.5	-112.5	-40.0	
	6	23	0.0	-27.5	-112.5	-40.0	
	12	5	30.0	-27.5	-37.5	35.0	
		23	0.0	-27.5	-112.5	-40.0	
	18	23	0.0	-27.5	-112.5	-40.0	
79016	0	23	0.0	-27.5	-112.5	-40.0	
	6	23	0.0	-27.5	-112.5	-40.0	
	12	23	0.0	-27.5	-112.5	-40.0	
	18	23	0.0	-27.5	-112.5	-40.0	
79017	0	23	0.0	-27.5	-112.5	-40.0	
	6	23	0.0	-27.5	-112.5	-40.0	
	12	23	0.0	-27.5	-112.5	-40.0	
	18	23	0.0	-27.5	-112.5	-40.0	
79018	0	23	0.0	-27.5	-112.5	-40.0	
	6	5	30.0	-27.5	-37.5	35.0	
		23	0.0	-27.5	-112.5	-40.0	
	12	23	0.0	-27.5	-112.5	-40.0	
	18	23	0.0	-27.5	-112.5	-40.0	
79019	0	23	0.0	-27.5	-112.5	-40.0	
	6	23	0.0	-27.5	-112.5	-40.0	
	12	23	0.0	-27.5	-112.5	-40.0	
	18	23	0.0	-27.5	-112.5	-40.0	
79020	0	5	30.0	-27.5	-37.5	35.0	
		23	0.0	-27.5	-112.5	-40.0	
	6	23	0.0	-27.5	-112.5	-40.0	
	12	23	0.0	-27.5	-112.5	-40.0	
	18	23	0.0	-27.5	-112.5	-40.0	

Day	Time	Satellite	Lat. Bounds		Long. Bounds		Comments
79021	0	21	30.0	-27.5	27.5	100.0	
		23	0.0	-27.5	-112.5	-40.0	
	6	23	0.0	-27.5	-112.5	-40.0	
	12	23	0.0	-27.5	-112.5	-40.0	
	18	23	0.0	-27.5	-112.5	-40.0	
79022	0	23	0.0	-27.5	-112.5	-40.0	
	6	5	30.0	-27.5	-37.5	35.0	
		23	0.0	-27.5	-112.5	-40.0	
	12	23	0.0	-27.5	-112.5	-40.0	
	18	23	0.0	-27.5	-112.5	-40.0	
79023	0	23	0.0	-27.5	-112.5	-40.0	
	6	23	0.0	-27.5	-112.5	-40.0	
	12	21					a few bad lines
		23	0.0	-27.5	-112.5	-40.0	
	18	23	0.0	-27.5	-112.5	-40.0	
79024	0	23	0.0	-27.5	-112.5	-40.0	
	6	23	0.0	-27.5	-112.5	-40.0	
	12	23	0.0	-27.5	-112.5	-40.0	
	18	23	0.0	-27.5	-112.5	-40.0	
79025	0	23	0.0	-27.5	-112.5	-40.0	
	6	5	30.0	-27.5	-37.5	35.0	
		23	0.0	-27.5	-112.5	-40.0	
	12	21					some bad lines
		23	0.0	-27.5	-112.5	-40.0	
	18	23	0.0	-27.5	-112.5	-40.0	
		25	-22.5	-27.5	177.5	-110.0	
79026	0	23	0.0	-27.5	-112.5	-40.0	
	6	23	0.0	-27.5	-112.5	-40.0	
	12	23	0.0	-27.5	-112.5	-40.0	
	18	21	30.0	-27.5	27.5	100.0	
		23	0.0	-27.5	-112.5	-40.0	
79028	0	23	2.5	-27.5	-112.5	-40.0	
	18	23	12.5	-27.5	-112.5	-40.0	
79030	6	21					a few bad lines
79031	0	23					some bad lines
79032	18	21	-7.5	-27.5	27.5	100.0	
			30.0	12.5	27.5	100.0	
79034	6	23	-22.5	-27.5	-112.5	-40.0	
79041	18	25					some bad lines
79050	18	5	30.0	-27.5	-37.5	35.0	
79051	0	5	30.0	-27.5	-37.5	35.0	
		23	30.0	-27.5	-112.5	-40.0	
	6	5	30.0	-27.5	-37.5	35.0	
		23	30.0	-27.5	-112.5	-40.0	
	12	23	30.0	-27.5	-112.5	-40.0	
	18	23	30.0	-27.5	-112.5	-40.0	
79052	0	5	30.0	-27.5	-37.5	35.0	
		23	30.0	-27.5	-112.5	-40.0	
	6	23	30.0	-27.5	-112.5	-40.0	
	12	23	30.0	-27.5	-112.5	-40.0	
79053	0	21					a few bad lines

Day	Time	Satellite	Lat. Bounds		Long. Bounds		Comments
79054	0	13	30.0	-27.5	102.5	175.0	
		23	-20.0	-27.5	-112.5	-40.0	
			30.0	25.0	-112.5	-40.0	
79055	6	23	-20.0	-27.5	-112.5	-40.0	
	18	5	30.0	-27.5	-37.5	35.0	
79056	0	23	-12.5	-27.5	-112.5	-40.0	
	6	23	-2.5	-27.5	-112.5	-40.0	
	12	23	-20.0	-27.5	-112.5	-40.0	
	18	23	-20.0	-27.5	-112.5	-40.0	
79057	0	23	-12.5	-27.5	-112.5	-40.0	
		25	30.0	-27.5	177.5	-110.0	
79058	0	23	-22.5	-27.5	-112.5	-40.0	
	18	23	-17.5	-27.5	-112.5	-40.0	
79060	0	23	30.0	-27.5	-112.5	-40.0	
	6	23	30.0	-27.5	-112.5	-40.0	
	12	23	30.0	-27.5	-112.5	-40.0	
	18	23	30.0	-27.5	-112.5	-40.0	
79061	0	23	30.0	-27.5	-112.5	-40.0	
	6	23	30.0	-27.5	-112.5	-40.0	
	12	23	30.0	-27.5	-112.5	-40.0	
79062	0	23	-12.5	-27.5	-112.5	-40.0	
	6	23	-2.5	-27.5	-112.5	-40.0	
	12	23	-20.0	-27.5	-112.5	-40.0	
	18	23	-17.5	-27.5	-112.5	-40.0	
79063	0	23	-12.5	-27.5	-112.5	-40.0	
	6	23	-2.5	-27.5	-112.5	-40.0	
79064	12	23	-20.0	-27.5	-112.5	-40.0	
79121	0	5	30.0	-27.5	-37.5	35.0	
	6	5	30.0	-27.5	-37.5	35.0	
79122	12	23	-10.0	-27.5	-112.5	-40.0	
		25	-20.0	-27.5	177.5	-110.0	
	18	23	-15.0	-27.5	-112.5	-40.0	
79123	0	23	-15.0	-27.5	-112.5	-40.0	
	18	23	-12.5	-27.5	-112.5	-40.0	
79124	0	23	-7.5	-27.5	-112.5	-40.0	
	6	23	-2.5	-27.5	-112.5	-40.0	
	18	23	-12.5	-27.5	-112.5	-40.0	
79125	0	21					a few bad lines
		23	-7.5	-27.5	-112.5	-40.0	
		25	-20.0	-27.5	177.5	-110.0	
	12	21					a few bad lines
79126	0	21	30.0	-27.5	27.5	100.0	
	6	21	30.0	-27.5	27.5	100.0	
	12	21	30.0	-27.5	27.5	100.0	
	18	21	30.0	-27.5	27.5	100.0	
79127	0	21	30.0	-27.5	27.5	100.0	
	6	21	30.0	-27.5	27.5	100.0	
		23					many bad lines
	12	21	30.0	-27.5	27.5	100.0	
	18	21	30.0	-27.5	27.5	100.0	
79128	0	21	30.0	-27.5	27.5	100.0	
	6	21	30.0	-27.5	27.5	100.0	
	18	23	-15.0	-27.5	-112.5	-40.0	

Day	Time	Satellite	Lat. Bounds		Long. Bounds		Comments
79129	0	23	-10.0	-27.5	-112.5	-40.0	
	6	23	-2.5	-27.5	-112.5	-40.0	
	12	23	-15.0	-27.5	-112.5	-40.0	
		25	-20.0	-27.5	177.5	-110.0	
	18	23	-15.0	-27.5	-112.5	-40.0	
79130	0	23	-15.0	-27.5	-112.5	-40.0	
	18	23	-15.0	-27.5	-112.5	-40.0	
		25	-20.0	-27.5	177.5	-110.0	
79131	0	21	30.0	-27.5	27.5	100.0	
		23	-10.0	-27.5	-112.5	-40.0	
	6	21	30.0	-27.5	27.5	100.0	
	12	21	30.0	-27.5	27.5	100.0	
	18	21	30.0	-27.5	27.5	100.0	
		23	-15.0	-27.5	-112.5	-40.0	
79132	0	21	30.0	-27.5	27.5	100.0	
		23	-10.0	-27.5	-112.5	-40.0	
	6	21	30.0	-27.5	27.5	100.0	
	12	5	17.5	-27.5	-37.5	35.0	
		21	30.0	-27.5	27.5	100.0	
		25	-17.5	-27.5	177.5	-110.0	
	18	21	30.0	-27.5	27.5	100.0	
		23	-22.5	-27.5	-112.5	-40.0	
79133	0	21	30.0	-27.5	27.5	100.0	
	6	21	30.0	-27.5	27.5	100.0	
	12	21	30.0	-27.5	27.5	100.0	
		25	30.0	-27.5	177.5	-110.0	
	18	21	30.0	-27.5	27.5	100.0	
		25	30.0	-27.5	177.5	-110.0	
79134	0	21	30.0	-27.5	27.5	100.0	
	6	21	30.0	-27.5	27.5	100.0	
	12	21	30.0	-27.5	27.5	100.0	
	18	21	30.0	-27.5	27.5	100.0	
		25	30.0	-27.5	177.5	-110.0	
79135	0	21	30.0	-27.5	27.5	100.0	
	6	21	30.0	-27.5	27.5	100.0	
	12	21	30.0	-27.5	27.5	100.0	
	18	21	30.0	-27.5	27.5	100.0	
79136	0	21	30.0	-27.5	27.5	100.0	
	6	21	30.0	-27.5	27.5	100.0	
	12	21	30.0	-27.5	27.5	100.0	
	18	21	30.0	-27.5	27.5	100.0	
79137	0	21	30.0	-27.5	27.5	100.0	
	6	21	30.0	-27.5	27.5	100.0	
	12	21	30.0	-27.5	27.5	100.0	
	18	21	30.0	-27.5	27.5	100.0	
79138	0	5	30.0	-27.5	-37.5	35.0	
		21	30.0	-27.5	27.5	100.0	
	6	21	30.0	-27.5	27.5	100.0	
	12	21	30.0	-27.5	27.5	100.0	
	18	21	30.0	-27.5	27.5	100.0	
79139	0	21	30.0	-27.5	27.5	100.0	
	6	21	30.0	-27.5	27.5	100.0	
	12	21	30.0	-27.5	27.5	100.0	
	18	21	30.0	-27.5	27.5	100.0	

Day	Time	Satellite	Lat. Bounds		Long. Bounds		Comments
79140	0	21	30.0	-27.5	27.5	100.0	
		25	30.0	-27.5	177.5	-110.0	
	6	21	30.0	-27.5	27.5	100.0	
		23	-2.5	-27.5	-112.5	-40.0	
		25	30.0	-27.5	177.5	-110.0	
	12	21	30.0	-27.5	27.5	100.0	
		23	-15.0	-27.5	-112.5	-40.0	
		25	-20.0	-27.5	177.5	-110.0	
	18	21	30.0	-27.5	27.5	100.0	
		23	-17.5	-27.5	-112.5	-40.0	
79141	0	21	30.0	-27.5	27.5	100.0	
		23	-17.5	-27.5	-112.5	-40.0	
	6	21	30.0	-27.5	27.5	100.0	
	12	21	30.0	-27.5	27.5	100.0	
	18	21	30.0	-27.5	27.5	100.0	
79142	0	21	30.0	-27.5	27.5	100.0	
		23	-15.0	-27.5	-112.5	-40.0	
	6	21	30.0	-27.5	27.5	100.0	
	12	21	30.0	-27.5	27.5	100.0	
	18	21	30.0	-27.5	27.5	100.0	
		23	-12.5	-27.5	-112.5	-40.0	
79143	0	21	30.0	-27.5	27.5	100.0	
	6	21	30.0	-27.5	27.5	100.0	
	12	21	30.0	-27.5	27.5	100.0	
	18	21	30.0	-27.5	27.5	100.0	
79144	0	21	30.0	-27.5	27.5	100.0	
		25	30.0	-27.5	177.5	-110.0	
	6	21	30.0	-27.5	27.5	100.0	
	12	21	30.0	-27.5	27.5	100.0	
	18	21	30.0	-27.5	27.5	100.0	
79145	0	5	30.0	-27.5	-37.5	35.0	
		21	30.0	-27.5	27.5	100.0	
		23	-10.0	-27.5	-112.5	-40.0	
	6	21	30.0	-27.5	27.5	100.0	
	12	21	30.0	-27.5	27.5	100.0	
	18	21	30.0	-27.5	27.5	100.0	
79146	0	21	30.0	-27.5	27.5	100.0	
79148	0	23	-10.0	-27.5	-112.5	-40.0	
	12	23	-15.0	-27.5	-112.5	-40.0	
		25	-20.0	-27.5	177.5	-110.0	
	18	23	-15.0	-27.5	-112.5	-40.0	
79149	0	23	-15.0	-27.5	-112.5	-40.0	
	18	23	-20.0	-27.5	-112.5	-40.0	
79150	12	23	-15.0	-27.5	-112.5	-40.0	
		25	-20.0	-27.5	177.5	-110.0	
	18	23	30.0	-27.5	-112.5	-40.0	
79151	18	25	-20.0	-27.5	177.5	-110.0	
79152	6	13	30.0	-27.5	102.5	175.0	
	12	21	30.0	17.5	27.5	100.0	
79154	12	21	27.5	20.0	27.5	100.0	
	18	21	30.0	-27.5	27.5	100.0	

Day	Time	Satellite	Lat. Bounds		Long. Bounds		Comments
79155	0	5	30.0	-27.5	37.5	35.0	
		21	30.0	-27.5	27.5	100.0	
	6	21	30.0	-27.5	27.5	100.0	
	12	21	30.0	-27.5	27.5	100.0	
	18	21	30.0	-27.5	27.5	100.0	
79156	12	25	-17.5	-27.5	177.5	-110.0	
	18	23	-15.0	-27.5	-112.5	-40.0	
79157	0	23	-15.0	-27.5	-112.5	-40.0	
	6	21	30.0	-27.5	27.5	100.0	
79158	0	5	30.0	-27.5	-37.5	35.0	
		23	0.0	-27.5	-112.5	-40.0	
	12	21	30.0	-27.5	27.5	100.0	
		23	-15.0	-27.5	-112.5	-40.0	
		25	-17.5	-27.5	177.5	-110.0	
	18	23	-15.0	-27.5	-112.5	-40.0	
79159	0	21	30.0	-27.5	27.5	100.0	
		23	-10.0	-27.5	-112.5	-40.0	
	6	21	30.0	-27.5	27.5	100.0	
	12	21	30.0	-27.5	27.5	100.0	
		23	-15.0	-27.5	-112.5	-40.0	
		25	-17.5	-27.5	177.5	-110.0	
	18	21	30.0	-27.5	27.5	100.0	
		23	-15.0	-27.5	-112.5	-40.0	
79160	0	5	30.0	-27.5	-37.5	35.0	
		21	30.0	-27.5	27.5	100.0	
		23	-15.0	-27.5	-112.5	-40.0	
	6	21	30.0	-27.5	27.5	100.0	
	12	21	30.0	-27.5	27.5	100.0	
	18	21	30.0	-27.5	27.5	100.0	
79161	0	21	30.0	-27.5	27.5	100.0	
	6	5	30.0	-27.5	-37.5	35.0	
		21	30.0	-27.5	27.5	100.0	
	12	21	30.0	-27.5	27.5	100.0	
	18	5	30.0	-27.5	-37.5	35.0	
		21	30.0	-27.5	27.5	100.0	
		23	-15.0	-27.5	-112.5	-40.0	
79162	0	5	30.0	-27.5	-37.5	35.0	
		21	30.0	-27.5	27.5	100.0	
79163	0	21	30.0	-27.5	27.5	100.0	
	6	21	30.0	-27.5	27.5	100.0	
	12	21	30.0	-27.5	27.5	100.0	
79164	0	21	30.0	-27.5	27.5	100.0	
	6	21	30.0	-27.5	27.5	100.0	
79166	0	21	30.0	-27.5	27.5	100.0	
	6	21	30.0	-27.5	27.5	100.0	
	12	23	-15.0	-27.5	-112.5	-40.0	
	18	5	30.0	-27.5	-37.5	35.0	
		23	-15.0	-27.5	-112.5	-40.0	
79167	18	23	-15.0	-27.5	-112.5	-40.0	
79168	0	23	-10.0	-27.5	-112.5	-40.0	
79170	18	23	-15.0	-27.5	-112.5	-40.0	
		25	30.0	-27.5	177.5	-110.0	

Day	Time	Satellite	Lat. Bounds		Long. Bounds		Comments
79171	0	23	-10.0	-27.5	-112.5	-40.0	
		25	30.0	-27.5	177.5	-110.0	
	6	23	-2.5	-27.5	-112.5	-40.0	
		25	30.0	-27.5	177.5	-110.0	
	12	25	30.0	-27.5	177.5	-110.0	
79172	0	23	-5.0	-27.5	-112.5	-40.0	
79173	12	25	30.0	-27.5	177.5	-110.0	
79174	0	5	30.0	-27.5	-37.5	35.0	
		23	-7.5	-27.5	-112.5	-40.0	
	6	21	30.0	-27.5	27.5	100.0	
	12	21	30.0	-27.5	27.5	100.0	
	18	21	30.0	-27.5	27.5	100.0	
79175	0	21	30.0	-27.5	27.5	100.0	
	6	21	30.0	-27.5	27.5	100.0	
	12	21	30.0	-27.5	27.5	100.0	
	18	21	30.0	-27.5	27.5	100.0	
79176	0	21	30.0	-27.5	27.5	100.0	
	6	21	30.0	-27.5	27.5	100.0	
	12	21	30.0	-27.5	27.5	100.0	
	18	21	30.0	-27.5	27.5	100.0	
79177	0	21	30.0	-27.5	27.5	100.0	
	6	21	30.0	-27.5	27.5	100.0	
	12	21	30.0	-27.5	27.5	100.0	
	18	21	30.0	-27.5	27.5	100.0	
79180	0	5	17.5	-27.5	-37.5	35.0	
		23	-7.5	-27.5	-112.5	-40.0	
	6	23	-5.0	-27.5	-112.5	-40.0	
	18	23	-2.5	-27.5	-112.5	-40.0	
79181	0	23	-7.5	-27.5	-112.5	-40.0	

4/AUVINE/05